Microelectrophoresis of Semiconductive Quantum Dots

By

Mengke Han

THE UNIVERSITY of ADELAIDE

A thesis submitted for the fulfilment of the degree of Master of Philosophy

in the

Faculty of Sciences

School of Physical Sciences

Aug 2017

Declaration of Authorship

I certify that this work contains no material which has been accepted for the award of any other degree or diploma in my name in any university or other tertiary institution and, to the best of my knowledge and belief, contains no material previously published or written by another person, except where due reference has been made in the text. In addition, I certify that no part of this work will, in the future, be used in a submission in my name for any other degree or diploma in any university or other tertiary institution without the prior approval of the University of Adelaide and where applicable, any partner institution responsible for the joint award of this degree.

I give consent to this copy of my thesis when deposited in the University Library, being made available for loan and photocopying, subject to the provisions of the Copyright Act 1968.

I also give permission for the digital version of my thesis to be made available on the web, via the University's digital research repository, the Library Search and also through web search engines, unless permission has been granted by the University to restrict access for a period of time.

Signed:

Date:

Table of contents

Abstract

Semiconductive quantum dots (QDs) with superior optical properties, have been used as unique fluorescent probes in biological sensing and labelling. The effective intracellular delivery of QDs is critical to those biological applications. Microelectrophoresis is a promising technique to precisely deliver monodispersed nanoparticles into target cells with negligible cell membrane damage and cell distortion. In addition, it can record the intracellular electrical activities of target cells at the same time. This thesis aims to achieve for the first time the intracellular delivery of QDs via microelectrophoresis technique.

Microelectrophoresis technique has been well established to eject charged substances from fine-tipped glass micropipettes into tissue and cells via electrical currents. However, few studies have paid any attention to exploring standard experimental protocols for the intracellular microelectrophoretic ejection of biocompatible nanoparticles. The success of microelectrophoresis is largely limited by the aggregation of nanoparticles and subsequent blockages in the tip of micropipettes during ejection, which is caused by the colloidal instability of nanoparticles when the attractive van der Waals forces between them prevail over the repulsive electrostatic forces. Thus, successful microelectrophoresis requires optimized suspensions with monodispersed nanoparticles within micropipettes to avoid blockage. To improve the delivery, the tip size, current magnitude and ejection duration should be screened in parallel for the optimal parameters.

To address the above-mentioned requirements, Chapter 2 provides an effective experimental protocol for the preparation of QDs suspensions for filling

micropipettes, which has balanced the stability of QDs against the electrolytic conductivity of suspensions. In Chapter 3, micropipettes have been designed and manufactured with suitable tip inner diameters (IDs) for the size distribution of QDs suspensions, which has been demonstrated in Chapter 4 via microinjection technique. Finally, in Chapter 5, QDs have been successfully ejected out of micropipettes via microelectrophoresis and observed under a fluorescence microscope. The success of microelectrophoresis technique in ejecting semiconductive QDs described in this thesis has paved the way for managing a variety of other biocompatible nanoparticles with proper surface functional groups in either intracellular or extracellular delivery for various biological research.

Acknowledgements

This was an enjoyable and memorable transdisciplinary research experience, where I have had the great chance to learn from and work with many scientists from various research fields such as nanomaterials, inorganic chemistry, electrochemistry, electrophysiology, neuroscience, optics and photonics. It is my great pleasure to acknowledge everyone for their support and guidance to me throughout my degree of Master of Philosophy (MPhil).

First of all, I would like to thank my supervisors Heike Ebendorff-Heidepriem, Steven Wiederman and Yinlan Ruan. This is a great team with a glass scientist, an electrophysiologist and a physicist. Without their guidance and support, it would have been impossible for me to achieve the research presented in the thesis. Thanks to all supervisors for editing this thesis.

I would like to acknowledge Jiangbo Zhao, Joseph Mahandas Fabian, Herbert Tze Cheung Foo, Jingxian Yu, Yunle Wei and Xuanzhao Pan for many discussions and advices, which helped me enormously throughout my MPhil. Thanks to Jiangbo Zhao also for help with proof-reading this thesis.

I acknowledge the support from some of the microscopists at Adelaide Microscopy; they are Ken Neubauer, Lyn Waterhouse and Agatha Labrinidis. A lot of the data presented in this thesis were measured by the well-maintained SEM, TEM and optical microscope instruments at Adelaide Microscopy. They are acknowledged also for many useful discussions regarding measurements and data analysis.

Finally and most importantly, I would like to give special thanks to my partner Hongwei Yu, my friend Yihong Zhao, my mum Wen Yuan and my dad Hui Han for their love, support and encouragement to me over years. Without the support from friends and family, I could not imagine that I can complete this thesis.

List of Figures

List of Tables

Abbreviations and Symbols for Units

Ω	Ohm
µL	Microliter
µM	Micromole per litre
°C	Celsius degree
µm	Micrometre
0D	Zero dimensional
1D	One dimensional
2D	Two dimensional
3D	Three dimensional
A/D	Analog-to-digital
Ag	Silver
Ag^+	Silver ion
AgCl	Silver chloride
AR	Analytical reagent
AU/a.u.	Arbitrary units
CdSe	Cadmium selenide
Cl^-	Chloride ion
cm	Centimeter
Conc.	Concentration
cP	Centipoise
DLS	Dynamic light scattering
DNA	Deoxyribonucleic acid
DOS	Electronic density of the states
e^-	Electron
EDTA	Ethylenediaminetetraacetic acid
eV	Electronvolt

FESEM	Field emission scanning electron microscope
H^+	Hydrogen ion
HCl	Hydrochloric acid
Hz	Hertz
ID	Inner diameter
IS	Ionic strength
K^+	Potassium ion
KCl	Potassium chloride
kHz	Kilohertz
LCD	Liquid crystal display
M	Mole per liter
MΩ	Megaohm
mL	Millilitre
mm	Millimeter
mM	Millimole per litre
ms	Millisecond
mV	Millivolt
mW	Milliwatt
nA	Nanoampere
Na^+	Sodium ion
NaCl	Sodium chloride
NaOH	Sodium hydroxide
NCs	Nanocrystals
nm	Nanometer
nM	Nanomole per litre
OD	Outer diameter
OH^-	Hydroxide ion
PCS	Photon correlation spectroscopy
PEG	Polyethylene glycol

pH	Potential of hydrogen
pKa	Acid dissociation constant
PL	Photoluminescence
QDs	Quantum dots
rad	Radian
RDB	Rhodamine b
rpm	Revolutions per minute
S	Sulfur
s	Second
SD	Standard deviation
SEM	Scanning electron microscope
STMD	Small target motion detector
TAE	Tris-acetate-EDTA
TEM	Transmission electron microscope
TiO_2	Titanium dioxide
UV	Ultraviolet
V	Volt
W	Watt
ZnS	Zinc sulfide

Chapter 1

1 Introduction

1.1 Background and Motivation

Understanding the complex spatiotemporal interplay of biomolecules in many fundamental, life science processes (from the cellular to the organismal level) relies on the employment of fast, sensitive, reliable and reproducible sensing techniques [1, 2]. Of various sensing mechanisms, fluorescence techniques are highly competent to fulfil these requirements [1]. They enable real-time imaging of live cells and offer nanoscale resolution with single-molecule sensitivity [1, 3].

Semiconductive QDs that are robust and bright light emitters, have become a new important class of fluorescent labels for *in vitro* and *in vivo* bioimaging research [4, 5]. They have functionalized surfaces suitable for bioconjugation, adaptable photophysical properties for multiplexed detection, and superior stability for longer investigation times [5]. Undoubtedly, the ability to achieve effective intracellular delivery of semiconductive QDs is critical to their biological applications [6, 7].

Current techniques of intracellular delivery of semiconductive QDs and a variety of other biocompatible nanoparticles can be categorised into the three main schemes of passive delivery, facilitated delivery and active delivery, based on their natural physiochemical characteristics [6]. In passive delivery, the surface functional groups and charges of QDs themselves can mediate their nonspecific cellular internalization [6, 8]. In facilitated delivery, the specific peptide sequences or polymer delivery reagents decorated on QDs surfaces

can facilitate their intracellular uptake via endocytosis [6, 9]. In active delivery, electroporation can apply high-voltage electric shocks (~ 1000 V/cm) across target cells to increase the permeability of the cell membrane and allow the intracellular delivery of QDs [6, 10]. Microinjection can use pressure to eject small volumes (usually femtoliters) of QDs suspensions from fine-tipped glass micropipettes into individual cells under a microscope [6, 7, 10].

These three strategies have their own set of benefits along with associated limitations. For passive delivery with simple surface functionalization, the nonspecific endocytosis and subsequent endosomal escape of QDs remain issues [6, 8]. For facilitated delivery, the specific ligands on QDs surfaces can significantly enhance their delivery to target cells with short incubation times, minimal toxicity, and overall loading efficiency [6, 11], but the endosomal sequestration and degradation of QDs are still unavoidable [6]. For active delivery, as it bypasses the endocytic pathway, the endosomal degradation of QDs can be avoided [6]. However, the high cell mortality and aggregation of QDs after electroporation, and the low throughput of microinjection remain liabilities [6, 7].

The research described in this thesis aims to develop a new method for delivering QDs into target cells using microelectrophoresis technique, which is also known as microiontophoresis [12, 13] or iontophoretic microinjection [14]. This technique can be categorised into active delivery as it can eject charged QDs from fine-tipped glass micropipettes via relatively small electrical currents (less than ± 100 nA) and has the potential to overcome some of the above-mentioned limitations of current techniques [15]. Compared to electroporation, it has the potential to precisely control the delivery of monodispersed QDs into target cells with negligible cell membrane damage

and cell distortion. Compared to microinjection, as most biological membranes *in vivo* maintain a resting membrane potential difference which may range from about -30 to -180 mV [16], microelectrophoresis technique can locate the position of target cells without a microscope by recording a potential difference once the micropipette is pierced into the target cell. Then it can monitor the intracellular electrical activities from target cells in response to environmental or intracellular stimuli during current passing [17]. In addition, it can minimize the troublesome diffusion of chemically and pharmacologically active agents from micropipettes by applying a retaining current [15]. However, like microinjection, microelectrophoresis has its inherent limitation of low throughput as each cell needs to be individually selected. Moreover, it can only be applied to deliver charged substances.

Although microelectrophoresis technique has been established since circa 1900 [12, 15], few studies have paid any attention to exploring standard experimental protocols for the ejection of biocompatible nanoparticles despite the rapid development in nanotechnology. The success of microelectrophoresis is largely limited by the aggregation of nanoparticles and subsequent blockages in the tip of micropipettes during ejection, which is caused by the colloidal instability of nanoparticles when the attractive van der Waals forces between them prevail over the repulsive electrostatic forces. Thus, optimized suspensions of monodispersed QDs are required to fill micropipettes for successful microelectrophoresis. Meanwhile, the tip size, current magnitude and ejection duration should be screened for an improved delivery.

The pioneering work of applying microelectrophoresis technique to the intracellular delivery of QDs described in this thesis can pave the way for utilizing not only charged semiconductive QDs but also a variety of other

charged biocompatible nanoparticles in intracellular and extracellular delivery for biological research.

1.1.1 Semiconductive QDs

QDs refer to nanoscale particles that exhibit quantum size effect, or known as quantum confinement, where the motion of electronic excitations is confined within the particles that have sizes comparable to the wavelength of the electron [18]. As a result, the continuous energy bands of the bulk materials collapse into discrete energy levels (Figure 1.1) [19]. The discrete structure of energy states leads to the discrete absorption spectra of QDs, which are in contrast to the continuous absorption spectra of their equivalent bulk materials [18]. However, in practical terms, small variations in the size of the QDs in a sample can translate into relatively large variations in the absorption and emission linewidths (Figure 1.2) [20]. In the case of semiconductive QD, besides the discrete energy levels, the energy gap that separates the conduction energy bands from the valence energy bands can be increased by reducing the particle size, leading to blue shifts in its absorption and emission spectra (Figure 1.2) [18, 21]. The minimum energy for an electron to get excited from the highest valence state to the lowest conduction state corresponds to the first absorption peak, which is also known as the absorption onset (Figure 1.2) [21]. Semiconductive QDs do not absorb energy of wavelengths longer than the absorption onset.

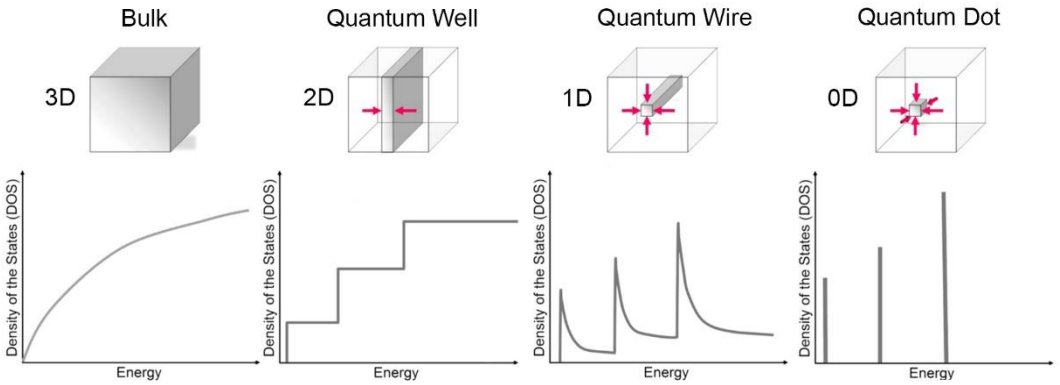

Figure 1.1 | Electronic density of the states (DOS) of a bulk three dimensional (3D) crystalline material, a two dimensional (2D) quantum well, a one dimensional (1D) quantum wire, and a zero dimensional (0D) QD. The insets show the corresponding spatial confinement from directions that are defined by arrows. Reproduced from [19].

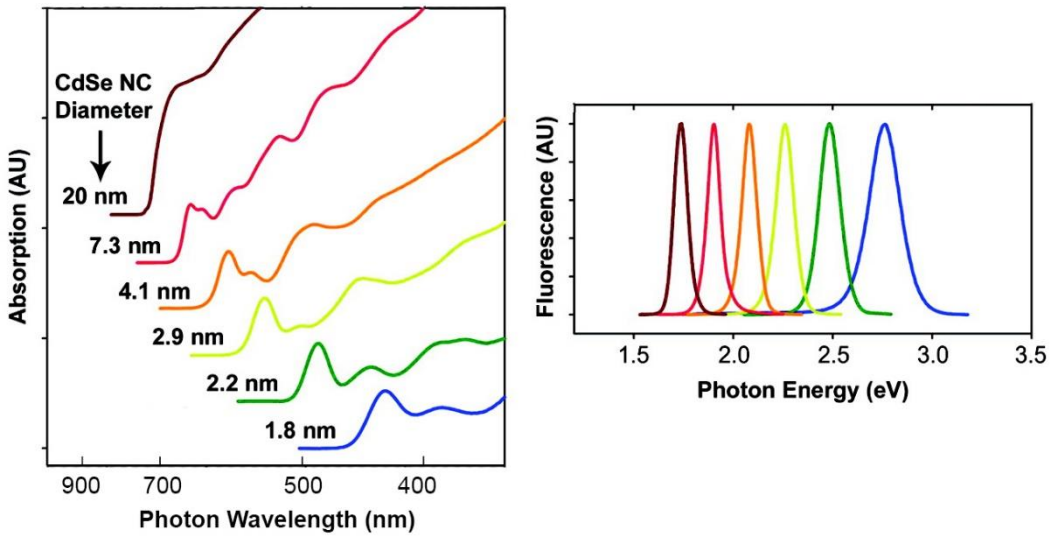

Figure 1.2 | Absorption (left) and emission (right) spectra of Cadmium Selenide (CdSe) semiconductor nanocrystals (NCs) showing quantum confinement. AU = arbitrary units. The first absorption peak, i.e. the peak with the lowest energy, is the absorption onset. Reproduced from [21].

When semiconductive QDs were first used as fluorescent probes in biological staining and diagnostics [22, 23], their superior optical properties as *in vivo* and *in vitro* fluorophores was noted in a variety of biological investigations [2]. Compared to conventional organic dyes and genetically encoded fluorescent

proteins, semiconductive QDs have high photoluminescence (PL) quantum yields even in the near-infrared region, larger molar absorption coefficients at the first absorption peaks, and larger two-photon excitation action cross-sections, resulting in bright fluorescence [1, 24]. Their size-tunable absorption and emission, and extremely broad absorption bands from the absorption onset enable flexible selections of excitation in multiplexed detection [2]. In addition, their high resistance to photobleaching and chemical degradation overcomes the limited effectiveness of utilizing traditional fluorescent labels in long-term imaging [2, 25]. In Table 1-1, under continuous wide-field illumination at 10.6 mW ($\approx$ 10.7 W cm^{-2}) excitation intensity, different fluorescent materials show different bleaching times at which the fluorescence intensity decreases to 50% of their initial values [25]. QDs show the minimal photobleaching, in contrast to the rapid bleaching of Alexa 647 (organic fluorophore), beads, Au nanoclusters and carbon dots [25]. Semiconductive QDs have been applied for detection and imaging in several areas of life sciences [1], and have become an important class of fluorescent labels in the toolkit of biological researchers [5].

Table 1-1 | Bleaching times of different fluorescent materials. Reproduced from [25].

Fluorescent materials	Bleaching time (s)
Quantum dots	1500
Carbon dots	150
Beads	85
Au nanoclusters	27
Alexa 647	8

1.1.2 Microelectrophoresis technique

Microelectrophoresis is the technique whereby an electrical current is used to control the ejection of relatively concentrated chemical substances in solution from the small orifice of micropipettes that are pulled from glass capillaries (Figure 1.3) [15, 26]. Iontophoresis can also be used to describe this technique but strictly should be restricted to describing the movement of ions by current flow [15]. The polarity of the applied ejecting current depends on the net charge on the substances to be ejected, i.e. negative currents are used to eject negatively charged molecules [17]. This technique can introduce minute amounts of drugs and chemicals into either the intracellular or extracellular phase of tissue, and conveniently record the electrical signals of cellular responses from excitable cells, e.g. muscle, glandular and neuronal cells [12, 15]. Excitable cells can generate action potentials at their membrane in response to depolarization and may transmit an impulse along the membrane [27].

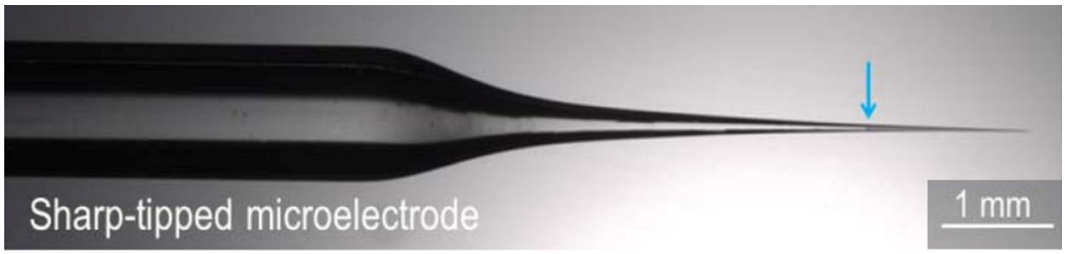

Figure 1.3 | Micrograph of a sharp-tipped micropipette that was pulled from a borosilicate glass capillary using a micropipette puller (Model P-97 Flaming/Brown). The blue arrow shows the meniscus of solution in the tip for microelectrophoresis. Reproduced from [26].

This powerful technique has a wide range of applications in modern biology [17]. Its ability to record intracellular electrical activities can be used to identify a single cell and delineate cellular architecture by ejecting fluorescent labels intracellularly in anatomical studies and fluorescence imaging [17, 28]. It can

be used to track the transfer of molecules between cells and neuronal pathways, and identify cell progeny in lineage studies [17, 29]. It can also be used to measure intracellular ion concentrations, e.g. pH (potential of hydrogen) and calcium ions [17, 30]. The basic principle of microelectrophoresis does not vary with compounds or applications. However, for different applications, several factors, including the tip size, current magnitude, ejection duration and in particular, the preparation of chemical solution for filling micropipette, should be considered carefully, since they are the most critical factors for successful microelectrophoresis [17].

1.2 State-of-the-art

This research project is developed on the basis of current knowledge and technologies in the area of biocompatible semiconductive QDs, iontophoresis, micropipettes manufacture and microinjection. The following sections provide a review of the literature for each topic.

1.2.1 Surface functionalization of semiconductive QDs

The exceptional optical properties of semiconductive QDs have promoted their applications in biological imaging. However, the preparation of semiconductive QDs for microelectrophoresis technique needs to consider not only their optical properties, but also their dispersity, stability, mobility and toxicity in a biological environment.

The optical properties of semiconductive QDs are determined by their chemical composition and structure, average size and size distribution [31]. One of most widely used semiconductive QDs for biological applications are made of CdSe cores coated with a layer of Zinc Sulfide (ZnS), because the synthesis technique and surface functionalization of CdSe/ZnS are well refined, commercialized by Sigma-Aldrich, Invitrogen, Evident and PlasmaChem with various sizes for the selections of desired optical properties [2]. The unique core/shell structure design has several advantages. Overcoating the core with a layer of inorganic materials with wider band gaps can improve the PL quantum yields by passivating surface nonradiative recombination sites [31]. In addition, the ZnS layer can protect the particles from oxidation and harsh biological environment, e.g. acidic buffers and

cellular organelles, and prevent the leakage of toxic CdSe into the surrounding environment [2, 31].

The dispersity and stability of semiconductive QDs are controlled by the chemical nature of their surface functional groups [1]. Since the aim of this thesis is to deliver QDs intracellularly via microelectrophoresis techniques, only charged QDs can move under the applied electric field. Different charged chemical groups can be used to modify the QDs surfaces, such as small charged adsorbants [32], charged surfactants [33], bulky polyelectrolytes [34] and additional inorganic shells (Figure 1.4) [1, 35]. The success of applying microelectrophoresis technique for intracellularly delivering QDs can provide a basic delivery strategy for a variety of other charged nanoparticles.

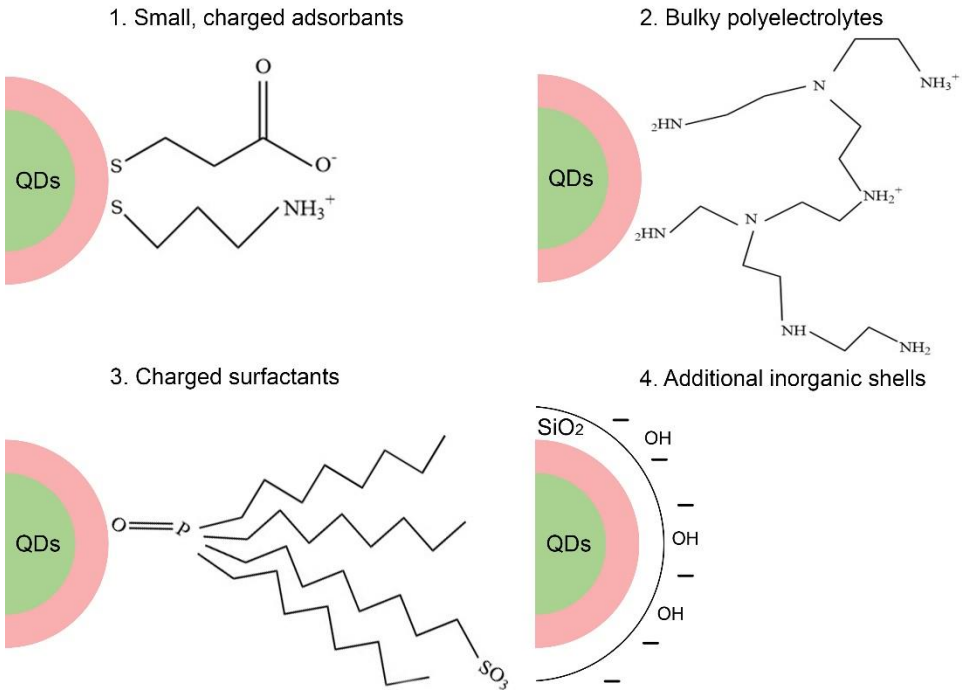

Figure 1.4 | Schematic illustration of surface functionalization strategies to prepare charged QDs, including small charged adsorbants (top left), bulky polyelectrolytes (top right), charged surfactants (bottom left) and additional inorganic shells (bottom right). Reproduced from [1].

1.2.2 Iontophoresis and zeta potential

To optimize the microelectrophoresis technique for delivering QDs, several important factors relating to the performance of microelectrophoresis are described as below, including zeta potential, electrophoretic mobility and hydrodynamic radius.

The microelectrophoretic ejection of chemical substances from glass micropipettes involves both iontophoresis and electroosmosis [15]. Iontophoresis is the movement of a charged species (molecule or particle) relative to the liquid where it is suspended, under the influence of an electric field [15]. Electroosmosis is the movement of a liquid relative to a stationary charged surface, which refers to the inner wall of glass micropipettes in this scenario, under the influence of an electric field [15]. In general, when the solutions within glass micropipettes contains concentrated and highly charged species, the motion of the species is faster than that of the liquid [15]. Thus, the contribution of electroosmosis to the total ejection is relatively small and can be ignored [15, 36].

In iontophoresis, a charged particle, which is mainly discussed in this thesis, experiences an electric force, balanced by its frictional drag through the medium [37]. The electric force (F_E) can be given by:

$$F_E = qE \qquad \text{Equation 1-1}$$

where E is the applied electric field, and q is the electric charge of the particle [38]. The frictional force (F_F, for a spherical particle) can be given by Stoke's law:

$$F_F = -6\pi\eta r v \qquad \text{Equation 1-2}$$

where η is the viscosity of the surrounding medium, r is the hydrodynamic radius of the particle, and v is the particle velocity [38]. During a short transient period when the electric force is first applied, a steady state, i.e. the balance of these forces, is attained [37].The transient time of macromolecules is typically on the order of 10^{-11} s [38]. After the transient period, the electric and frictional forces are equal, but opposite in direction:

$$qE = 6\pi\eta r v \qquad \text{Equation 1-3}$$

For a given charged particle, a physical constant, electrophoretic mobility (μ_e), can be defined by [38]:

$$\mu_e = \frac{v}{E} = \frac{q}{6\pi\eta r} \qquad \text{Equation 1-4}$$

In Equation 1-4, it is evident that small, highly charged particles have high mobilities whereas large, negligibly charged particles have low mobilities [37]. However, the conclusion is based on the ideal condition where particles are fully charged and extrapolated to infinite dilution [37]. In practice, electrophoretic mobility is determined by the Henry equation:

$$\mu_e = \frac{2\varepsilon\zeta f(K_a)}{3\eta} \qquad \text{Equation 1-5}$$

where ε is the dielectric constant of the medium and $f(K_a)$ is Henry's function, which is generally approximated as 1.50 by Smoluchowski approximation in polar media with moderate electrolyte concentrations, or 1.00 by Huckel approximation in non-polar media [39]. ζ is the zeta potential of the particle, which can be explained by the electrical double layer structure existing around the particle as illustrated in Figure 1.5 [40].

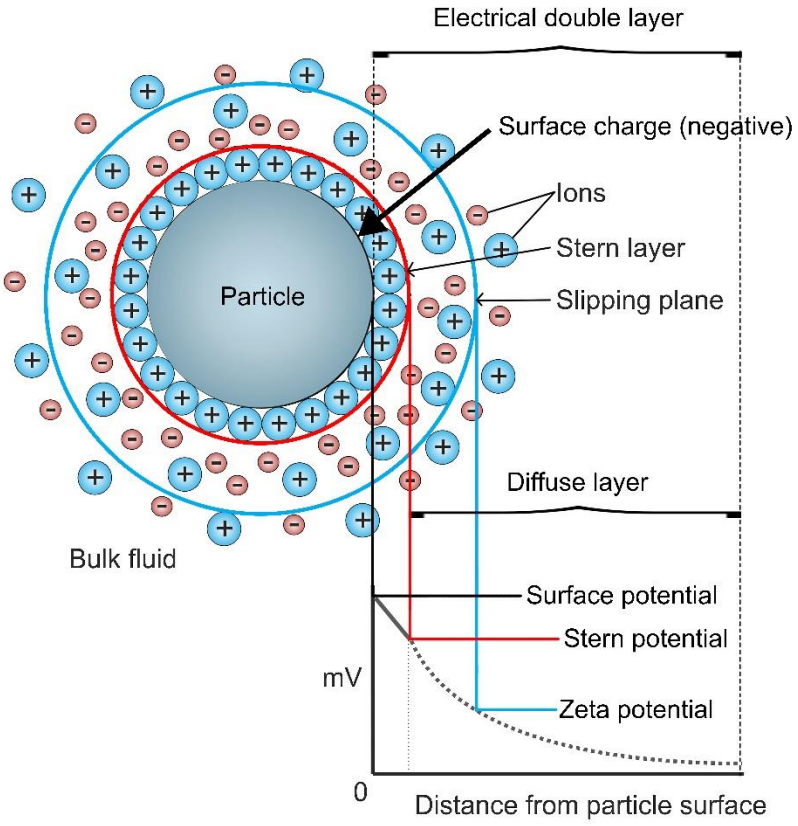

Figure 1.5 | Schematic illustration of electrical double layer structure and zeta potential: ionic concentration and potential differences as a function of distance from the charged surface of a particle suspended in a medium. Reproduced from [40].

The net charge on the particle surface affects the distribution of ions in the surrounding interfacial region, and attracts oppositely charged ions close to the surface [41]. In the Stern layer, ions are strongly bound to the particle, whereas in the diffuse layer, ions are less firmly attached [42]. The thickness of the diffuse layer is called the Debye length (k^{-1}, nm):

$$k^{-1} = \sqrt{\frac{\varepsilon\varepsilon_0 k_B T}{2N_A I e^2}} \qquad \text{Equation 1-6}$$

where ε_0 is the dielectric permittivity of a vacuum, k_B is the Boltzmann constant, T is the absolute temperature, N_A is Avogadro's number, I is the ionic strength and e is unit charge. The slipping plane is a notional boundary within the diffuse layer to divide ions, which forms a stable entity and moves with the particle at the same speed [38]. The radius of the particle and the thickness of slipping plane make the total hydrodynamic radius [43]. The potential existing at the edge of the hydrodynamic radius is known as zeta potential [38, 43]. Based on Equation 1-5, it is essential to prepare highly charged QDs in suspension with high zeta potentials and electrophoretic mobilities for successful microelectrophoresis.

The magnitude of zeta potential is highly dependent on the pH and ionic strength (IS) of the medium as shown in Figure 1.6 [37, 44]. In respect of the pH of the medium, for a suspended particle with a negative zeta potential, the more alkali added to this suspension, the more negative charge the particle tends to acquire [41]. If acid is added to this suspension, the negative charge can be neutralised at a pH value, which is called the isoelectric point [41]. The zeta potential of the particle at the isoelectric point is zero [41]. The more acid added, the more positive the zeta potential becomes [41]. However, for

particles having surface functional groups with very high or low acid dissociation constant (pKa) values (< 3 or > 11), the zeta potential can remain constant over a wide pH range [45].

In respect of the IS of the medium, inorganic ions in solution can affect the zeta potential in two distinct ways. The increase in IS compresses the Debye length as shown in Equation 1-6 [41], resulting in a stronger electrostatic screening effect and a lower zeta potential. But the isoelectric point remains the same when there is no specific adsorption of ions on particles (Figure 1.6) [44]. Otherwise, the isoelectric point shifts depending on the adsorption process [46].

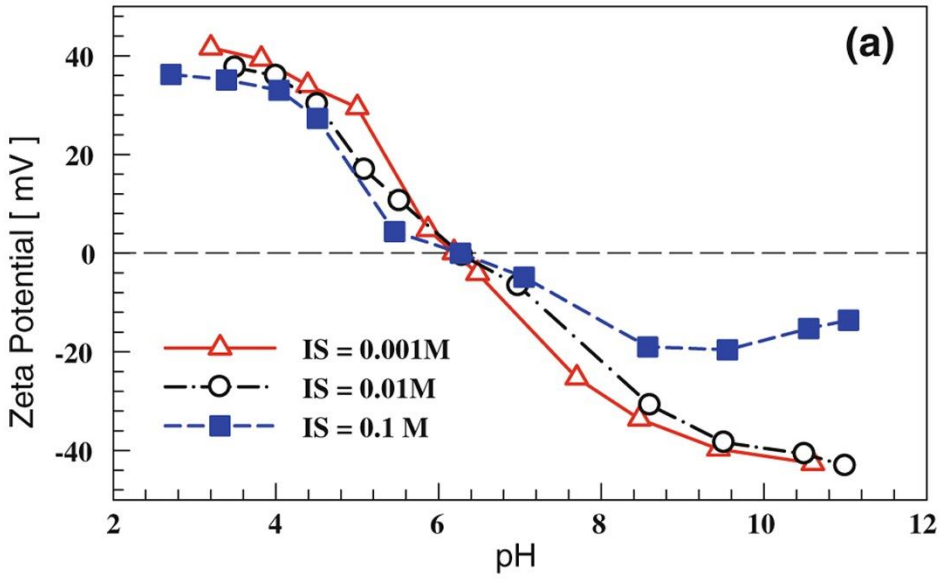

Figure 1.6 | The influence of solution IS and pH on the zeta potential of titanium dioxide (TiO2) nanoparticles. Reproduced from [44].

In addition, particles with high zeta potentials are stable due to the strong electrostatic repulsion between each other to inhibit aggregation and avoid blockage of the tip during microelectrophoresis [41, 47]. In contrast, particles in a highly unstable suspension with low or zero zeta potential tend to rapidly

aggregate and impede microelectrophoresis [41]. Thus, the magnitude of zeta potential can indicate the stability of particles, which is critical to successful microelectrophoresis. The stability dividing line is generally considered to be ± 30 mV for aqueous systems [48].

To determine the zeta potential of particles in suspension, electrophoretic mobility can be directly measured with Zetasizer nano ZSP via laser doppler velocimetry technique and converted to zeta potential via the Henry equation [49]. In a classic microelectrophoresis system, i.e., folded capillary cell, particles move to the oppositely charged electrode when a potential is applied across the suspension as shown in Figure 1.7 [49, 50]. The incident laser beam illuminates the particles and the scattered light at a certain angle is collected by the detector [49]. A reference beam is modulated at a certain frequency [49]. The frequency difference between the reference beam and the scattered beam due to the movement of particles is proportional to particle velocities [49]. The extracted velocity per unit field strength is the electrophoretic mobility (Equation 1-4), which can generate the zeta potential via the Henry equation (Equation 1-5) [49].

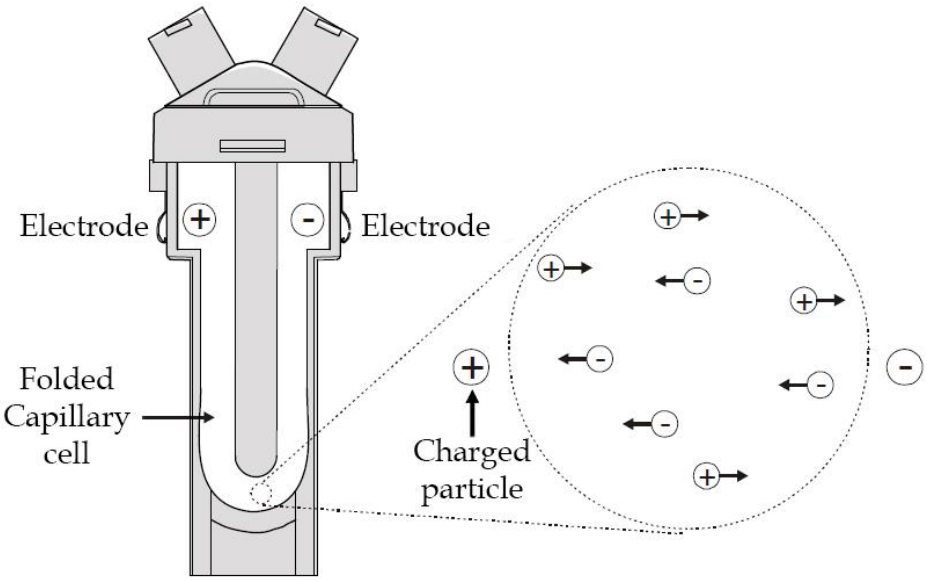

Figure 1.7 | Schematic illustration of a folded capillary cell. Reproduced from [50].

1.2.3 Size distribution of semiconductive QDs

Successful microelectrophoresis requires not only the high electrophoretic mobility of QDs but also micropipettes with suitable tip sizes that allow the ejection of QDs and avoid physical damage to tissue and cells at the same time.

For intracellular microelectrophoresis, it is essential that the tips remain as small as possible (less than 0.1 μm) for successful penetration into cells without damage [15, 17]. For extracellular microelectrophoresis, it is advantageous to ensure that the tip sizes are less than 0.5 μm to avoid the massive leakage of extremely active compounds from micropipettes and the possibility of tissue damage [15]. However, semiconductive QDs have their sizes (typically 2 - 10 nm) comparable with the tip size of micropipettes that are routinely used. Tips that are too small can impede the ejection of QDs and subsequently cause the aggregation of QDs in the tips, resulting in microelectrophoresis failure. Thus, it is essential to prepare monodispersed QDs in suspension. Their

hydrodynamic radii are critical to the selection of suitable tip sizes for successful microelectrophoresis.

First, the accurate primary sizes and shapes of QDs can be measured by transmission electron microscope (TEM). The primary sizes can be used to evaluate the dispersity of QDs in aqueous medium. If the hydrodynamic radii of QDs in aqueous medium are less than twice of their primary sizes, it can be concluded that the QDs are aggregation-free and vice versa [51]. The hydrodynamic radius of QDs can be measured by Zetasizer nano ZSP via dynamic light scattering (DLS) technique, which provides reliable and convenient measurements of the size of particles from 0.3 nm to 10 μm in diameter as specified.

DLS technique, which is also known as photon correlation spectroscopy (PCS), uses a laser beam to illuminate particles and analyses the intensity fluctuations in the scattered light that are caused by constantly Brownian motion of particles in liquid medium [51]. Brownian motion is the movement of particles due to the random collision with the molecules of the liquid that surrounds the particles [52]. Particles with different sizes have different speeds of Brownian motion and the higher the temperature the faster the Brownian motion. For larger particles with slower Brownian motion, the intensity fluctuation in time at one point on the detector is slower than that of smaller particles [51]. The digital correlator in Zetasizer measures the degree of similarity between two signals at this point over a period and plots a correlation function that reduces with time [51]. For smaller particles, the rate of decay for the correlation function is much faster than that of lager particles [51]. Finally, the hydrodynamic radius and size distribution of particles are produced by extracting algorithms between the decay rates and size classes [51].

1.2.4 Micropipettes and electrodes

Micropipettes with suitable tip sizes for microelectrophoresis can be manufactured on a micropipette puller, e.g. Model P-97 Flaming/Brown. In P-97, a glass capillary is heated at the centre until molten and stretched at the same time [53]. The tip draws out, breaks and separates while the glass is still soft but cooling down [53]. One capillary can be pulled to produce two micropipettes ready for use at a time. The tip size of micropipettes can be measured by scanning electron microscope (SEM).

Silver/silver chloride (Ag/AgCl) electrodes are the most frequently used electrodes in microelectrophoresis to apply electric forces on QDs that are filled in the micropipette and record the intracellular electrical activities of target cells. A thin Ag/AgCl wire can be inserted into the QDs suspension from the blunt end of the micropipette, as the working electrode. Another Ag/AgCl wire is placed in the outer medium as the counter electrode. The two electrodes are connected to the copper wires at the opposite poles of the current source to form a completed electrical circuit where charged QDs filled in the micropipette can move to the counter electrode under the applied electric field as shown in Figure 1.8.

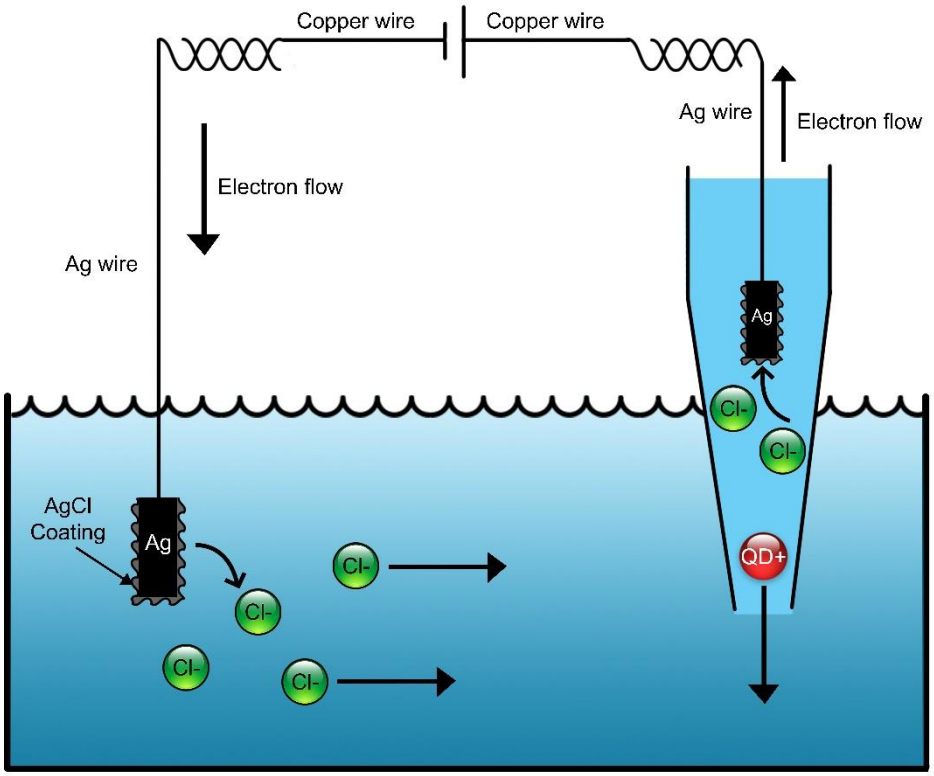

Figure 1.8 | The silver/silver chloride electrode. Reproduced from [54].

To prepare a Ag/AgCl wire, Ag wire can be immersed into 1 M sodium chloride (NaCl) solution and anodized by applying voltage across the solution where a platinum electrode is used as the cathode. The Ag wire surface darkens once it gets coated with a matte thin layer of AgCl pellet.

In microelectrophoresis, the current is transformed smoothly from a flow of electrons in the copper wires to a flow of ions in solution as shown in Figure 1.8 [54]. The Ag/AgCl electrode reaction can be presented by:

$$Ag + Cl^{-} \leftrightarrow AgCl + electron\ (e^{-}) \qquad \text{Equation 1-7}$$

If electrons flow from the copper wire through the silver wire to the coated AgCl pellet, they convert the AgCl to Ag atoms and the chloride ions (Cl^-) enter the solution and move along the direction of the electric field to the anode [54]. If electrons flow in the reverse direction, Ag atoms in the silver wire that is coated with AgCl pellet give up their electrons and combine with Cl^- ions that are in the solution to make insoluble AgCl pellet [54]. Thus, Ag/AgCl electrode is reversible, i.e. electrons can flow in both directions, but exhaustible [54]. If AgCl on the cathode is exhausted by the current flow, bare silver wire could come in contact with the solution [54]. Silver ions (Ag^+) that are leaking from the cathode wire can poison many proteins [54]. The resulting poorly reversible surface reactions due to other ions in the solution and trace impurities in the silver wire can cause electrode polarization [54]. Thus, it is important to check and maintain the AgCl coating routinely.

To record the intracellular electrical activities of target cells with high fidelity, strong electrolyte solutions, e.g. 2 - 4 M potassium chloride (KCl), are typically filled into micropipettes [54, 55]. On the one hand, KCl solutions with high concentrations, such as 3 M, can offer a resistivity less than 5 - 10 Ωcm [55], which can keep the resistance of micropipettes as low as possible, suppress voltage noise and provide a wider recording bandwidth [54]. On the other hand, they can prevent erroneous measurement of the resting membrane potential by negating the positive liquid junction potential between the filling solution and the cell cytoplasm, which is caused by the difference in the mobilities of the cellular anions and cations [54]. The predominant cellular anions are low mobility ions, e.g. negatively charged large proteins, whereas the cations are small with high mobility [54]. Highly concentrated KCl solution makes the liquid junction potential independent of changes in the composition of the cellular solution due to the similar mobility of potassium ions (K^+) and Cl^- [54].

However, the disadvantage of using highly concentrated KCl solution is that K^+ and Cl^- can enter the target cells. This can cause a hyperosmotic load that swells the cell and alters the normal anion and cation composition [54]. Fine tipped micropipettes can minimize this effect but result in noise, diminish current passing ability and limit recording bandwidth due to their high resistance [54]. Thus, in practice, it is important to obtain a balance between the concentration of KCl in the filling solutions and the tip sizes of micropipettes [54].

For the microelectrophoresis of QDs, it seems easy to obtain stable and monodispersed QDs with high electrophoretic mobilities by simply regulating the pH of suspensions. Meanwhile, the IS of suspensions should be as low as possible to avoid the decrease in zeta potentials. However, Ag/AgCl electrodes can only perform well in solutions containing substantial Cl^- as shown in Equation 1-7 [54]. The high concentration of KCl in suspensions can greatly reduce the zeta potentials and repulsive energy barrier of QDs by compressing the Debye length, resulting in rapid aggregation and unsuccessful microelectrophoresis [41]. Thus, it is essential to determine a suitable concentration of KCl in QDs suspensions to maintain the stability of QDs and permit the high-fidelity intracellular recording at the same time.

1.2.5 Microinjection technique and agarose gel

After fine-tipped micropipettes are manufactured with hypothetically suitable tip sizes, the successful microelectrophoretic ejection of QDs should be demonstrated before delivering QDs into target cells.

It is reasonable that the successful detection of fluorescence signals from ejected QDs can demonstrate the successful microelectrophoretic ejection. However, if no fluorescence signal is detected, it is irrational to conclude that the tip size of micropipette is not large enough to allow the ejection of QDs, provided that the QDs are monodispersed and the possible aggregation factor is excluded. Besides the size mismatch, there are several factors that could lead to unsuccessful fluorescence detection, for example, ineffective ejecting current or insufficient ejection duration can result in a negligible amount of ejected QDs with low fluorescence intensity under the detection limit of fluorescence microscopes. To firstly exclude the possibility of the size mismatch, microinjection technique is utilized to eject QDs via pressure [12]. If the microinjection of QDs succeeds, it can be concluded that the tip size is suitable for the microelectrophoretic ejection of QDs. If the microinjection of QDs fails, the tip size should be further increased, and the size match should be demonstrated before attempting to test microelectrophoresis.

To ease detecting the fluorescence signals from ejected QDs in microinjection, agarose gels are utilized as the outer medium to confine the diffusion of ejected QDs by their unique macromolecular netted texture. Agarose is isolated from the seaweed genera *Gelidium* and *Gracilaria*, and consists of repeated agarobiose (L- and D-galactose) subunits to form linear polymers (Figure 1.9) [56-58]. During gelation, agarose polymers associate non-covalently by hydrogen bond and form a porous network of channels and bundles, which could provide sufficient space to hold a large amount of water or electrolyte [56]. In microinjection, ejected QDs in the outer medium do not experience the driving force due to the applied pressure any more. They enter the agarose gels and accumulate because of the confinement effect of the agarose gel network structure, resulting in a high local concentration and fluorescence intensity.

Thus, the bright fluorescence from ejected QDs can be observed under a fluorescence microscope to demonstrate the size match and successful microinjection.

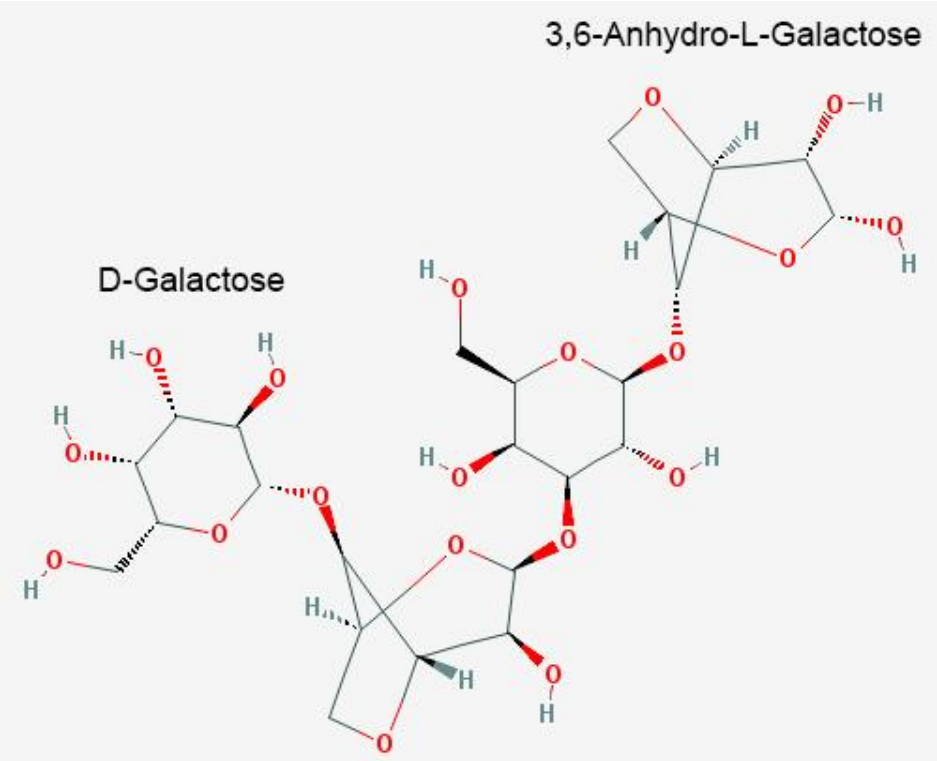

Figure 1.9 | Segmental 2D structure of agarose polymers. Reproduced from [58].

1.3 Research Objectives

The objectives of this work presented in this thesis are to:

1. Develop an effective experimental protocol for the preparation of semiconductive QDs suspensions for successful microelectrophoresis.

2. Manufacture micropipettes with suitable tip sizes that are large enough for the ejection of semiconductive QDs and as small as possible to avoid physical damage to target cells.

3. Demonstrate the successful microinjection and microelectrophoresis of semiconductive QDs.

1.4 Thesis structure

This thesis describes the pioneering work of applying microelectrophoresis technique for delivering semiconductive QDs into target cells. The flowchart below (Figure 1.10) illustrates the connection between the chapters in this thesis.

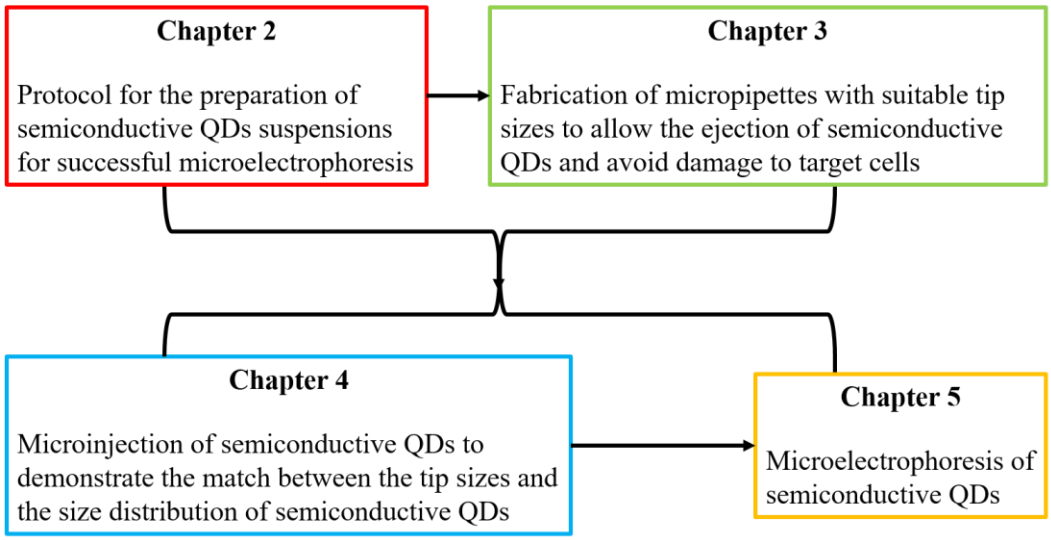

Figure 1.10 | A flow chart showing the connection between chapters in this thesis.

Chapter 2 describes the experimental protocol for the preparation of semiconductive QDs suspensions for successful microelectrophoresis. The prepared QDs suspensions achieved the best balance between the stability of QDs (preferring to high zeta potential and low IS) and the electrolytic conductivity of suspensions (preferring to strong IS) for intracellular recording. The zeta potentials of QDs in suspensions were reliably measured to demonstrate the optimized protocol.

Chapter 3 describes the manufacture of micropipettes with suitable tip IDs. The manufactured micropipettes could record the neuronal activities of small target motion detectors (STMD) neurons in the lobula plate of dragonflies with negligible cell membrane damage. Meanwhile, their tip IDs were suitable for the ejection of QDs, which was demonstrated via microinjection technique in Chapter 4 and microelectrophoresis technique in Chapter 5.

Chapter 4 describes the successful microinjection of QDs and demonstrates that the tip IDs of manufactured micropipettes are suitable for microelectrophoresis. Microinjection technique was applied to eject QDs via pressure into agarose gels. The diffusion of ejected QDs was obstructed by agarose gels, resulting in a relatively high local concentration and fluorescence intensity of QDs. The bright fluorescence from ejected QDs was successfully observed under a fluorescence microscope.

Chapter 5 demonstrates the successful microelectrophoresis of QDs by observing the bright fluorescence from ejected QDs under a fluorescence microscope.

Chapter 6 concludes the thesis and provides an outlook for the future development of microelectrophoresis technique to intracellularly and extracellularly deliver semiconductive QDs and a variety of other biocompatible nanoparticles for biological studies.

Appendix summarizes the materials and instruments used in this thesis and presents the parameter setting of Zetasizer and the quality assessment of zeta potential data.

1.5 References

1. Resch-Genger, U., et al., *Quantum dots versus organic dyes as fluorescent labels.* Nat Meth, 2008. **5**(9): p. 763-775.
2. Medintz, I.L., et al., *Quantum dot bioconjugates for imaging, labelling and sensing.* Nature materials, 2005. **4**(6): p. 435-446.
3. Zhang, J., et al., *Creating new fluorescent probes for cell biology.* Nature Reviews Molecular Cell Biology, 2002. **3**: p. 906.
4. Alivisatos, A.P., W. Gu, and C. Larabell, *Quantum dots as cellular probes.* Annu Rev Biomed Eng, 2005. **7**: p. 55-76.
5. Wegner, K.D. and N. Hildebrandt, *Quantum dots: bright and versatile in vitro and in vivo fluorescence imaging biosensors.* Chemical Society Reviews, 2015. **44**(14): p. 4792-4834.
6. Delehanty, J.B., H. Mattoussi, and I.L. Medintz, *Delivering quantum dots into cells: strategies, progress and remaining issues.* Anal Bioanal Chem, 2009. **393**(4): p. 1091-105.
7. Derfus, A.M., W.C.W. Chan, and S.N. Bhatia, *Intracellular Delivery of Quantum Dots for Live Cell Labeling and Organelle Tracking.* Advanced Materials, 2004. **16**(12): p. 961-966.
8. Jaiswal, J.K., et al., *Long-term multiple color imaging of live cells using quantum dot bioconjugates.* Nat Biotech, 2003. **21**(1): p. 47-51.
9. Ruan, G., et al., *Imaging and tracking of tat peptide-conjugated quantum dots in living cells: new insights into nanoparticle uptake, intracellular transport, and vesicle shedding.* J Am Chem Soc, 2007. **129**(47): p. 14759-66.
10. Sun, C., et al., *Intracellular Tracking of Single Native Molecules with Electroporation-Delivered Quantum Dots.* Analytical Chemistry, 2014. **86**(22): p. 11403-11409.
11. Hardman, R., *A Toxicologic Review of Quantum Dots: Toxicity Depends on Physicochemical and Environmental Factors.* Environmental Health Perspectives, 2006. **114**(2): p. 165-172.
12. Lalley, P.M., *Microiontophoresis and Pressure Ejection*, in *Modern Techniques in Neuroscience Research*, U. Windhorst and H. Johansson, Editors. 1999, Springer Berlin Heidelberg: Berlin, Heidelberg. p. 193-212.
13. Kirkpatrick, D.C. and R.M. Wightman, *Evaluation of Drug Concentrations Delivered by Microiontophoresis.* Analytical chemistry, 2016. **88**(12): p. 6492-6499.
14. Fraser, S.E., *Iontophoretic dye labeling of embryonic cells.* Methods in cell biology, 1996. **51**: p. 147-160.
15. Curtis, D.R., *Microelectrophoresis.* Physical techniques in biological research, 1964. **5**(Part A): p. 144-190.
16. Tekle, E., R.D. Astumian, and P.B. Chock, *Electro-permeabilization of cell membranes: Effect of the resting membrane potential.* Biochemical and Biophysical Research Communications, 1990. **172**(1): p. 282-287.
17. Mobbs, P., et al. *Techniques for dye injection and cell labelling*. in *Microelectrode techniques. The Plymouth workshop handbook. Cambridge, UK: The Company of Biologists Ltd*. 1994. Citeseer.

18. Hollingsworth, J.A. and V.I. Klimov, *Soft chemical synthesis and manipulation of semiconductor nanocrystals.* Nanocrystal Quantum Dots, 2010. **2**: p. 1-61.
19. Mino, L., et al., *Low-dimensional systems investigated by x-ray absorption spectroscopy: a selection of 2D, 1D and 0D cases.* Journal of Physics D: Applied Physics, 2013. **46**(42): p. 423001.
20. Wise, F., *Quantum dots call the shots.* SPIE's OE Mag, 2002: p. 24-27.
21. Smith, A.M. and S. Nie, *Semiconductor Nanocrystals: Structure, Properties, and Band Gap Engineering.* Accounts of Chemical Research, 2010. **43**(2): p. 190-200.
22. Bruchez, M., et al., *Semiconductor Nanocrystals as Fluorescent Biological Labels.* Science, 1998. **281**(5385): p. 2013-2016.
23. Chan, W.C. and S. Nie, *Quantum dot bioconjugates for ultrasensitive nonisotopic detection.* Science, 1998. **281**(5385): p. 2016-8.
24. Petryayeva, E., W.R. Algar, and I.L. Medintz, *Quantum dots in bioanalysis: a review of applications across various platforms for fluorescence spectroscopy and imaging.* Applied spectroscopy, 2013. **67**(3): p. 215-252.
25. Reineck, P., et al., *Brightness and Photostability of Emerging Red and Near-IR Fluorescent Nanomaterials for Bioimaging.* Advanced Optical Materials, 2016. **4**(10): p. 1549-1557.
26. Lee, S.-K., W.F. Boron, and M.D. Parker, *Monitoring Ion Activities In and Around Cells Using Ion-Selective Liquid-Membrane Microelectrodes.* Sensors (Basel, Switzerland), 2013. **13**(1): p. 984-1003.
27. Holmes Bullock, T., *Neuron doctrine and electrophysiology.* Science, 1959. **129**: p. 997-1002.
28. Purves, R., *Microelectrode methods for intracellular recording and ionophoresis*. 1981: Academic Press.
29. Gardner, R., *Clonal analysis of early mammalian development.* Philosophical Transactions of the Royal Society of London B: Biological Sciences, 1985. **312**(1153): p. 163-178.
30. Blinks, J.R., et al., *Measurement of Ca2+ concentrations in living cells.* Progress in biophysics and molecular biology, 1982. **40**: p. 1-114.
31. Dabbousi, B.O., et al., *(CdSe) ZnS core− shell quantum dots: synthesis and characterization of a size series of highly luminescent nanocrystallites.* The Journal of Physical Chemistry B, 1997. **101**(46): p. 9463-9475.
32. Chan, W.C. and S. Nie, *Quantum dot bioconjugates for ultrasensitive nonisotopic detection.* Science, 1998. **281**(5385): p. 2016-2018.
33. Gao, X., et al., *In vivo cancer targeting and imaging with semiconductor quantum dots.* Nature biotechnology, 2004. **22**(8): p. 969-976.
34. Nann, T., *Phase-transfer of CdSe@ ZnS quantum dots using amphiphilic hyperbranched polyethylenimine.* Chemical communications, 2005(13): p. 1735-1736.
35. Parak, W.J., et al., *Conjugation of DNA to silanized colloidal semiconductor nanocrystalline quantum dots.* Chemistry of Materials, 2002. **14**(5): p. 2113-2119.
36. Curtis, D., D. Perrin, and J. Watkins, *The excitation of spinal neurones by the ionophoretic application of agents which chelate calcium.* Journal of neurochemistry, 1960. **6**(1): p. 1-20.

37. Lauer, H. and G. Rozing, *High performance capillary electrophoresis.* Agilent Technologies, Germany, 2010.
38. Grossman, P.D. and J.C. Colburn, *Capillary electrophoresis: Theory and practice*. 2012: Academic Press.
39. Henry, D. *The cataphoresis of suspended particles. Part I. The equation of cataphoresis*. in *Proceedings of the Royal Society of London A: Mathematical, Physical and Engineering Sciences*. 1931. The Royal Society.
40. Liese, A. and L. Hilterhaus, *Evaluation of immobilized enzymes for industrial applications.* Chemical Society Reviews, 2013. **42**(15): p. 6236-6249.
41. Zhang, W., *Nanoparticle aggregation: principles and modeling*, in *Nanomaterial*. 2014, Springer. p. 19-43.
42. Russel, W.B., D.A. Saville, and W.R. Schowalter, *Colloidal dispersions*. 1989: Cambridge university press.
43. Collins, A., *Nanotechnology cookbook: practical, reliable and jargon-free experimental procedures*. 2012: Elsevier.
44. Suttiponparnit, K., et al., *Role of Surface Area, Primary Particle Size, and Crystal Phase on Titanium Dioxide Nanoparticle Dispersion Properties.* Nanoscale Research Letters, 2011. **6**(1): p. 27-27.
45. Yoon, R.-H. and J.L. Yordan, *Zeta-potential measurements on microbubbles generated using various surfactants.* Journal of Colloid and Interface Science, 1986. **113**(2): p. 430-438.
46. Reyes Bahena, J., et al., *Fluoride adsorption onto α-Al2O3 and its effect on the zeta potential at the alumina–aqueous electrolyte interface.* Separation Science and Technology, 2002. **37**(8): p. 1973-1987.
47. Hanaor, D., et al., *The effects of carboxylic acids on the aqueous dispersion and electrophoretic deposition of ZrO2.* Journal of the European Ceramic Society, 2012. **32**(1): p. 235-244.
48. Greenwood, R. and K. Kendall, *Selection of suitable dispersants for aqueous suspensions of zirconia and titania powders using acoustophoresis.* Journal of the European Ceramic Society, 1999. **19**(4): p. 479-488.
49. Clogston, J.D. and A.K. Patri, *Zeta Potential Measurement*, in *Characterization of Nanoparticles Intended for Drug Delivery*, S.E. McNeil, Editor. 2011, Humana Press: Totowa, NJ. p. 63-70.
50. Instruments, M., *Zetasizer nano series user manual.* MAN0317, 2004. **1**.
51. Pecora, R., *Dynamic light scattering: applications of photon correlation spectroscopy*. 2013: Springer Science & Business Media.
52. Nelson, E., et al., *Dynamical theories of Brownian motion*. Vol. 3. 1967: Princeton university press Princeton.
53. Halliwell, J., M. Whitaker, and D. Ogden. *Using microelectrodes*. in *Microelectrode Techniques–The Plymouth Workshop Handbook 2nd Ed. Cambridge: The Company of Biologists Ltd*. 1994.
54. Axon Instruments, I., *The Axon guide for electrophysiology & biophysics laboratory techniques*. 1993: Axon Instruments.
55. Bretschneider, F. and J.R. De Weille, *Introduction to electrophysiological methods and instrumentation*. 2006: Academic Press.
56. Serwer, P., *Agarose gels: Properties and use for electrophoresis.* ELECTROPHORESIS, 1983. **4**(6): p. 375-382.

57. Lee, P.Y., et al., *Agarose Gel Electrophoresis for the Separation of DNA Fragments.* Journal of Visualized Experiments : JoVE, 2012(62): p. 3923.
58. *National Center for Biotechnology Information. PubChem Compound Database; CID=11966311*.

2 Suspension preparation of semiconductive QDs

2.1 Introduction

The successful intracellular delivery of QDs via microelectrophoresis technique requires the particles to be stable and monodispersed in the suspension as well as tolerate high electrophoretic mobilities in the micropipette. In addition, for the high-fidelity intracellular recording, the prepared QDs suspension should have an appropriate KCl concentration to obtain a proper electrolytic conductivity. The preparation of QDs suspensions agreeing with above-mentioned requirements is the core work in this Chapter.

To fulfil the two requirements above, three methods for the QDs suspension preparation are proposed as shown in Figure 2.1.

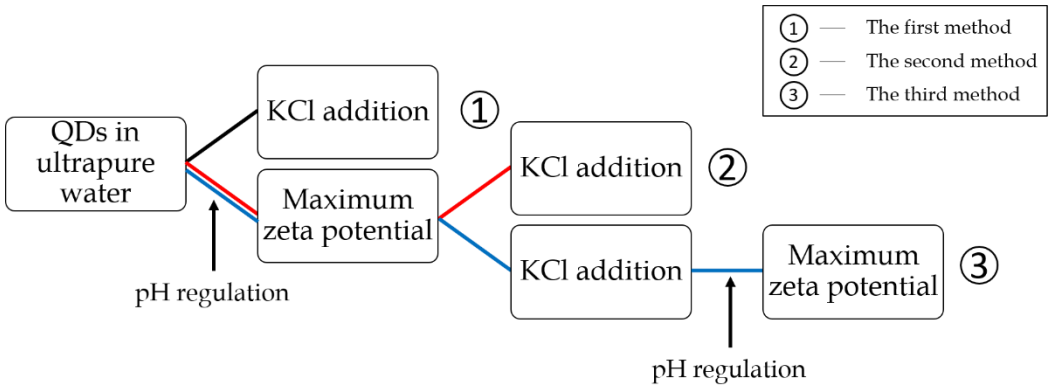

Figure 2.1 | The flow chart of three proposed methods for QDs suspension preparation. The black, red and blue flow paths represent the first, second and third methods respectively.

As described in Chapter 1, the high concentration of KCl in suspensions can greatly reduce the zeta potentials of QDs, resulting in rapid aggregation and unsuccessful microelectrophoresis [1]. Therefore, to retard the rapid QDs aggregation, the first method disperses QDs in ultrapure water and then gradually adds concentrated KCl solution into the diluted QDs suspension to reach a desired KCl concentration.

The regulation of pH can provide additional ions with the same surface charges, i.e. hydrogen or hydroxyl ions, for nanoparticles in suspension [1]. The acquired ions can bind to nanoparticles and buffer the negative effect of KCl on the zeta potentials [1]. Therefore, the second method disperses QDs in ultrapure water and then regulates the pH of the suspension to a certain value where the most stable state of QDs exists (maximum modulus of zeta potential) before gradually adding KCl into the suspension.

To further stabilizes QDs, the third method regulates the pH back to the value where the most stable state of QDs exists after adding KCl, which provides more similarly charged ions for QDs.

A series of experiments were conducted to compare the performance of these three methods.

2.2 Experimental procedures

2.2.1 Materials

One of the requirements for the protocol is to obtain semiconductive QDs with high surface charge in the filling suspensions for microelectrophoresis. Thus, CdSe/ZnS core/shell structured Qdot® 655 ITK™ Amino (PEG) Quantum Dots (655-QDs) with amine-derivatized polyethylene glycol (PEG) surface functionalization is chosen in this thesis as illustrated in Figure 2.2. Similar to primary aliphatic amine, the pKa of the amine terminus of 655-QDs is in the range of 9 – 11 [2]. In a basic solution, the primary amine loses a hydrogen ion and charges negatively [3], which can be coupled to biomolecules by amine-reactive crosslinking chemistries (Figure 2.2) [4]. In respect of optical properties, 655-QDs have emission maxima of 655 nm near the infrared range (Figure 2.3). They are bright and photostable, and have been used for various labeling and tracking applications [5, 6]. For example, they were used to reveal the complex interactions in the microenvironment of tumor through multiplexed imaging [7]. They were employed to detect several biomarkers of inflammation, such as Myeloperoxidase, Interleukin-1a and Tumor Necrosis Factor-a to indicate clinical disease severity and facilitate determination of therapeutic success [8].

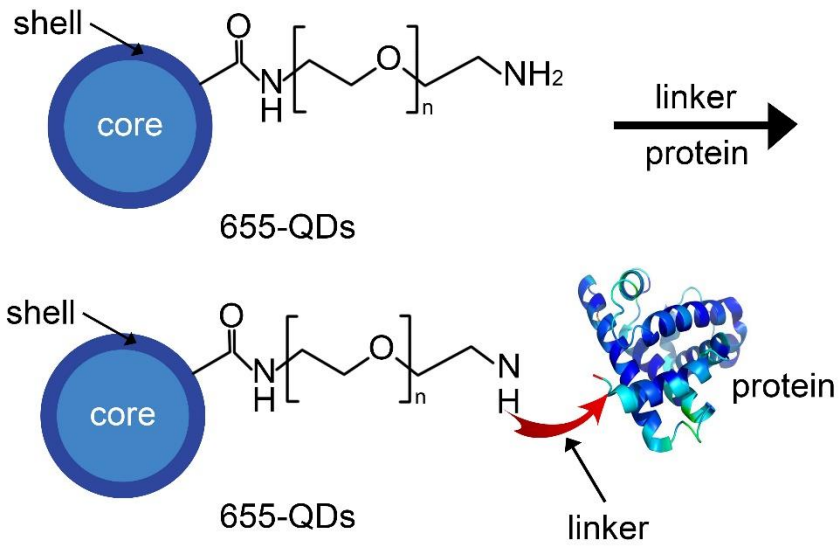

Figure 2.2 | Schematic illustration of the surface functional groups of 655-QDs. Reproduced from [4].

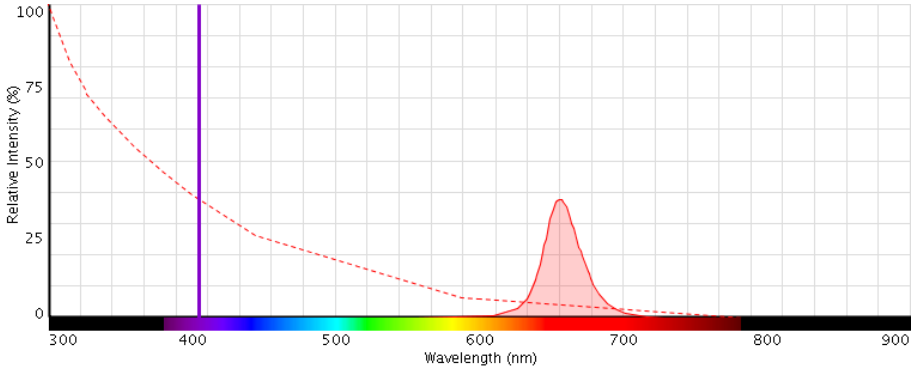

Figure 2.3 | Absorption (dash line) and fluorescence (solid line) spectra under 405 nm laser excitation (violet line) of 655-QDs. Reproduced from [9].

2.2.2 Preparation of QDs suspension for TEM imaging

It is critical to choose a suitable concentration of QDs in suspensions for microelectrophoresis. The QDs concentration should not be too high to cause QDs aggregation, which could impede microelectrophoresis. It also should not be too low to eject insufficient amount of QDs into target cells, which could

result in a low intracellular fluorescence intensity of QDs and thus the failure of fluorescence imaging. TEM can be used to provide references for the choice of QDs concentration for successful microelectrophoresis. As shown in Figure 2.4, when preparing TEM sample, a drop of ethanol with a certain concentration of QDs is placed onto the support film of TEM grid. After few minutes, ethanol fully evaporates, QDs form a certain density on the grid in 2D space. It can be assumed that QDs have enough 3D space to monodisperse in the suspension if they monodisperse without overlap in the 2D space. Thus, TEM image is indicative of the density of QDs in suspension and suggests the proper choice of QDs concentration for successful microelectrophoresis.

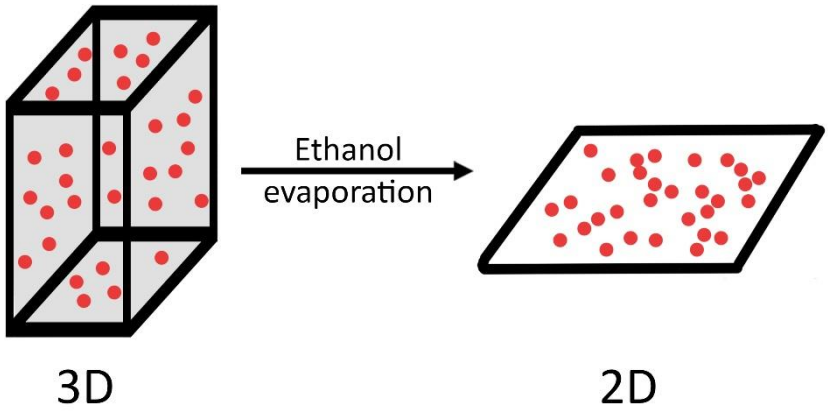

Figure 2.4 | Schematic illustration of TEM sample preparation.

The original 8 μM 655-QDs suspension in borate buffer (50 mM borate) from Thermo Fisher was gently vortexed for 1 minute. Then, 1 μL original 655-QDs suspension was pipetted into 1.5 mL ethanol in an Eppendorf Flex-tube, resulting in a QDs concentration of 5 nM. To obtain a better dispersion of 655-QDs particles, the sample was gently vortexed for 1 minute and sonicated at 43 ± 2 kHz at 25.0 °C for 10 minutes before dropped onto the support film of TEM grid.

2.2.3 Intracellular recording tests for the determination of KCl concentration

To minimize the passive effect of KCl on the stability of QDs, it is essential to find the lowest concentration of KCl that is feasible for intracellular recording. The tip size of micropipettes should also be carefully considered. Thus, KCl solutions with different concentrations were backfilled into micropipettes with different tip IDs that were manufactured from aluminosilicate glass capillaries using different programs in the Model P-97 micropipette puller as described later in Chapter 3. Once the tip ID of a micropipette in SEM image (Figure 2.5) showed good size, i.e., suitable for the size distribution of QDs, the related program was used to manufacture new micropipettes for the intracellular recording tests. The micropipette used in intracellular recording could be regarded as identical micropipette used in SEM imaging, as Model P-97 is designed with good reproducibility. However, changes in the tip ID between micropipettes that are pulled with the same program is unavoidable. For example, the standard deviation (SD) of the tip IDs of 59 micropipettes that are pulled with the same program is ± 44 nm with a mean of 194 nm. The distribution of tip ID of these 59 micropipettes in each range, i.e., 110-120 nm, 120-130 nm, etc., is shown in Figure 2.6. The tip ID range of 160-170 nm is the range with the largest probability. The relatively large variation of the tip ID can be caused by the ineffective canister in the puller that is filled with drierite, which is used to remove moisture from the air when pulling micropipettes to minimize environmental effects on micropipette reproducibility. Maintenance will be applied in the future to improve the puller robustness.

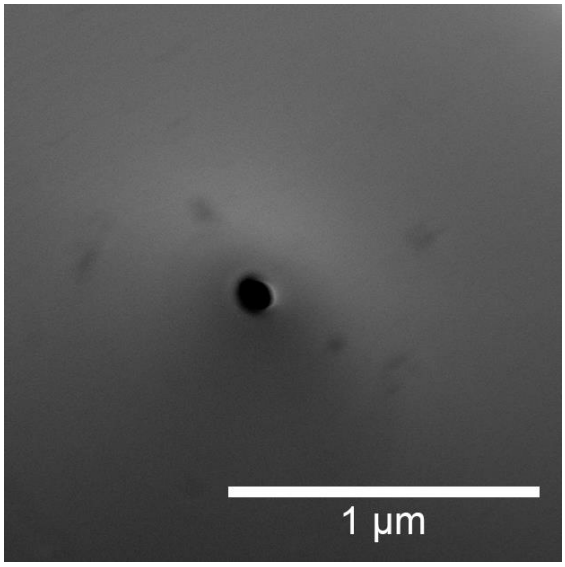

Figure 2.5 | High resolution SEM image of a micropipette with tip ID estimated at 130 nm. The orifice of the micropipette is the black hole at the centre of the image.

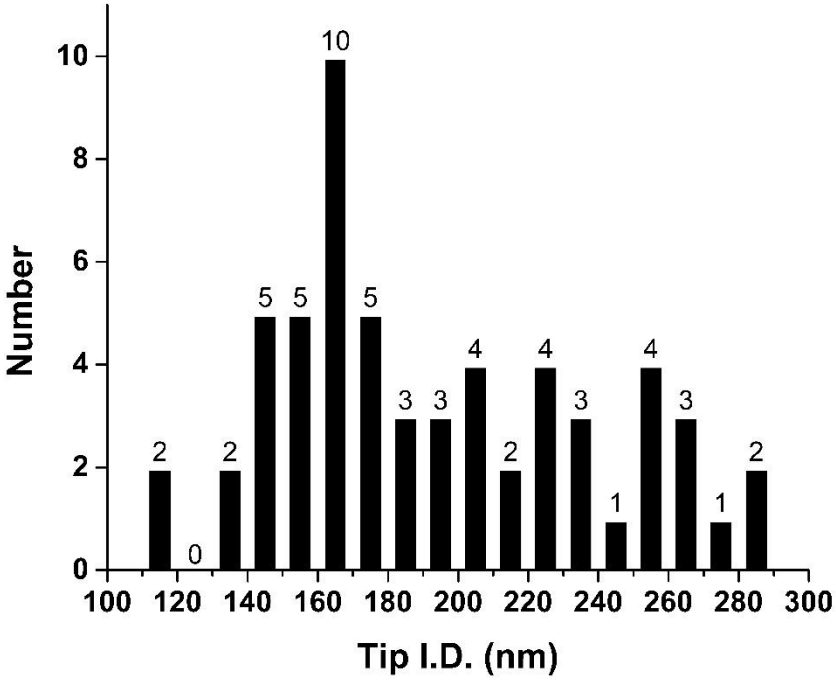

Figure 2.6 | The distribution of tip ID of 59 micropipettes pulled with the same program.

The quality of micropipettes was tested by recording intracellular electrical activities from STMD neurons in the lobula plate of dragonflies. These

experiments were conducted in the Visual Physiology and Neurobotics Laboratory in the Adelaide Medical School as shown in Figure 2.7. A wild-caught dragonfly (*Hemicordulia tau*) was immobilized with a mixture of beeswax and gum rosin (solid form of resin) (1:1) on a plastic stage and the head was tilted forward to access the posterior surface [10]. The working Ag/AgCl electrode was connected to a bridge amplifier and the counter Ag/AgCl electrode was inserted onto the brain surface of the dragonfly to form an electrical circuit. With a micromanipulator, micropipettes pierced into single neurons through a hole cut above the lobula (3rd optic neuropil). The dragonfly faced the centre of a high refresh rate (144 Hz) liquid crystal display (LCD) monitor, upon which visual stimuli was presented using custom software. The resistance of a micropipette was measured by applying a small current, e.g. 1 nA, through the micropipette from the bridge amplifier. Data were digitized at 5 kHz with a 16-bit analog-to-digital (A/D) converter and analysed off-line with MATLAB [10]. The visual stimulus elicited voltage changes across the cell membranes of neurons and the digitized data indicated the successful intracellular recording of neurons in real time.

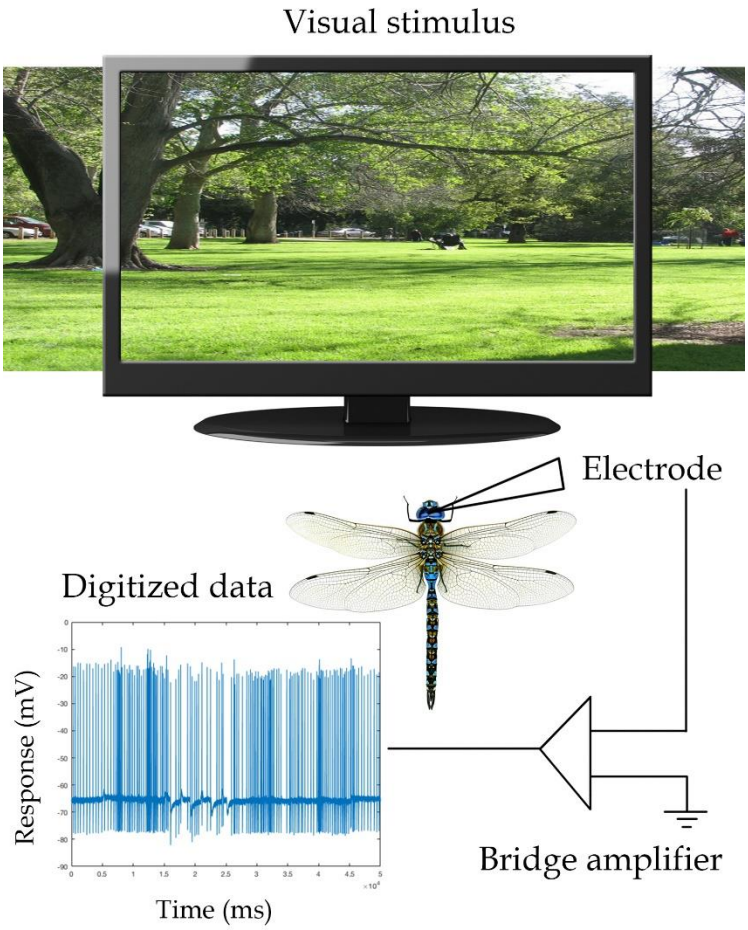

Figure 2.7 | Schematic illustration of experiment setup for intracellular recording of dragonflies.

2.2.4 Preparation of QDs samples with varying pH

In the following experiments (section 2.2.4, 2.2.5 and 2.2.6), all operations were conducted in the fume cupboard. The foremost step was to calibrate the pH meter by three standard pH buffers, pH 4.00 ± 0.02, pH 7.00 ± 0.02 and pH 9.22 ± 0.02 at 20.0 °C. The original 8 μM 655-QDs suspension from Thermo Fisher was gently vortexed for 1 minute before dilution. In addition, the concentration of 655-QDs in each sample was 10 nM. All chemical reagents were centrifuged at 4000 rpm for 50 seconds before addition to remove possible large size aggregates and impurities.

It is essential to understand the relationship between the pH of the suspension and the zeta potential of 655-QDs and find the pH value where the most stable state of QDs exists. Thus, 655-QDs suspensions with varying pH values from 3 to 11 were prepared and the zeta potentials were measured by Zetasizer nano ZSP.

1. **655-QDs dilution**: Pipette 12.5 μL original 655-QDs suspension into 10 mL fresh ultrapure water (18.2 MΩ·cm at 25.0 °C) in glass beaker A (10 mL) with stir bar rotating continuously at 200 rpm. Pipette another 8.75 μL original 655-QDs suspension into 7 mL fresh ultrapure water in glass beaker B (10 mL) with stir bar rotating continuously at 200 rpm.

2. **Sample 5 preparation**: When the pH reading of the diluted suspension in beaker A is stable (change in value was less than ± 0.05 unit within 1 minute), record the pH and temperature readings and pipette 1.5 mL diluted suspension into a 1.5 mL Eppendorf Flex-tube labelled with Sample 5 for further treatment.

3. **Samples 6 – 9 preparations**: Gradually add 0.1 M sodium hydroxide (NaOH) solution into the rest diluted suspension in beaker A to reach a stable pH value of 7.80 as listed in Table 2-1. Record the pH and temperature readings and pipette 1.5 mL suspension into a 1.5 mL Eppendorf Flex-tube labelled with Sample 6 for further treatment. Orderly prepare the other samples in the same way.

4. **Samples 1 – 4 preparations**: Gradually add 0.1 M hydrochloric acid (HCl) solution into the diluted suspension in beaker B to reach a stable pH value of 5.44 as listed in Table 2-1. Record the pH and temperature readings and pipette 1.5 mL suspension into a 1.5 mL Eppendorf Flex-tube labelled with Sample 4 for further treatment. Orderly prepare the other samples in the same way.

Table 2-1 | Temperature and pH values of Samples 1 - 9. The sequence of samples is ascending with pH.

Sample	1	2	3	4	5	6	7	8	9
Temperature (°C)	22.9	22.9	22.9	23.0	22.8	22.7	22.7	22.8	22.8
pH	2.80	3.79	4.77	5.44	6.80	7.80	8.83	9.81	10.79

2.2.5 Preparation of QDs samples by the first method

QDs suspensions were prepared by the first method.

1. **655-QDs dilution**: Pipette 8.75 μL original 655-QDs suspension into 7 mL fresh ultrapure water in a glass beaker (10 mL) with stir bar rotating continuously at 200 rpm.

2. **Sample 10 preparation**: When the pH reading of the diluted suspension is stable, record the pH and temperature readings and pipette 1.5 mL diluted suspension into a 1.5 mL Eppendorf Flex-tube labelled with Sample 10 for further treatment.

3. **Samples 11 preparation**: Gradually add 2 M KCl solution into the rest diluted suspension to reach the final concentration of KCl as 0.01 M. Record the pH and temperature readings and pipette 1.5 mL suspension into a 1.5 mL Eppendorf Flex-tube labelled with Sample 11 for further treatment.

2.2.6 Preparation of QDs samples by the second and third methods

QDs suspensions were prepared by the second and third methods.

1. **655-QDs dilution**: Pipette 18.75 μL original 655-QDs suspension into 15 mL fresh ultrapure water in a glass beaker (20 mL) with stir bar rotating continuously at 200 rpm.

2. **Sample 12 preparation and aliquot**: When the pH reading of the diluted suspension is stable, record the pH and temperature readings and pipette 1.5 mL diluted suspension into a 1.5 mL Eppendorf Flex-tube labelled with Sample 12 for further treatment. Divide the rest diluted suspension in half into two beakers C and D.

3. **Samples 13 and 15 preparations**: Gradually add 0.1 M NaOH solution into the diluted suspension in beaker C and D to reach a stable pH value around 9.81. Record the pH and temperature readings and pipette 1.5 mL suspension into 1.5 mL Eppendorf Flex-tubes labelled as Sample 13 and 15 for further treatment, respectively.

4. **Sample 14 and 16 preparations**: Gradually add 2 M KCl solution into the rest diluted suspension in beaker C and D to reach the final concentration of KCl as 0.01 M. Record the pH and temperature readings and pipette 1.5 mL suspension into 1.5 mL Eppendorf Flex-tubes labelled as Sample 14 and 16 for further treatment, respectively.

5. **Sample 17 preparation**: Gradually add 0.1 M NaOH solution into the rest diluted suspension in beaker D to reach a stable pH value around 9.81. Record the pH and temperature readings and pipette 1.5 mL suspension into a 1.5 mL Eppendorf Flex-tube labelled with Sample 17 for further treatment.

The flow chart describing the preparation process of the three methods is presented in Figure 2.12. All the Samples 1 – 17 in the Eppendorf Flex-tubes were sonicated from 4.0 °C to 24.0 °C without external heat for 20 minutes to obtain a better dispersion and centrifuged at 3000 rpm for 40 seconds to remove possible large size aggregates and impurities. Then 1 mL supernatants were pipetted by 1 mL syringes from centrifuged Samples 1 - 17 into clean folded capillary cells for subsequent measurements in Zetasizer nano ZSP. The parameter setting used for the Zetasizer measurements is presented in the Appendix.

2.2.7 Measurement procedure for the size distribution of QDs

The size distribution of 655-QDs in sample 17 was measured by Zetasizer nano ZSP via DLS technique. The sample was in the same folded capillary cell that

was used in the zeta potential measurement. The parameter setting used for the Zetasizer measurement is presented in the Appendix.

2.3 Results and discussion

2.3.1 The impact of KCl concentration on intracellular recording

The results of intracellular recording tests of micropipettes with different IDs and KCl concentrations are presented in Table 2-2. The relation between the resistance of micropipettes with tip ID of 20 and 30 nm, the noise of resting membrane potential and the KCl concentration of filling solution are plotted in Figure 2.8.

Table 2-2 | The concentration (Conc.) of KCl, tip ID, resistance of micropipette, and noise in intracellular recording tests.

Test	KCl Conc. (M)	Tip ID (nm)	Resistance of micropipette (MΩ)	Noise (mV)
1	2.00	20	140	0.5
2	0.50	20	200	1.5
3	0.10	20	506 - 550	3.6
4	0.05	20	450	8.3
5	0.01	20	300	4.1
6	2.00	30	40 - 80	0.5
7	2.00	32	38 - 39	0.5
8	0.01	30	150	0.6
9	0.01	130	130	3.2

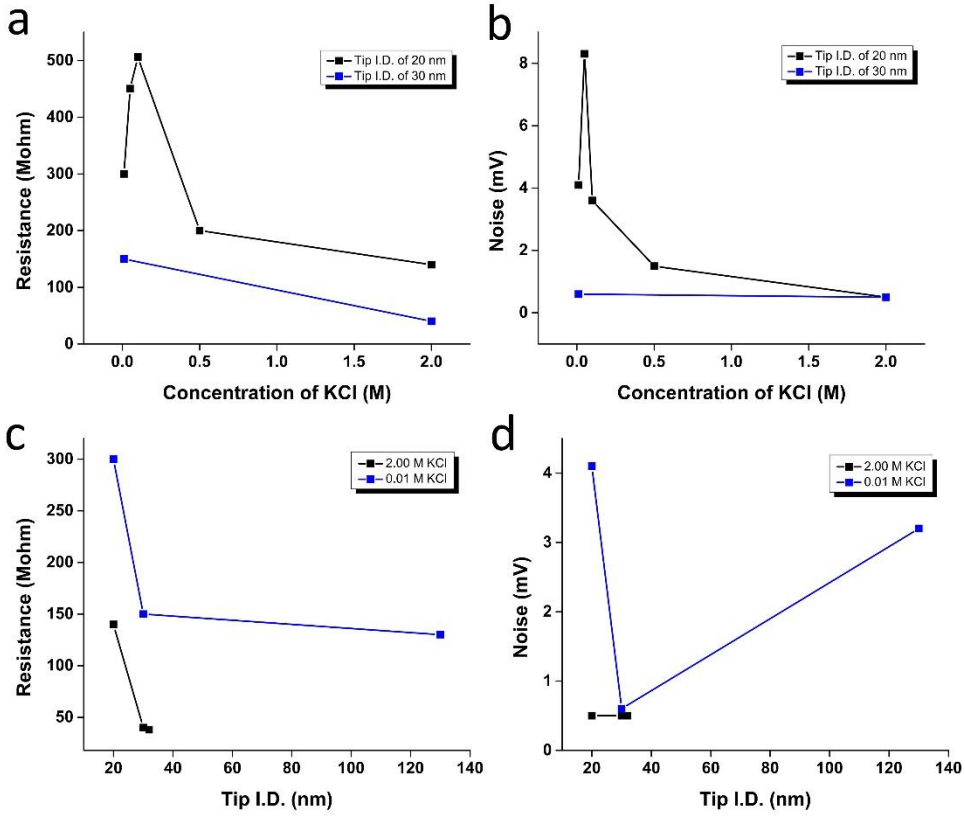

Figure 2.8 | The impact of KCl concentration and tip ID on intracellular recording. **a, b,** The influence of KCl concentration on the resistance and noise of micropipettes with tip ID of 20 and 30 nm. **c, d,** The influence of tip ID on the resistance and noise of micropipettes filled with 2.00 and 0.01 M KCl.

The neuronal activities from STMD neurons in dragonflies were recorded in real time when they were presented with visual stimulus on the monitor. In Test 8, the resting membrane potential of the visual neuron was around -65 mV and they generated spikes with amplitudes up to -15 mV in response to the visual stimulus as shown in Figure 2.9a. Between spikes, the changes in the resting membrane potential are enlarged as shown in Figure 2.9b. The standard deviation (SD) of the membrane potential is calculated as the noise, which is 0.6 mV in Test 8.

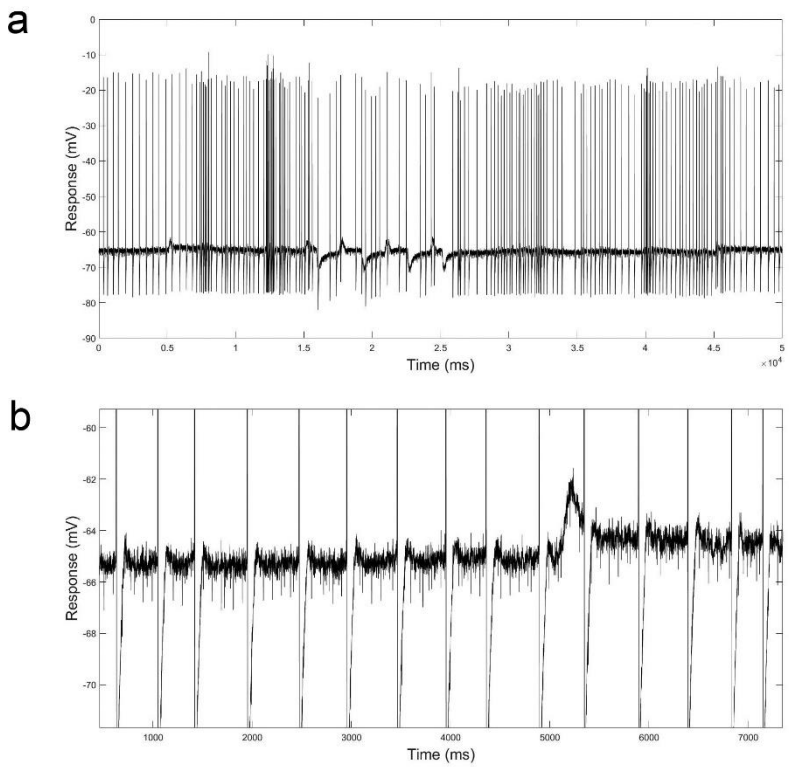

Figure 2.9 | a, The intracellular electrical activities of a visual neuron in the dragonfly in response to visual stimulus in Test 8. **b,** The partial enlargement of the resting membrane potential. The SD of the membrane potential between spikes is calculated as the noise.

It is worth noting that intracellular recording is highly dependent on the quality of the individual cell recording. The results in Table 2-2 provide an approximate reference for the choice of the tip ID and the concentration of KCl. However, although the method of testing the micropipettes in living neurons has many confounding factors in data interpretation, this method can evaluate the toughness of the micropipette tip for penetrating brain tissue. In addition, it can examine whether the tip ID is small enough to avoid physical damage to neuronal cells by monitoring their intracellular electrical activities. If the micropipette can record the intracellular electrical activities for a long period of time, it can be concluded that it can penetrate target neuronal cells with negligible cell membrane damage. All the micropipettes used in 8 tests

recorded the intracellular activities for a long period of time, thus they successfully penetrated the cells with negligible cell membrane damage.

For micropipettes with tip ID of 20 and 30 nm, the resistance of micropipette and voltage noise increase with reducing KCl concentration (Figure 2.8a and b). The results are in line with the theory that highly concentrated KCl solutions can keep the resistance of micropipettes as low as possible, reduce voltage noise and provide a wider recording bandwidth [11]. The large resistance of micropipette in Test 3 was caused by the blockage in the tip of micropipette. The tip may be clogged with pieces of brain tissue when the micropipette was forced to pierce into the brain tissues by micromanipulator. The blockage sign was irreversible after applying electrical clearing where large amounts of positive and negative currents, and buzz function with powerful high-frequency oscillations were used to clear the tip.

As shown in Figure 2.8c and d, for KCl solution with a relatively high concentration of 2.00 M, the increase in tip ID of micropipettes dramatically reduces the resistance of micropipette. For KCl solution with a relatively low concentration of 0.01 M, the increase in tip ID of micropipettes results in slight change in the resistance of micropipettes. Although the tip resistance is determined by the overall narrowness of the taper, e.g. the length and shape of the taper [12], the comparison between the two groups of tests could roughly indicate that the increase in tip ID has larger effect on the resistance of micropipette containing KCl solutions with relatively high concentrations whereas has minor effect on the resistance of micropipette containing KCl solutions with relatively low concentrations.

The KCl concentration of 0.01M was used in the suspension preparation of 655-QDs in the subsequent experiments to avoid QDs aggregation and remain the ability of intracellular recording simultaneously. 655-QDs particles are more stable in the suspension with relatively low IS, thus the lower KCl solution concentration is preferred for stability. In addition, as shown in Figure 2.8c and d, although the relatively low concentration of 0.01 M increases the resistance of micropipettes and noise voltage, for delivering 655-QDs intracellularly via microelectrophoresis, where the resistance of micropipette has no effect on the mobility of 655-QDs particles under the electrical field, the increase of the resistance of micropipettes and noise voltage can be neglected, as long as the micropipette can locate the position of target cells and record the intracellular electrical activities for a period of time.

2.3.2 Size, shape and density of QDs

The TEM image of 5 nM 655-QDs in ethanol is shown in Figure 2.10a. The dark dots are 655-QDs particles. One of them is designated with a red circle. To confirm that the dark dots are 655-QDs particles, an element composition analysis was conducted on Philips CM 200 TEM in Adelaide Microscopy with the same sample. Cadmium, Selenium, Sulfur (S) elements were detected, which is identical to the chemical composition specification from Thermo Fisher (CdSe/ZnS).

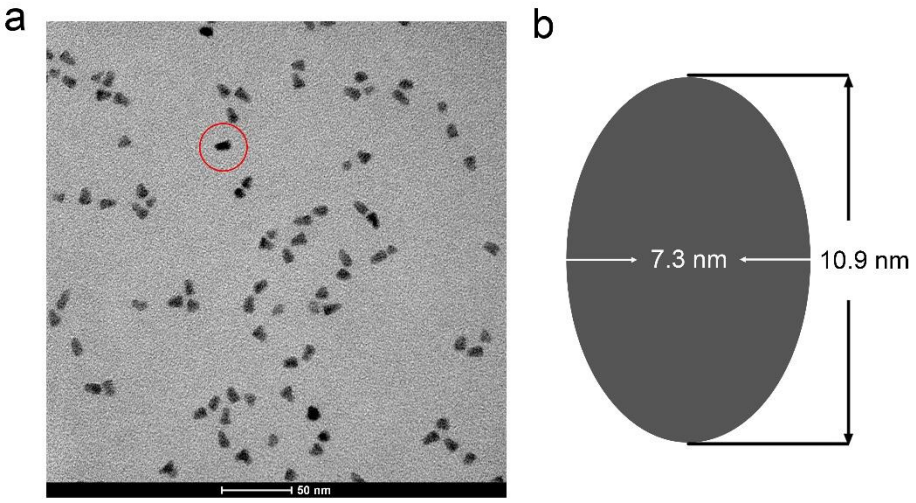

Figure 2.10 | The accurate size and shape of 655-QDs. **a,** High resolution TEM image of 5 nM 655-QDs. One of them is designated with a red circle. **b,** An ellipse with the major axis of 10.9 nm and the minor axis of 7.3 nm that represents the average shape and size of 655-QDs.

The average shape of 655-QDs particles is estimated as an ellipse with the major axis of 10.9 ± 1.9 nm and the minor axis of 7.3 ± 1.1 nm as shown in Figure 2.10b. The result is based on the size analysis of 80 particles, i.e., the average of 80 particles' major axes is 10.9 nm, which is comparable with the specification from Thermo Fisher (13 – 21 nm).

The size, shape and density of 655-QDs particles were informative for subsequent experiments:

1. For a 3D nanoparticle, it is impossible to describe its size with a single value unless it is a sphere. All particle size analysis techniques measure some properties of a particle and report its size as the equivalent spherical diameter. DLS technique in Zetasizer nano ZSP measures the average diffusion coefficient of particles in Brownian motion and reports their sizes as the equivalent diameters of spheres that have the

same average diffusion coefficient. Thus, the more spherical the nanoparticles, the more accurate the reported sizes from Zetasizer nano ZSP. The shape of 655-QDs particles is nearly elliptical with the axial ratio of 1.49 (10.9 nm/7.3 nm). Thus, the hydrodynamic radius and size distribution results from Zetasizer nano ZSP is convincing and noticeably echo the range of the actual size of 655-QDs particles, which is critical to guide the successful microelectrophoresis. Because of this, the diameter calculated from the diffusional properties of the particle will be indicative of the apparent size of the dynamic hydrated particle.

2. A convenient criterion for aggregation-free nanoparticles is that their hydrodynamic radii should be less than twice of their primary sizes [13]. The twice of major and minor axes of 655-QDs is 21.8 and 14.6 nm. Therefore, the upper limit of hydrodynamic radii of monodispersed 655-QDs is 21.8 nm.

3. DLS technique extracts the diffusion coefficient of particles in Brownian motion via monitoring the change of scattered light. To acquire accurate diffusion coefficient and then the size distribution, it is ideal to make the sample concentration avoid multiple scattering which could result from the restricted diffusion and serious aggregation of particles due to higher sample concentration. The ideal sample also should avoid low scattered light intensity due to lower sample concentration, which can both lead to erroneous results. The density of 5 nM 655-QDs in ethanol provides a reference for the choice of the concentration of 655-QDs in the suspension for microelectrophoresis. In Figure 2.10a, 655-QDs are well dispersed without overlapping and there is sufficient blank space around them even if the number of 655-QDs particles is doubled.

However, the space could be compact when the number is tripled. Thus, the concentration of 655-QDs was determined as 10 nM in suspensions. The feasibility of 10 nM is examined in the following sections.

2.3.3 Relation between pH and the zeta potential of QDs

The zeta potentials of 655-QDs in the Samples 1 - 9 are listed in Table 2-3. The zeta potential and SD of each sample is the average of three measurements. The relationship between the pH of the suspension and the zeta potential of 655-QDs is plotted in Figure 2.11.

Table 2-3 | The zeta potential of 655-QDs in the Samples 1 - 9.

Sample	Temperature (°C)	pH	Zeta potential with ± 1 SD (mV)
1	22.9	2.80	26.0 ± 1.1
2	22.9	3.79	28.2 ± 0.6
3	22.9	4.77	16.2 ± 0.2
4	23.0	5.44	-2.0 ± 0.1
5	22.8	6.80	-16.6 ± 0.4
6	22.7	7.80	-21.3 ± 0.1
7	22.7	8.83	-31.1 ± 1.7
8	22.8	9.81	-32.5 ± 1.5
9	22.8	10.79	-27.1 ± 1.7

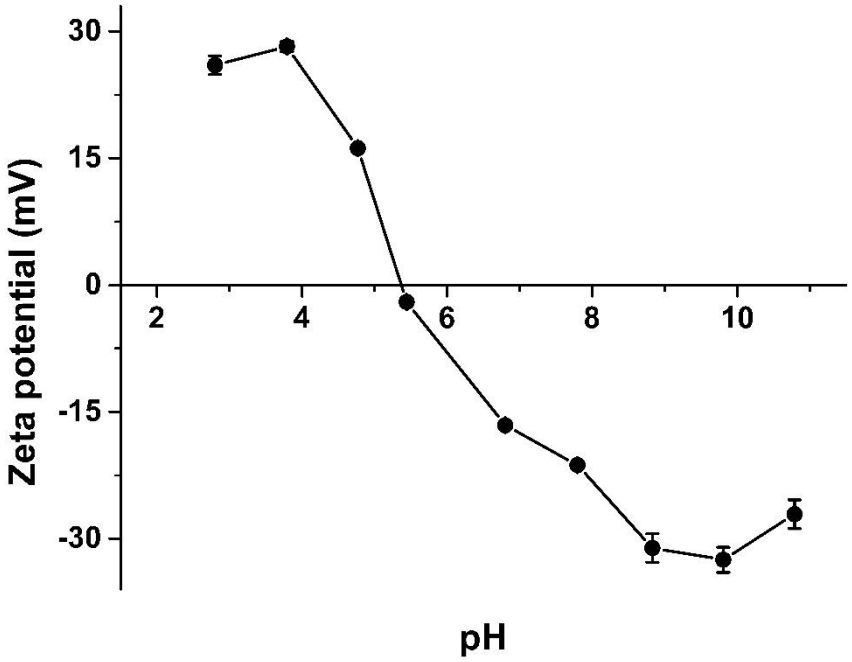

Figure 2.11 | The relationship between pH of the suspension and the zeta potential of 655-QDs. Error bars, ± 1 SD with *n*=3 each.

The relationship between the pH of the suspension and the zeta potential of 655-QDs in Figure 2.11 is in line with the theory. The net charge at the surface of 655-QDs is negative determined by its surface functionalization, amine-derivatized PEG. The net charge affects the distribution of ions in the surrounding interfacial region, and attracts oppositely charged ions close to the surface of 655-QDs particles to form an average negative zeta potential, -16.6 mV, at pH 6.80, 22.8 °C in Sample 5. The more alkali (NaOH) added to the medium the more negative charge the 655-QDs particles acquire and conversely the more acid (HCl) added, the more positive the charge.

The maximum modulus of zeta potential is around pH 9.81 where the most stable state of 655-QDs exists in Sample 8. Although the stable state of 655-QDs also exists around pH 3.79 in Sample 2, strong acid environment (pH < 4) is not recommended by Thermo Fisher for using 655-QDs where the polymer coating

can dissociate and then the exposed core/shell structure starts dissolving. In addition, due to the high concentration and high mobility of hydrogen ions (H^+) in the micropipettes in microelectrophoresis, a large amount of H^+ can result in a lowering of the pH in the vicinity of the tip of micropipettes [14]. Such a localized change in pH has been proposed to account for the excitation of central nervous system neurons [15], which can interfere with the intracellular recording. However, 655-QDs do not degrade in strong basic environment (pH > 9) as suggested by Thermo Fisher. In addition, compared to the electrophoretic mobility of H^+ (36.25 μmcm/Vs in water at 25.0 °C), hydroxide ions (OH^-) have a relatively low electrophoretic mobility (20.50 μmcm/Vs in water at 25.0 °C), resulting in less effect on neuronal activity [16].

2.3.4 Results and comparison of the three methods for QDs suspension preparation

The pH, temperature, concentration of KCl and zeta potential of 655-QDs for each sample in the three methods are listed in Table 2-4. The zeta potential and SD of each sample is the average of three measurements. The settings of Zetasizer nano ZSP are the same as described previously. To ease comparing the performance of these three methods, the flow chart of sample preparation is shown in Figure 2.12. The zeta potential and pH of samples are plotted in Figure 2.13. Sample 13 and 15 originate from the same diluted suspension, which has the same pH and temperature as Sample 12.

Table 2-4 | The zeta potential of 655-QDs and Conc. of KCl in Samples 10 – 17 prepared by the three methods.

Method	Sample	Temperature (°C)	pH	KCl Conc. (M)	Zeta potential with ± 1 SD (mV)
1	10	22.7	6.91	0.00	-26.3 ± 1.5
1	11	22.4	6.45	0.01	-8.6 ± 0.6
2	12	25.1	6.83	0.00	-20.8 ± 0.8
2	13	24.6	9.78	0.00	-40.4 ± 0.9
2	14	23.5	9.00	0.01	-19.6 ± 1.4
3	15	20.3	9.83	0.00	-38.6 ± 0.8
3	16	20.5	9.00	0.01	-16.5 ± 1.4
3	17	20.2	9.78	0.01	-21.1 ± 1.5

As shown in Figure 2.12, in the first method, the original 655-QDs suspension from Thermo Fisher is diluted in ultrapure water. Then 2 M KCl solution is diluted into the suspension to the final concentration of 0.01 M. In the second method, before the dilution of 2 M KCl, the pH of the suspension is increased to the value where the most stable state of 655-QDs exists (maximum zeta potential). In the third method, the pH of diluted 655-QDs suspension is also increased to the value with maximum zeta potential as for the second method. The additional operation of the third method is that the pH is increased back to the value after the dilution of 2 M KCl.

As shown in Figure 2.13 and Table 2-4, the pH and zeta potential of Sample 10 and 12 are not consistent, though they have the same composition, i.e., 10 nM QDs in ultrapure water. The same situation occurs between Sample 13 and 15, Sample 14 and 16. On the one hand, the error in pipetting could lead to slight differences in the concentration of compounds between samples. On the other hand, the temperature change when mixing different solutions has effect on the pH measurement. Another reason for the relatively large pH difference

between Sample 10 and 12 is the inherent instability of pH of ultrapure water. Ultrapure water refers to water which has been purified to the highest standards by removing all contaminants such as organic and inorganic compounds, dissolved gases and particulate matters [17]. The purified water has very low conductivity because all the conductive components have been removed, which makes accurate pH measurement very difficult to achieve [17].

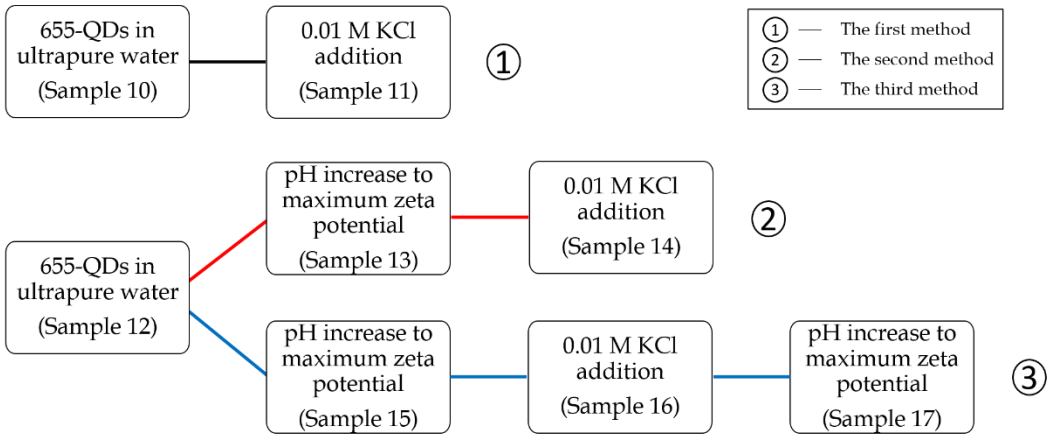

Figure 2.12 | The flow chart of the three methods.

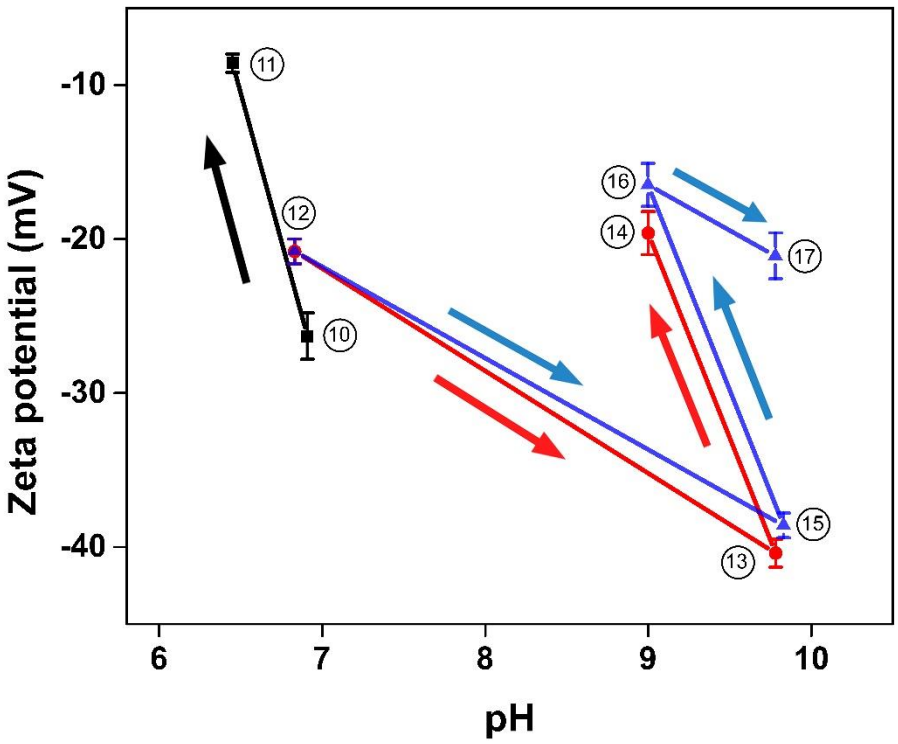

Figure 2.13 | The zeta potential and pH of Samples 10 - 17. The black, red and blue plots represent samples prepared by the first, second and third method respectively. Error bars, ± 1 SD with *n*=3 each. The black, red and blue arrows represent the sequence of samples in the three methods respectively.

The results provide several conclusions:

1. In all three methods, the addition of 0.01 M KCl increases the IS of QDs suspensions and reduces their zeta potentials by compressing the Debye length, which is in line with the theory of the electrical double layer structure. However, the zeta potential modulus of Sample 14 and 16 are larger than that of Sample 11. In Sample 14 and 16, the pH of suspension is increased to the value where the most stable state of 655-QDs exists before the addition of 0.01 M KCl. Negatively charged OH^- are added into the slipping plane of 655-QDs, which buffer the negative effect of K^+ and Cl^- on the magnitude of zeta potential.

2. The zeta potential of Sample 11 is less than the stability dividing line (± 30 mV), which indicates that K^+ and Cl^- in the suspension reduce the electrostatic repulsion between 655-QDs particles, resulting in an unstable colloidal system and possible rapid aggregation of 655-QDs. In contrast, Sample 14 and 16 have larger modulus of zeta potentials, 655-QDs have moderate electrostatic repulsion between each other to inhibit aggregation.

3. In all three methods, the pH of QDs suspensions decrease after the addition of 0.01 M KCl. The increase of IS can alter the activity coefficient of H^+ in aqueous medium. The pH meter measures the activity of H^+ rather than the concentration of H^+ [18]. The activity of a substance B (α_B) can be given by:

$$\alpha_B = x_B \gamma_B \qquad \text{Equation 2-1}$$

where γ_B is the activity coefficient and x_B is the mole fraction of the substance B [19]. In an ideal solution, the activity coefficient of a substance is close to 1 [19]. In general, the activity coefficient is a function of temperature, pressure and composition, and must be determined experimentally for each solution [19]. The addition of KCl increased the activity of H^+ and reduced the pH of the suspension. The pH became closer to the isoelectric point and passively affected the zeta potential of 655-QDs.

4. The pH of Sample 16 is increased back to the value where the most stable state of QDs exists after the addition of 0.01 KCl. The zeta potential modulus of Sample 17 is larger than that of Sample 16. This method can further stabilize QDs particles by providing more negatively charged OH^- in the slipping plane.

5. Although the zeta potential of Sample 17, -21.1 mV, is less than the stability dividing line (± 30 mV), 655-QDs have moderate electrostatic repulsion between each other to inhibit aggregation. Sample 17 fulfils the requirements of successful microelectrophoresis, where 655-QDs are stable and the suspension has a KCl concentration of 0.01 M for intracellular recording.

2.3.5 The size distribution of QDs

The size distribution result of Sample 17 is presented in Figure 2.14 and Table 2-5 with the peak sizes, the SD of three measurements, and the intensity, volume and number percentage of each peak listed.

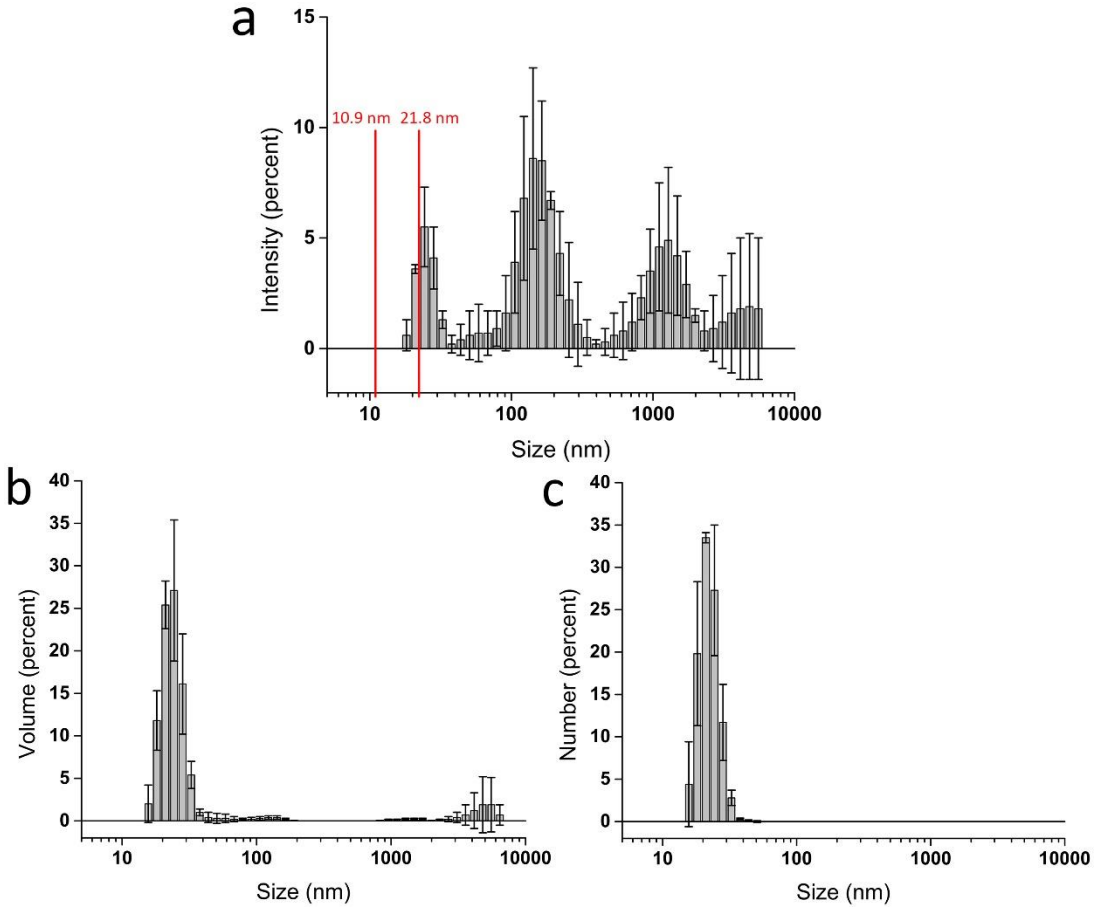

Figure 2.14 | The size distribution by intensity plots of three measurements of Sample 17. Error bars, ± 1 SD with *n*=3 each. The red lines indicate the primary size of 655-QDs at 10.9 nm (major axis) and the twice of their primary size at 21.8 nm.

Table 2-5 | The size distribution by intensity results of Sample 17. The sequence of the peaks is ascending with the peak size. ± 1 SD with *n*=3 each.

Peak	Size ± SD (nm)	Intensity ± SD (percent)	Volume ± SD (percent)	Number ± SD (percent)
1	25.3 ± 0.1	15.1 ± 2.4	90.1 ± 8.6	100.0
2	166.6 ± 29.8	44.5 ± 6.4	1.8 ± 0.8	
3	2101.0 ± 1548.0	34.0 ± 2.5	8.1 ± 9.4	

The size distribution by intensity is the raw data from DLS measurements. It is based on the intensity of light scattered by particles in the different size ranges, which are sensitive to the presence of large particles, aggregates and dust. Although particles in Peak 1 scatter less intensity of light than particles in Peak 2, the total volume and number of all particles in Peak 1 should be much larger than that of particles in Peak 2, so that they could scatter large enough light intensity comparable with Peak 2. The large hydrodynamic radii of particles in Peak 3 are assumed to be caused by the presence of air bubbles or dust.

Zetasizer nano ZSP uses Mie theory and the material properties to convert the intensity distribution to the size distribution by volume and number [20]. The volume distribution displays the total volume of particles in different size ranges. The number distribution shows the total number of particles in different size ranges. The material properties, refractive index and absorption of 655-QDs, were entered as 2.550 and 0.010 in Zetasizer [21]. DLS technique tends to overestimate the width of peaks in intensity distribution and this effect is magnified in the transformations to volume and number distributions. Thus, the size distribution by volume and number results should only be used for estimating the relative amounts of material in separate peaks as suggested from the instrument manufacturer. The size distribution by volume and number results indicate that a large number of particles in Peak 1 possesses a large volume in Sample 17. The particles in Peak 2 are assumed to be a small amount of aggregates of 655-QDs. Peak 3 is caused by air bubbles or dust that could be introduced during the measurement.

The shapes of 655-QDs particles are nearly elliptical with the major axis of 10.9 nm measured via TEM (see section 2.3.2). The hydrodynamic radii of most 655-QDs particles are 25.3 nm. DLS technique reports the hydrodynamic radii of

particles as the equivalent diameters of spheres that have the same average diffusion coefficient in Brownian motion. Thus, it is normal to have difference between primary sizes and reported hydrodynamic radii. A convenient criterion for aggregation-free nanoparticles is that their hydrodynamic radii should be less than twice of their primary sizes [13]. Although the hydrodynamic radii of 655-QDs are slightly larger than the upper limit, i.e., twice of major axis (21.8 nm), it is reasonable to conclude that most 655-QDs particles are monodispersed. The size distribution results of 655-QDs in Sample 17 are in line with the zeta potential results. The moderate zeta potential, -21.1 mV, provides moderate electrostatic repulsion between 655-QDs particles.

The choice of suitable tip ID should consider the sum of hydrodynamic radii of QDs and other dispersed ions that pass through the tip for conductivity [22]. The twice of the major axis of 655-QDs is 25.3 nm and the hydrated radii of K^+, Cl^- and sodium ions (Na^+) are 0.331, 0.332, and 0.358 nm, respectively [23]. Therefore, the tip ID of micropipette should be over 50 nm but less than 150 nm to avoid physical damage to cells. In this thesis, the primary application of microelectrophoresis of QDs focuses on the intracellular delivery of QDs into neuronal cells in dragonflies. In the previous section, the micropipette in Test 8 with tip ID estimated at 130 nm can penetrate neurons with negligible cell membrane damage and record the intracellular activities for a long period of time. Thus, the upper limitation of tip ID is determined as 150 nm.

2.4 Conclusions

The results are in line with the theoretical basis of the electrical double layer structure. The net charge at the surface of 655-QDs is negative, which is

determined by its surface functionalization, amine-derivatized PEG. The net charge affects the distribution of ions in the surrounding interfacial region, and attracts oppositely charged ions close to the surface of 655-QDs particles to form an average negative zeta potential when they are dispersed in ultrapure water. After introducing KCl to the concentration of 0.01 M into the suspension, the K^+ and Cl^- reduce the zeta potential of 655-QDs by compressing the Debye length and weaken the electrostatic repulsion among them, leading to an unstable system with a low modulus of zeta potential. However, if the pH of the suspension is first increased to the point where the most stable state of 655-QDs exists beforehand, 655-QDs particles acquire more OH^- and achieve the most stable state to buffer the following addition of KCl in the surrounding suspension. The addition of KCl decreases the pH of the suspension and passively effect the zeta potential of 655-QDs. Thus, the pH of the suspension is increased back to the point where the most stable state of 655-QDs exists after introducing KCl. This method provides more OH^- for 655-QDs particles and actively increases the modulus of zeta potential of 655-QDs. In addition, the concentration of KCl satisfies the requirement of electrolytic conductivity for intracellular recording at the same time.

The size distribution results of 655-QDs in Sample 17, which is ready to be used for microelectrophoresis, determines the lowest limit of the tip ID of micropipettes. 655-QDs particles are monodispersed with hydrodynamic radii of 25.3 nm respectively in three DLS measurements. Considering the hydrodynamic radii of 655-QDs and other dispersed ions, the tip ID of micropipettes should be over 50 nm but less than 150 nm to avoid physical damage to target cells.

In the following chapters, 655-QDs suspensions were prepared in the same way as Sample 17 for microinjection and microelectrophoresis experiments, which are simply called 655-QDs-17 suspensions.

The protocol developed in Chapter 2 provides a general methodology for suspension preparation of various charged biocompatible nanoparticles for microelectrophoresis technique and for pre-treatment of nanoparticles in biological imaging and many other applications, where monodispersed nanoparticles are needed in a relatively high IS environment. This methodology can gently preserve the surface functionalization of nanoparticles and is straightforward to operate.

2.5 References

1. Zhang, W., *Nanoparticle aggregation: principles and modeling*, in *Nanomaterial*. 2014, Springer. p. 19-43.
2. Wanwimolruk, S., D.J. Birkett, and P.M. Brooks, *Structural requirements for drug binding to site II on human serum albumin.* Mol Pharmacol, 1983. **24**(3): p. 458-63.
3. Ryman-Rasmussen, J.P., J.E. Riviere, and N.A. Monteiro-Riviere, *Surface Coatings Determine Cytotoxicity and Irritation Potential of Quantum Dot Nanoparticles in Epidermal Keratinocytes.* Journal of Investigative Dermatology, 2007. **127**(1): p. 143-153.
4. ThermoFisher.
5. Xiao, Y., et al., *Dynamics and mechanisms of quantum dot nanoparticle cellular uptake.* Journal of nanobiotechnology, 2010. **8**(1): p. 13.
6. Nikiforov, T.T. and J.M. Beechem, *Development of homogeneous binding assays based on fluorescence resonance energy transfer between quantum dots and Alexa Fluor fluorophores.* Analytical biochemistry, 2006. **357**(1): p. 68-76.
7. Peng, C.-W., et al., *Patterns of cancer invasion revealed by QDs-based quantitative multiplexed imaging of tumor microenvironment.* Biomaterials, 2011. **32**(11): p. 2907-2917.
8. Karwa, A., et al., *Imaging biomarkers of inflammation in situ with fun ctionalized quantum dots in the dextran sodium sulfate (DSS) model of mouse colitis.* Inflammation Research, 2007. **56**(12): p. 502-510.

9. https://www.thermofisher.com/au/en/home/life-science/cell-analysis/labeling-chemistry/fluorescence-spectraviewer.html?ICID=svtool&UID=QD655SA. 2017.
10. Wiederman, S.D. and D.C. O'Carroll, *Discrimination of Features in Natural Scenes by a Dragonfly Neuron.* Journal of Neuroscience, 2011. **31**(19): p. 7141-7144.
11. Axon Instruments, I., *The Axon guide for electrophysiology & biophysics laboratory techniques*. 1993: Axon Instruments.
12. Instrument, S., *P-97 Pipette Cookbook.* Rev. D, Novato, CA, 2008.
13. Liu, J., et al., *Aggregation control of quantum dots through ion-mediated hydrogen bonding shielding.* Acs Nano, 2012. **6**(6): p. 4973-4983.
14. Gruol, D.L., et al., *Hydrogen ions have multiple effects on the excitability of cultured mammalian neurons.* Brain Res, 1980. **183**(1): p. 247-52.
15. Frederickson, R.C., L.M. Jordan, and J.W. Phillis, *The action of noradrenaline on cortical neurons: effects of pH.* Brain Res, 1971. **35**(2): p. 556-60.
16. Duso, A.B. and D.D.Y. Chen, *Proton and Hydroxide Ion Mobility in Capillary Electrophoresis.* Analytical Chemistry, 2002. **74**(13): p. 2938-2942.
17. Riché, E., et al., *High-purity water and pH.* American Laboratory, 2006. **38**(13): p. 22.
18. Peech, M., *Hydrogen-ion activity.* Methods of soil analysis. Part 2. Chemical and microbiological properties, 1965(methodsofsoilanb): p. 914-926.
19. DeHoff, R., *Thermodynamics in materials science*. 2006: CRC Press.
20. Bohren, C.F. and D.R. Huffman, *Absorption and scattering of light by small particles*. 2008: John Wiley & Sons.
21. Hondow, N., et al., *Quantitative characterization of nanoparticle agglomeration within biological media.* Journal of Nanoparticle Research, 2012. **14**(7): p. 977.
22. Bear, M.F., B.W. Connors, and M.A. Paradiso, *Neuroscience*. Vol. 2. 2007: Lippincott Williams & Wilkins.
23. Nightingale, E.R., *Phenomenological Theory of Ion Solvation. Effective Radii of Hydrated Ions.* The Journal of Physical Chemistry, 1959. **63**(9): p. 1381-1387.

3 Manufacture of micropipettes

3.1 Introduction

As described in Chapter 1, fine-tipped micropipettes filled with chemical solutions can penetrate into cells and eject chemical substances via microelectrophoresis and microinjection techniques [1, 2]. The structure of a micropipette is illustrated in Figure 3.1 [3]. For microelectrophoresis and microinjection techniques, the most important property of a micropipette is its ID near the tip, which should be large enough for the ejection of chemical substances with different sizes. However, to impale cells with the minimal physical damage, a rule of thumb is that the outer diameter (OD) near the tip should be 0.5 % or less of the diameter of the target cell [3]. Thus, the proper tip size of micropipettes for ejecting 655-QDs intracellularly should fit the size distribution of 655-QDs in suspension and avoid physical damage to target cells.

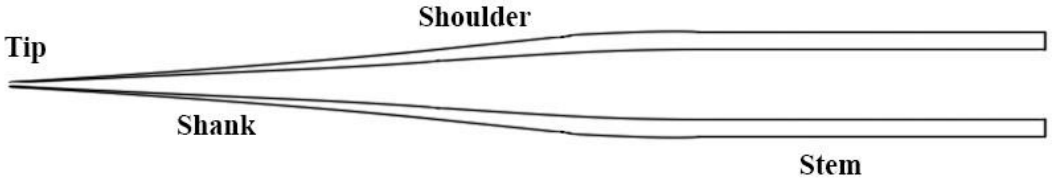

Figure 3.1 | A schematic illustration of the structure of a micropipette, including tip, shank, shoulder and stem. Reproduced from [3].

A horizontal micropipette puller, model P-97 Flaming/Brown from Sutter Instrument, is used to manufacture micropipettes with suitable tip sizes for ejecting 655-QDs. In the micropipette puller, a box filament for heating

encircles the centre of the glass capillary that is fixed by two symmetrical clamps on the puller bars (Figure 3.2a). An air nozzle for cooling is placed under the centre of the filament (Figure 3.2b) [4]. A new feature of model P-97 compared to previous series is the humidity controlled chamber surrounding the filament to minimize environmental effects on micropipette reproducibility [5].

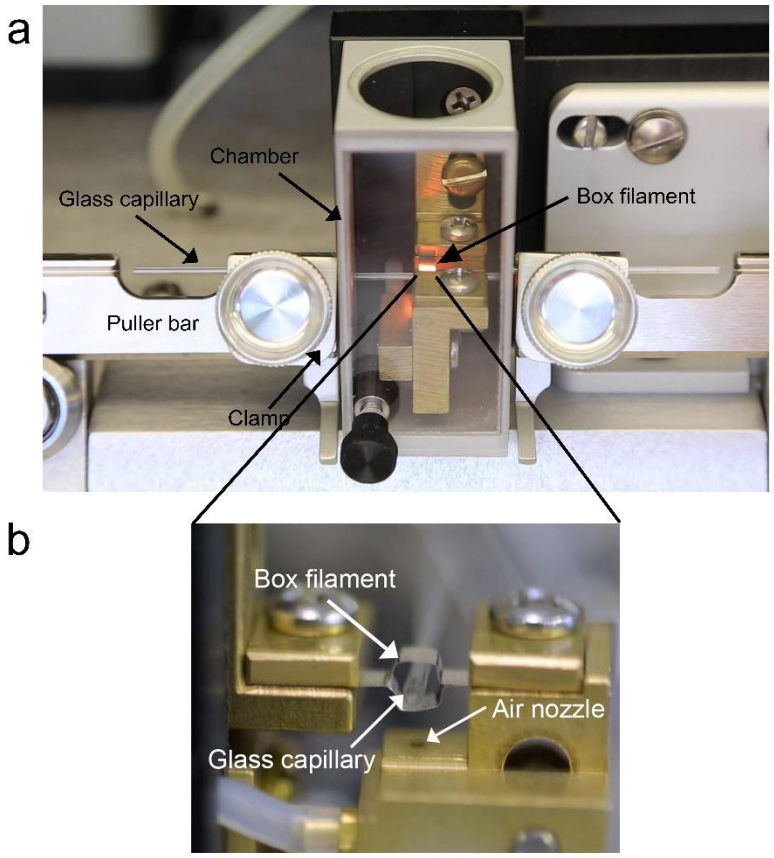

Figure 3.2 | Micropipette puller, Model P-97. **a,** The box filament in the chamber, glass capillary, puller bars and clamps in the micropipette puller (front view). **b,** The box filament, glass capillary and air nozzle in the micropipette puller (side view). Reproduced from [4]. Only half of the glass capillary is shown.

Manufacturing micropipettes in P-97 is programmed for controllable fabrication with good reproducibility. A program consists of one or more pull cycles that are executed in sequence [5]. One cycle consists of five

programmable parameters, including HEAT, PULL, VELOCITY, either TIME or DELAY, and PRESSURE [5]. A typical pull cycle in a program is described below [5]:

1. The box filament heats the glass capillary at the HEAT value.

2. The glass becomes soft and a weak pull from puller bars draws the glass out until they reach the VELOCITY value.

3. When the VELOCITY value is reached, the heat turns off and the air nozzle turns on at the PRESSURE value.

4. If TIME is over zero, a hard pull at the PULL value is executed after a 40 ms delay and the air nozzle is activated for the programmed TIME. If DELAY is over zero, the air nozzle is activated for 300 ms and a hard pull at the PULL value is activated after the programmed DELAY.

There are two regimes of pulling in the micropipette puller. The so-called weak pull where the puller bars draw the soft glass out at a relatively low speed, does not break the capillary with the heating on. In contrast, the so-called hard pull where the puller bars move at a relatively high speed, breaks the capillary when the glass cools down with the air nozzle on. Varying these parameters in a program results in different tip sizes, shank lengths and shapes of micropipettes. Typically, higher HEAT and PULL result in a finer tip and a longer shank [5]. Higher PRESSURE and lower VELOCITY result in a shorter shank length [5].

The aim of this Chapter is to provide several efficient programs for fabricating micropipettes with suitable tip ID for the ejection of QDs.

3.2 Experimental procedures

3.2.1 Manufacture of micropipettes

Aluminosilicate glass capillaries were chosen to manufacture micropipettes in this thesis. Compared to borosilicate glass, aluminosilicate provides increased hardness, improved chemical durability, and reduced electrical conductivity [4]. In particular, the ratio of the inner to outer diameter (OD) in a borosilicate micropipette is consistent over its total taper length, whereas in aluminosilicate micropipettes, the ratio increases remarkably towards the tip, which allows extremely fine tips to be formed when fabricating sharp micropipettes with long taper lengths and small tip sizes [4]. Thus, aluminosilicate micropipettes are more suited for the ejection of QDs and avoiding physical damage to target cells.

A filament is attached to the inner wall of aluminosilicate capillary, which is different from the heating filament in the micropipette puller. It is a glass rod with approximately 160 μm diameter to lead solutions from the blunt end to the tip of micropipettes via capillary force [4]. When a capillary is pulled to create a micropipette, its ID and the diameter of filament gradually reduce in size.

Manufactured micropipettes were stuck onto a carbon tape covered, vertical metal stage and coated with 3 nm thickness platinum for SEM image.

3.3 Results and discussion

3.3.1 Tip sizes of micropipettes

The parameters of two cycles in the programs and the resulting tip ID of micropipettes are listed in Table 3-1. If VELOCITY (VEL) is over zero, one unit of TIME represents 0.5 ms. If VELOCITY is zero, one unit of TIME represents 10 ms. The micrograph of a micropipette pulled with Program 5 and the SEM image of another micropipette pulled with the same program is shown in Figure 3.3.

Table 3-1 | The parameters of the pulling programs and the tip ID of micropipettes. The sequence of programs is ascending with the tip sizes.

Program	Parameters						Tip ID (nm)
	PRESSURE	Cycle 1	HEAT	PULL	VEL	TIME	
		Cycle 2	HEAT	PULL	VEL	TIME	
1	550	Cycle 1	520	0	10	1	70
		Cycle 2	460	160	60	100	
2	550	Cycle 1	520	0	10	1	77
		Cycle 2	460	150	60	100	
3	550	Cycle 1	520	0	10	1	83
		Cycle 2	460	180	60	100	
4	550	Cycle 1	520	0	10	1	83
		Cycle 2	460	200	60	100	
5	575	Cycle 1	520	0	10	1	84
		Cycle 2	450	200	60	100	
6	575	Cycle 1	520	0	10	1	130
		Cycle 2	460	200	60	100	

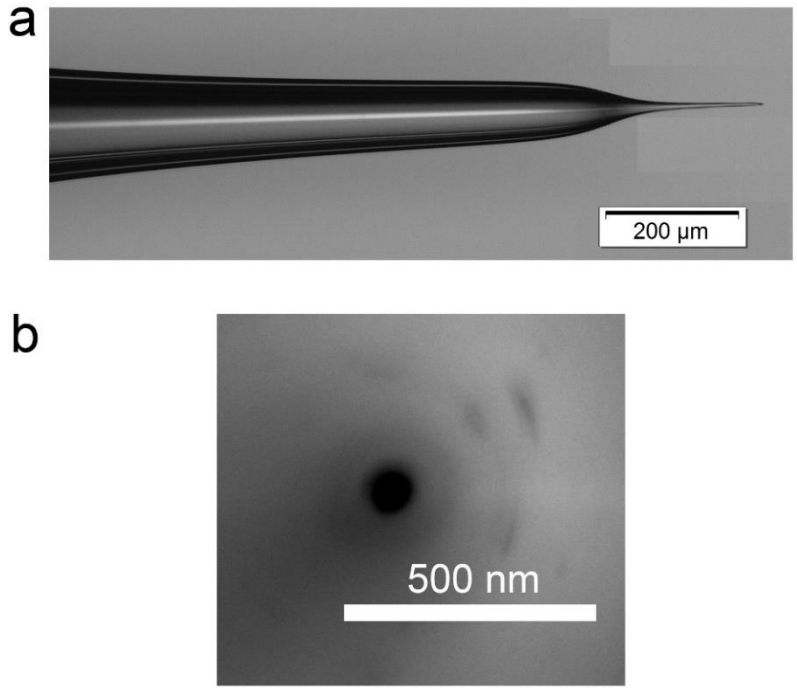

Figure 3.3 | a, Micrograph of an aluminosilicate glass micropipette pulled with Program 5. Scale bar, 200 µm. **b,** High resolution SEM image of a micropipette pulled with Program 5. Scale bar, 500 nm. The tip ID is 84 nm. The orifice of the micropipette is the black hole near the centre of the image.

The HEAT value in the first cycle of all the 6 programs is set as 520, which is based on the ramp value (522) of aluminosilicate glass capillary when heated by the FB255B box filament, which is the amount of heat required to melt a specific type of glass depending on the type of heating filament [4].

Program 1 consists of two cycles. In cycle 1, heat is applied at programmed HEAT value of 520. When the velocity of the puller bars reaches the VELOCITY value of 10, the heat turns off and the air nozzle turns on at the PRESSURE value of 550. Then a hard pull of 0, i.e., no pull, is applied after a 40 ms delay and the air nozzle is activated for the programmed TIME at 0.5 ms. In cycle 2, heat is applied at HEAT value of 460. When the velocity of puller bars reaches the VELOCITY value of 60, the heat turns off and the air nozzle turns on at the

PRESSURE value of 550. Then a hard pull of 60 value is applied to break the glass capillary in half after a 40 ms delay and the air nozzle is activated for 50 ms.

Model P-97 is designed to achieve good reproducibility of micropipette tip size. Change in the tip ID of micropipettes that are pulled with the same program is unavoidable but acceptable for microelectrophoresis and microinjection techniques (see section 2.2.3). Micropipettes that have been processed for SEM imaging are not usable for microelectrophoresis or microinjection and vice versa. In practice, the variation in tip ID can be simply estimated from the resistance of micropipettes. Typically, a larger tip has a lower resistance when other conditions are the same.

The tip IDs in Table 3-1 satisfy the theoretical requirement determined from the size distribution results of 655-QDs in Sample 17 (0.01 M KCl with pH at 9.78, see section 2.3.5) for successful ejection. The minimum tip ID estimated at 70 nm of micropipette pulled with Program 1, exceeds the overall theoretical size, 50 nm, of ejecting compounds, including 655-QDs, dissolved ions and other possible impurities [6].

3.4 Conclusions

Proper tip sizes of micropipettes are critical to successful microelectrophoresis and microinjection. In this chapter, manufacture of micropipettes with theoretically feasible tip IDs for the ejection of 655-QDs is described.

In Sample 17, 655-QDs particles are monodispersed with hydrodynamic radii of 25.3 nm. Considering other dissolved ions and possible impurities, the tip ID of micropipettes should be over 50 nm but less than 150 nm to avoid physical damage to target cells. Several programs in the micropipette puller were developed to fabricate micropipettes with suitable tip IDs.

The theoretical fit between the size distribution of 655-QDs and the tip ID for ejection is demonstrated in Chapter 4 via microinjection technique.

3.5 References

1. Curtis, D.R., *Microelectrophoresis.* Physical techniques in biological research, 1964. **5**(Part A): p. 144-190.
2. Lee, S.-K., W.F. Boron, and M.D. Parker, *Monitoring Ion Activities In and Around Cells Using Ion-Selective Liquid-Membrane Microelectrodes.* Sensors (Basel, Switzerland), 2013. **13**(1): p. 984-1003.
3. Purves, R., *Microelectrode methods for intracellular recording and ionophoresis*. 1981: Academic Press.
4. Instrument, S., *P-97 Pipette Cookbook.* Rev. D, Novato, CA, 2008.
5. Instrument, S., *P-97 Flaming/BrownTM Micropipette Puller Operation Manual Rev. 2.30-DOM (20140825)*. 2014.
6. Bear, M.F., B.W. Connors, and M.A. Paradiso, *Neuroscience*. Vol. 2. 2007: Lippincott Williams & Wilkins.

4 Microinjection of semiconductive QDs

4.1 Introduction

To demonstrate the hypothetical match between the tip ID of micropipettes and the size distribution of QDs for ejection, microinjection technique and agarose gel are utilized.

Microinjection technique has been used to deliver uncharged or poorly charged chemical substances via pressure from small orifices of micropipettes that are pulled from glass capillaries, either extracellularly or intracellularly, where the target cell has to be visible under microscope [1]. The driving force on 655-QDs particles relies on the pressure applied within micropipettes. Particles that are ejected out of micropipettes do not experience the driving force any more. Thus, in microinjection, 655-QDs particles can be more localized and confined in the outer medium. In this way, the relatively higher local concentration offers the great advantage for optical detection due to the brighter fluorescence.

To further confine the movement and diffusion of ejected 655-QDs particles in microinjection, agarose gels with the unique structure are used as the outer medium. Agarose consists of repeated agarobiose (L- and D-galactose) subunits to form linear polymers [2, 3]. During gelation, agarose polymers associate non-covalently by hydrogen bond and form a porous network of channels and bundles, which could offer sufficient space to hold a large amount of liquid medium [3-5]. The field emission scanning electron microscopy (FESEM) image of a 2.0 % agarose gel is shown in Figure 4.1 [6].

The mechanical property of agarose gels, their network mesh size (pore size), depends on the agarose type and concentration, and setting temperature, etc [7].

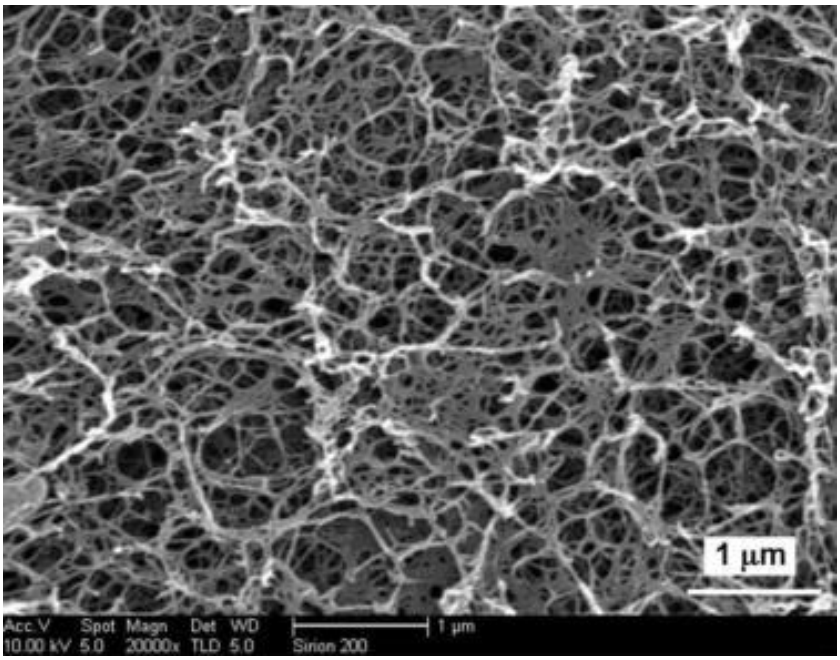

Figure 4.1 | FESEM image of a 2.0 % agarose gel (after drying). Scale bar, 1 µm. The agarose gel solution was prepared over 90°C and then cooled down to room temperature and dried. Reprinted with permission from Elsevier [6].

The unique network structure of agarose gels makes them suitable for molecular sieving. Agarose gel electrophoresis has been used as an effective and routine method in molecular biology for separating deoxyribonucleic acid (DNA) fragments, proteins and particles with the size up to 10 - 20 nm [2]. For example, agarose gel electrophoresis under an electrical field allows the negatively charged DNA to move through the agarose gel matrix toward the positively charged anode [2]. DNA has a uniform mass/charge ratio, thus DNA molecules are separated by size within an agarose gel in a pattern such that the distance travelled is inversely proportional to the log of its molecular weight, i.e., shorter DNA fragments migrate through the network structure of

the gel more quickly than longer ones [3]. Thus, the approximate length of DNA fragments can be determined by running a collection of DNA fragments of known length alongside as a DNA ladder [3]. In addition, agarose gels can be used as phantoms that resemble some of the properties of living organs and tissues for studies on the diffusion of substances in the living tissues and simulate the actual process [8]. Inspired by the molecular sieving capability of agarose gels and their convenient preparation protocol, as well as their high optical transmittance under ultraviolet (UV) laser excitation [9], agarose gels are used to confine the movement and diffusion of 655-QDs that are ejected out of the micropipettes in microinjection for fluorescence detection. The 655-QDs ejected out of the micropipettes will be immediately confined within the agarose gel and stay localized, which ensures the high local concentration of QDs and achieve brighter fluorescence.

The successful detection of fluorescence signals from ejected 655-QDs in agarose gels can indicate the successful microinjection that is attributed to the match between the tip ID and the size distribution of 655-QDs.

4.2 Materials and Method

4.2.1 Measurement procedure for the fluorescence spectrum of QDs

The fluorescence spectra of 1 nM 655-QDs in ultrapure water was measured with iHR320 imaging spectrometer under 0.1 mW 405 nm laser excitation. The experiment setup is illustrated in Figure 4.2 [10]. Two UV-visible transparent optical fibres (200 μm core diameter) were arranged at 90° for excitation and collection. The 405 nm laser was coupled into one fibre to guide the excitation

beam to the sample in a PMMA cuvette. The other fibre collected the fluorescence from the sample and guided it to the spectrometer.

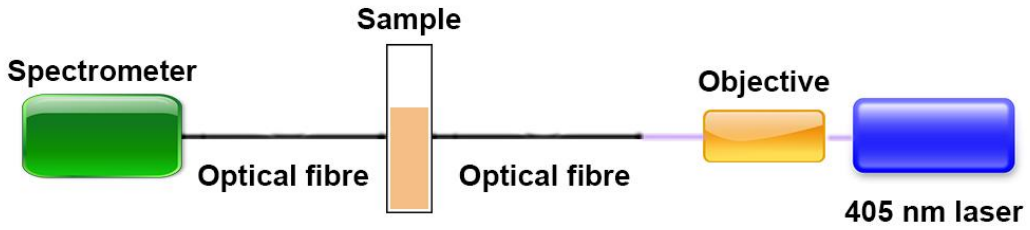

Figure 4.2 | Experiment setup of fluorescence measurement. Reproduced from [10].

4.2.2 Preparation of agarose gels

Agarose gels were prepared with different agarose concentrations (2.0 % and 0.7 %) and used as the outer medium in microinjection experiments to confine the diffusion of ejected 655-QDs. The percentage concentration of an agarose gel reflects the weight of agarose (in g) in 100 mL buffer used, i.e., 2 g agarose in 100 mL buffer can make a 2.0 % gel.

To make 2.0 % agarose gels, 1g agarose powder was mixed with 50 mL 1 x TAE buffer (Tris-acetate-EDTA, pH 8.3 at 23.9°C) in a 100 mL erlenmeyer flask. The mixture was microwaved for 1 – 3 minutes and swirled until the agarose was completely dissolved. Then, 100 µL liquid agarose (around the melting temperature of 88 °C as specified) was pipetted into a homemade mould to form a pie shape with a thickness of 6 mm and a diameter of 1 cm. The agarose gel completely solidified around the setting temperature of 23 °C. According to the melting and setting temperature of TopVision Agarose from

specification, the pore size of 0.7 % and 2.0 % agarose gels are estimated at 800 nm and 200 nm respectively [7].

To test whether agarose gels could localize 655-QDs particles and provide a reference for the fluorescence detection of ejected 655-QDs in the agarose gels after microinjection, special 2.0 % agarose gels that were doped with 655-QDs particles were prepared and observed under the fluorescence microscope. When the agarose was still liquid but cooling down in the mould, 100 μL 40 nM 655-QDs in ultrapure water was pipetted into the agarose gel and quickly mixed by pipetting up and down several times.

4.2.3 Microinjection of QDs

The pico-litre injector Model PLI-10 was used to supply ejection pressure. To prove the feasibility of the experiment setup and compare the behaviour of nanoparticles and small molecules in microinjection, the widely used fluorophore, rhodamine b (RDB) was prepared as filling solutions in Test 1 and 2. RDB was dissolved in ultrapure water in an Eppendorf Flex-tube to the concentration of 100 μM and gently vortexed for 1 minute. The solution was sonicated from 4.0 °C to 24.0 °C without external heat for 20 minutes and centrifuged at 3000 rpm for 40 seconds. The supernatants of RDB solution and 655-QDs-17 suspension (see preparation in section 2.2.6) were pipetted by 1 mL syringes and backfilled into micropipettes via 34 Gauge MicroFil™ flexible plastic syringe needles separately.

The schematic side elevation and micrograph (top view) of experiment setup is shown in Figure 4.3. The experiments were conducted on a vibration-proof

table in full dark environment to avoid photobleaching of 655-QDs. The micropipette was filled with 100 μM RDB solution and confined within a glass capillary that was stuck on the glass slide to avoid vibration and crack. The ID of the glass capillary was slightly larger than the OD of the micropipette. The micropipette was held by the injection pipette holder and the position was adjusted by the micromanipulator. The agarose gel pie was placed in front of the glass capillary on the glass slide. It was surrounded by 1x TAE buffer and covered with a coverslip to prevent water evaporation. All the glass slides and coverslips were cleaned by ethanol and water, and dried out by nitrogen before experiments. The micropipette was slowly pierced into the agarose gel controlled by the micromanipulator.

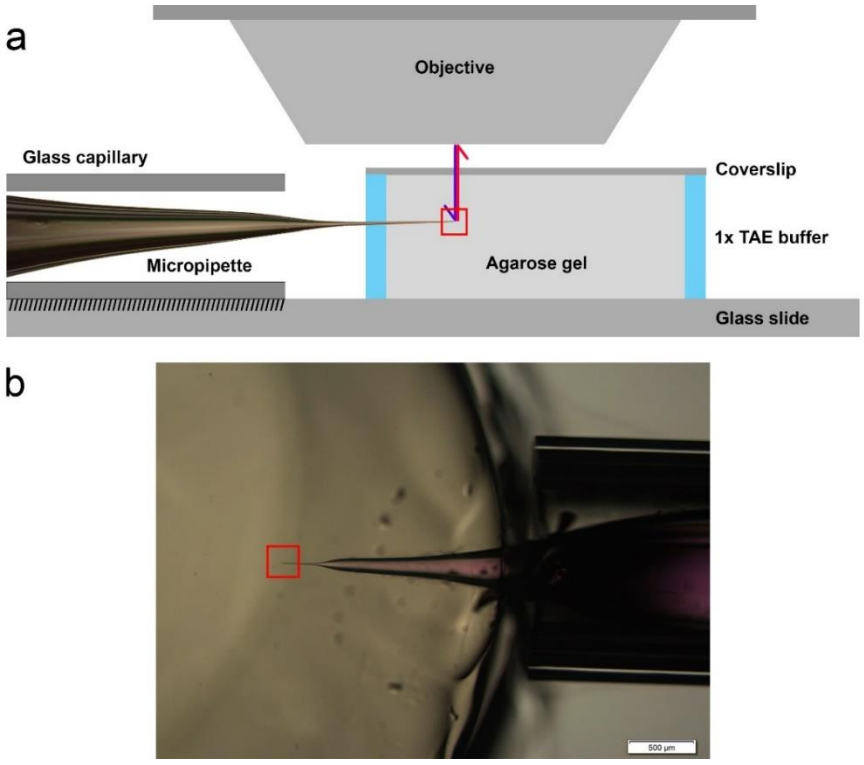

Figure 4.3 | Experiment setup of microinjection experiments. The area to be observed under the microscope after microelectrophoresis is designated with red frames. **a,** Schematic illustration of experiment apparatus (side view). The violet and red arrows represent the excitation light from the objective and the fluorescence from ejected 655-QDs particles respectively. **b,** Micrograph of the experiment setup (top view). Scale bar, 500 μm.

4.2.4 Fluorescence microscopy: measurement of the fluorescence signals of ejected QDs

The Olympus BX51 upright optical microscope at Adelaide Microscopy was used to obtain micrographs (white light illumination) and fluorescence images (mercury lamp illumination) of target objects. For fluorescent imaging, the excitation light from the mercury lamp and the emission signal can be filtered by two interference filters to achieve different excitation and emission range (using long pass filter) as listed in Table 4-1. The exposure time is how long the camera will be exposed to the light (photons) emitted from the sample.

Table 4-1 | Interference filters equipped on Olympus BX51 optical microscope.

Interference filter	Excitation range (nm)	Dichroic mirror (nm)	Emission range (nm)
1	330-385	400	420
2	400-440	455	475

4.3 Results and discussion

4.3.1 Fluorescence spectra of QDs

The fluorescence spectrum of 1 nM 655-QDs in ultrapure water is shown in Figure 4.4. The fluorescence peak wavelength is at 654 nm, which is identical to the specification from Thermo Fisher.

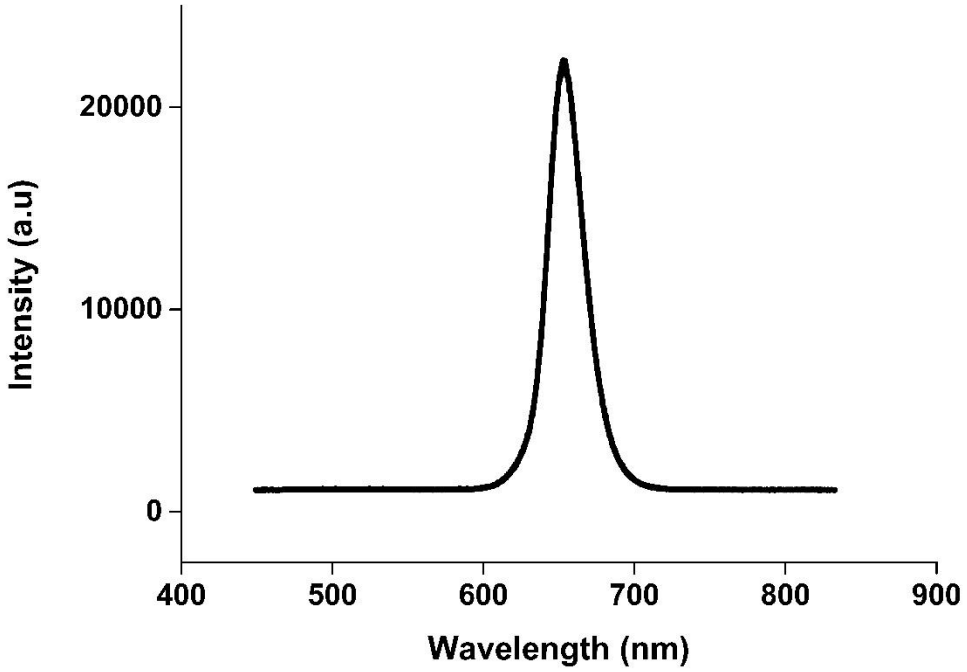

Figure 4.4 | Fluorescence spectrum of 1 nM 655-QDs in ultrapure water (a.u. = Arbitrary Units).

4.3.2 Fluorescence image of agarose gels doped with QDs

The fluorescence image of 655-QDs in a 2.0 % agarose gel is shown in Figure 4.5. 655-QDs particles formed aggregates in the agarose gel due to the macromolecular netted texture of agarose gel and its approximate 200 nm pore size. Thus, it is promising to utilize the structural characteristics of agarose gels to confine the movement of 655-QDs that are ejected out of the micropipettes in microinjection. Figure 4.5 also provides a reference for detecting prospective fluorescence from 655-QDs within agarose gels in microinjection experiments.

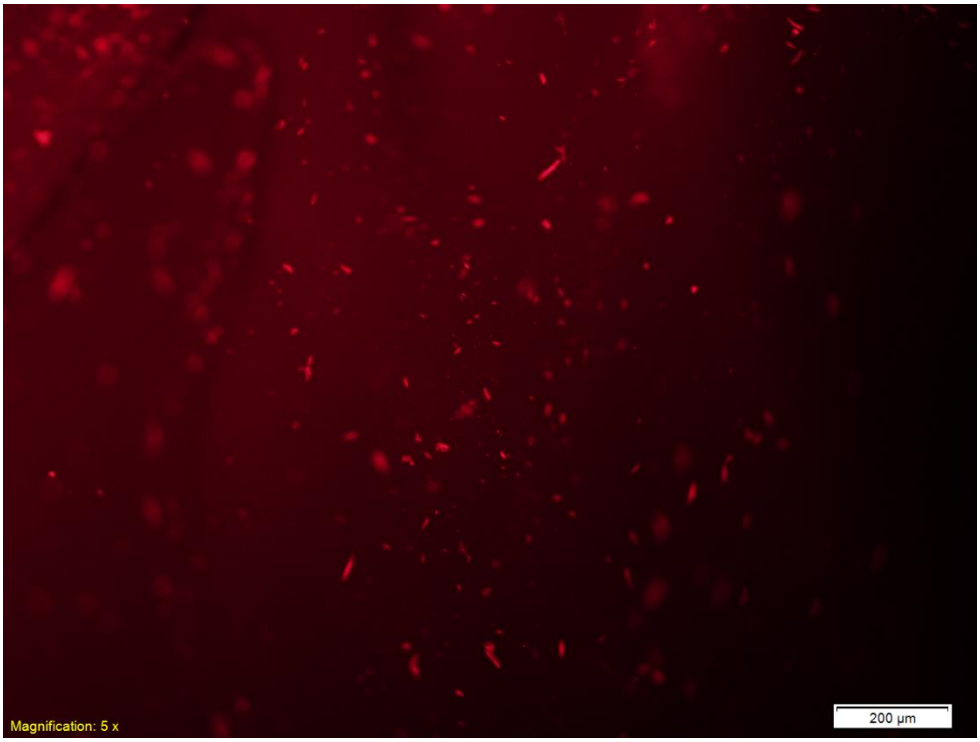

Figure 4.5 | Fluorescence image of 655-QDs in a 2.0 % agarose gel (filter 2; exposure time: 5.4 ms). The red dots are 655-QDs aggregates. Scale bar, 200 µm.

4.3.3 Microinjection of QDs

Four tests were conducted to demonstrate the successful microinjection of RDB and 655-QDs into agarose gels. For each test, the compound concentration, the tip ID of micropipette, agarose gel concentration, pressure and ejection duration, and the exposure time of fluorescence imaging are listed in Table 4-2.

Table 4-2 | The Conc. of compounds that were filled within micropipettes, the tip ID of micropipettes, agarose gels Conc., pressure and ejection duration for each microinjection experiment.

	Compound		Micropipette	Agarose gel	Microinjection		Fluorescence imaging	
Test	Name	Conc. (nM)	Tip ID (nm)	Conc. (%)	Pressure (p.s.i.)	Duration (minute)	Exposure time (ms)	Filter
1	RDB	100,000	31,400	2.0	3	3	67	2
2	RDB	100,000	130	2.0	49	100		
3	QDs	10	130	0.7	10	100	1100	2
4	QDs	10	130	2.0	10	100	1100	2

Test 1 was to verify the feasibility of the experiment setup for microinjection, where RDB was ejected through a hand-broken micropipette with a tip ID of 31.4 μm under a low pressure (3 p.s.i) and short ejection duration (3 minutes). In Test 2, a new micropipette with the tip ID of 130 nm was used to eject RDB solution with the same concentration. To achieve a high local concentration of RDB in the agarose gel for fluorescence detection, the ejection pressure was gradually increased to 49 p.s.i and ejection time was extended to 100 minutes. In Test 3 and 4, freshly prepared 655-QDs-17 suspensions were backfilled into micropipettes with tip ID estimated at 130 nm and ejected via 10 p.s.i pressure for 100 minutes into 0.7 % and 2.0 % agarose gels respectively.

In Test 1, a large amount of RDB diffused from the position where the tip of micropipette was pierced into the agarose gel (Figure 4.6). The result demonstrates the feasibility of the experiment setup for microinjection.

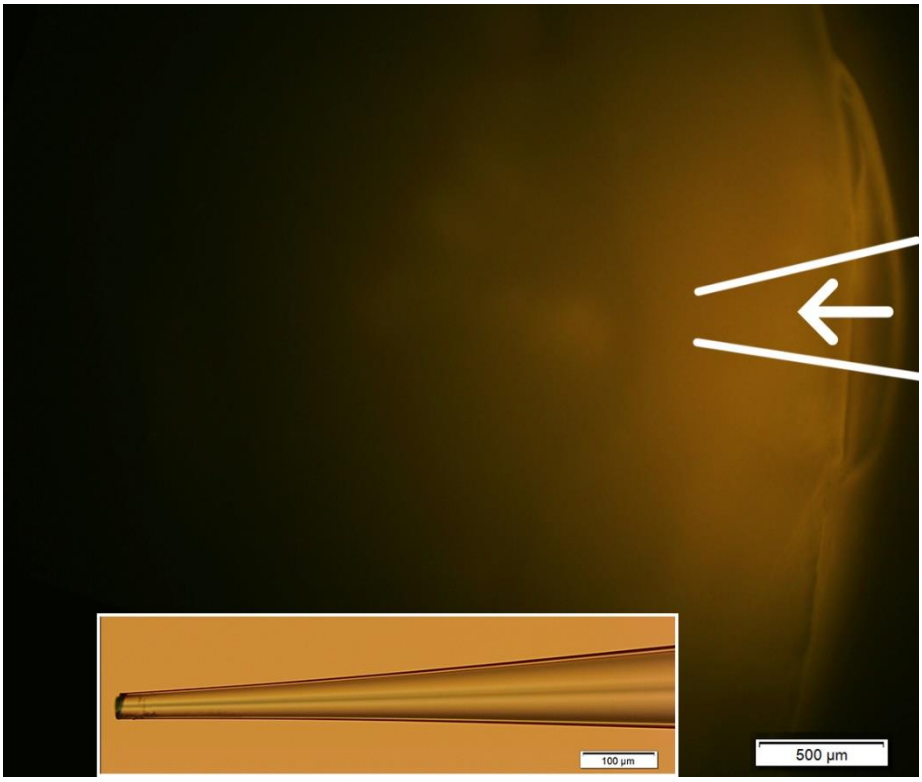

Figure 4.6 | Fluorescence image of ejected RDB molecules in the agarose gel in Test 1. Scale bar, 500 µm. The micropipette was pierced into the gel from the right and removed before imaging. The position of micropipette is shown by the white lines and arrow. The inset shows the micrograph of the hand-broken micropipette with a tip ID of 31.40 µm that was used in Test 1. Scale bar, 100 µm.

After Test 2, the micropipette was removed from the agarose gel. There was no fluorescence detected from RDB near the tip position in the agarose gel. However, bright fluorescence from RDB molecules was observed in the tip of micropipette (Figure 4.7a). Similarly in Test 3, the bright fluorescence from 655-QDs was also observed in the tip of micropipette as shown in Figure 4.7b. However, fluorescence signals from ejected 655-QDs was observed near the tip position in the agarose gel (Figure 4.8b). Thus, it is assumed that RDB and 655-QDs were both successfully ejected out of the micropipettes. However, the molecular size of RDB is much smaller than 655-QDs and the pore size of 2.0 % agarose gels. Thus, the macromolecular netted texture of agarose gels has no confinement effect on the RDB molecules. RDB molecules were quickly

diffusing in the agarose gel and resulted in a low local concentration, which was hard to be detected under the fluorescence microscope. Oppositely, 655-QDs were confined in a small area, resulting in a high local concentration for fluorescence detection. This can explain the phenomenon of the bright fluorescence from RDB and 655-QDs in the micropipette tips where RDB molecules and 655-QDs that were not ejected out of the tip was pushed backwards by the inner wall of the micropipette rather than clogging the tip.

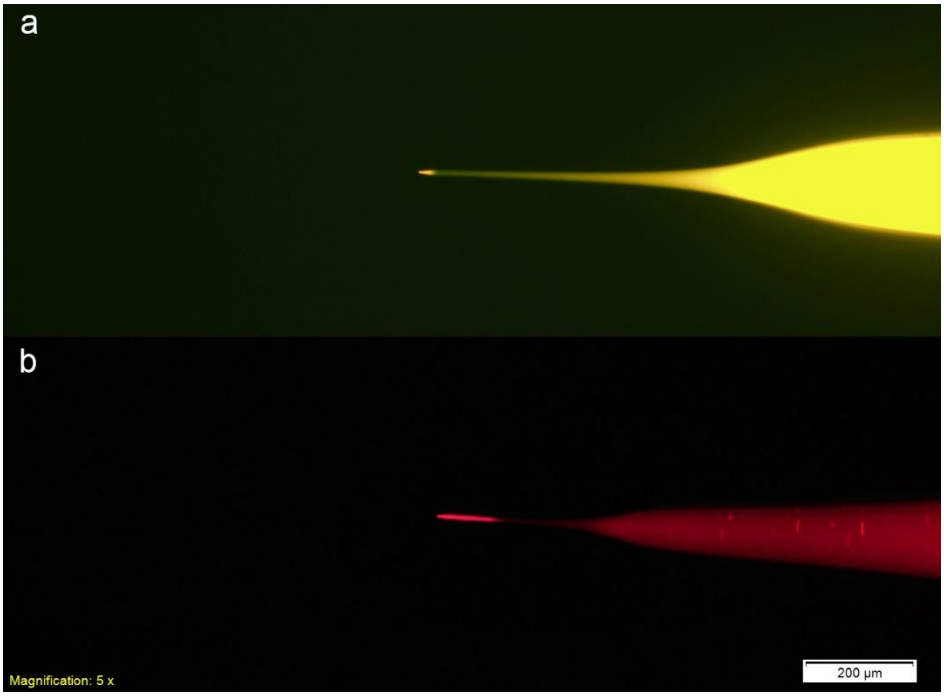

Figure 4.7 | Fluorescence image of micropipettes that were removed from the agarose gel in Test 2 (**a**) (filter 2; exposure time: 292.9 ms) and 3 (**b**) (filter 2; exposure time: 50 ms). Scale bar, 200 µm. The micropipettes in (a) and (b) have the same tip ID of 130 nm.

The micrographs and fluorescence images of ejected 655-QDs in the 0.7 % and 2.0 % agarose gels in Test 3 and 4 are shown in Figure 4.8. The micrograph and corresponding fluorescence image were captured without adjusting the position of the glass slide or focus. A red dot was observed near the tip position in both 0.7 % and 2.0 % agarose gels under the fluorescence microscope and

magnified with the same magnification in the insets. The minimum square in each inset represents one pixel, and one pixel represents 1.66 μm^2 area (1.29*1.29 µm).

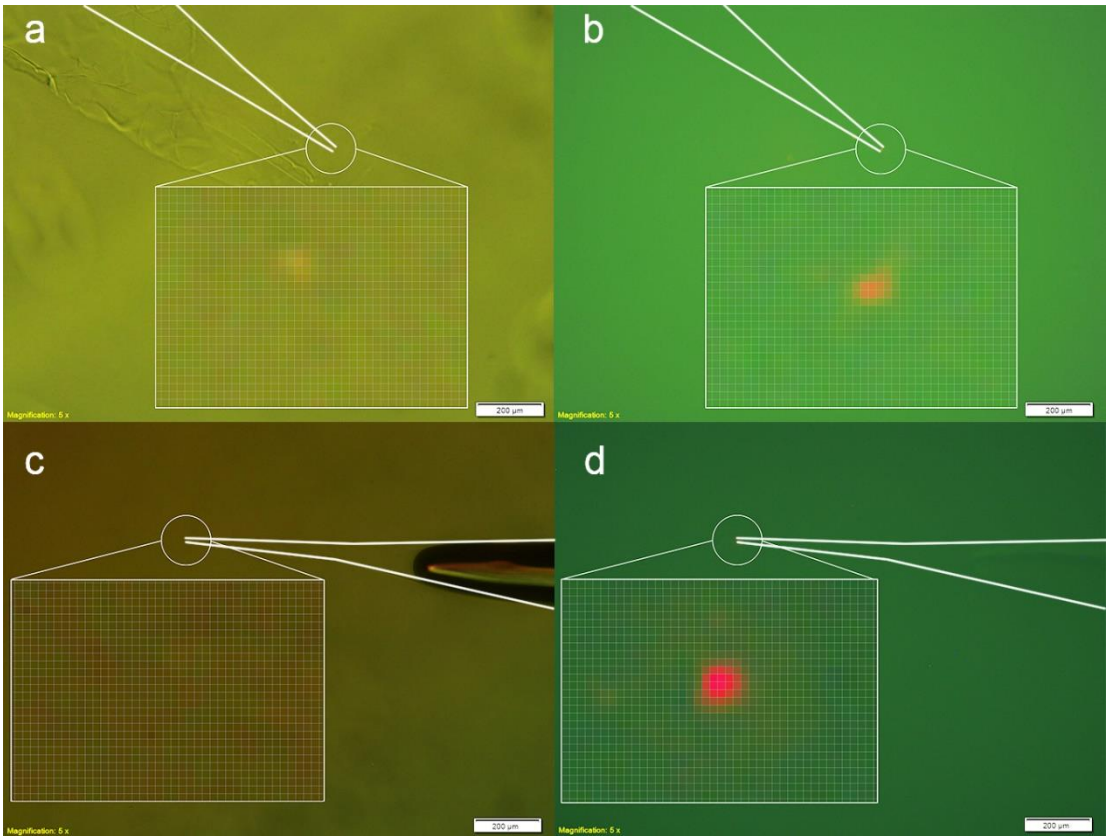

Figure 4.8 | The results of Test 3 and 4. The position where the tip of micropipettes was pierced into the agarose gel is designated with white lines and circles. Scale bar, 200 µm. **a, c,** Micrographs of the 0.7 % and 2.0 % agarose gels in Test 3 and 4 respectively. **b, d,** Fluorescence images of the 0.7 % and 2.0 % agarose gels in Test 3 and 4 respectively.

The results of Test 3 and 4 demonstrate the successful ejection of 655-QDs particles via microinjection technique and confirm the size match between the tip ID (130 nm) and the size distribution of 655-QDs-17 suspensions. Under the same pressure and ejection duration, the increase of agarose gel concentration results in reduced pore size. The confinement effect of the macromolecular netted texture of agarose gels on the movement and diffusion of 655-QDs

particles became stronger. The detected fluorescence intensity of 655-QDs in the 2.0 % agarose gel is brighter than that in the 0.7 % agarose gel as shown in Figure 4.8, which demonstrates that a larger amount of 655-QDs are confined outside the tip of micropipette in the 2.0 % agarose gel.

4.4 Conclusions

This chapter demonstrated the successful microinjection of 655-QDs into agarose gels. 655-QDs were ejected out of the micropipettes with tip ID estimated at 130 nm without blockage. They were well-confined in a small space by the macromolecular netted texture of agarose gels and were observed under the fluorescence microscope. Thus, the tip ID estimated at 130 nm is proved being large enough to allow the ejection of 655-QDs-17 suspensions and can be used for microelectrophoresis.

4.5 References

1. Lalley, P.M., *Microiontophoresis and Pressure Ejection*, in *Modern Techniques in Neuroscience Research*, U. Windhorst and H. Johansson, Editors. 1999, Springer Berlin Heidelberg: Berlin, Heidelberg. p. 193-212.
2. Serwer, P., *Agarose gels: Properties and use for electrophoresis.* ELECTROPHORESIS, 1983. **4**(6): p. 375-382.
3. Lee, P.Y., et al., *Agarose Gel Electrophoresis for the Separation of DNA Fragments.* Journal of Visualized Experiments : JoVE, 2012(62): p. 3923.
4. Arnott, S., et al., *The agarose double helix and its function in agarose gel structure.* Journal of Molecular Biology, 1974. **90**(2): p. 269-284.
5. Chang, C., et al., *Strongly fluorescent hydrogels with quantum dots embedded in cellulose matrices.* Journal of Materials Chemistry, 2009. **19**(41): p. 7771-7776.
6. Liu, S., et al., *Micro/nano-scaled carbon spheres based on hydrothermal carbonization of agarose.* Colloids and Surfaces A: Physicochemical and Engineering Aspects, 2015. **484**: p. 386-393.

7. Narayanan, J., J.-Y. Xiong, and X.-Y. Liu. *Determination of agarose gel pore size: Absorbance measurements vis a vis other techniques*. in *Journal of Physics: Conference Series*. 2006. IOP Publishing.
8. Vilca-Quispe, L., et al., *Diffusion of Methylene Blue in Phantoms of Agar Using a Photoacoustic Technique.* International Journal of Thermophysics, 2010. **31**(4): p. 987-997.
9. Pomfret, R., G. Miranpuri, and K. Sillay, *The substitute brain and the potential of the gel model.* Annals of neurosciences, 2013. **20**(3): p. 118.
10. Han, M., et al., *An optical fibre sensor for remotely detecting water traces in organic solvents.* RSC Advances, 2016. **6**(85): p. 82186-82190.

5 Microelectrophoresis of semiconductive QDs

5.1 Introduction

As described in Chapter 4, agarose gels have successfully confined the diffusion of ejected 655-QDs in microinjection, resulting in a high local concentration and fluorescence intensity of 655-QDs for successful fluorescence detection. However, unlike in microinjection where the pressure only exists within micropipettes, the driving force on 655-QDs in microelectrophoresis is ascribed to the applied electric field constantly pushing the charged QDs onto the counter electrode. The network structure of 2.0 % agarose gels (pore size estimated at 200 nm) is not enough to confine the continuous movement of 655-QDs for effective accumulation. Thus, two methods were used to demonstrate the successful microelectrophoretic ejection of QDs:

- One method is to conduct the microelectrophoresis of QDs for a long period of time and detect the fluorescence signals from ejected QDs that are accumulated and adsorbed on the counter electrode, which is hereafter referred to as *long-term ejection*.

- The other method is inspired by the rapid aggregation of QDs in an environment with high ionic strength (IS) [1, 2]. Agarose gels can be immersed in 3 M KCl solution to create an outer medium with high IS. Thus, ejected QDs can rapidly flocculate in the agarose gels due to the compressed electrical double layer, and generate large aggregates with

bright fluorescence for successful fluorescence detection. This method is hereafter referred to as *3 M KCl accumulation*.

5.2 Experimental procedures

5.2.1 Preparation of QDs in 3 M KCl solutions

To confirm that QDs can rapidly aggregate in high IS solutions, 655-QDs were suspended in 3 M KCl solution and their size distribution was measured by Zetasizer nano ZSP.

The original 8 μM 655-QDs suspension from Thermo Fisher Scientific was gently vortexed for 1 minute and then 1.8 μL original suspension was pipetted into 1.5 mL centrifuged 3 M KCl solution in an Eppendorf Flex-tube labelled with "655-QDs_3M-KCl". The sample was vortexed for 1 minute and sonicated from 4.0 °C to 24.0 °C without external heat for 20 minutes. 1 mL of the sample was pipetted by a 1 mL syringe into a clean folded capillary cell for subsequent measurements in Zetasizer nano ZSP. The parameter setting used for the Zetasizer measurement is presented in the Appendix.

5.2.2 Preparation of agarose gels

In Chapter 4, it is concluded that 2.0 % agarose gels have better confinement effect on the diffusion of 655-QDs than 0.7 % agarose gels. Thus, 2.0 % agarose gels were prepared in 1x TAE buffer and then immersed in 3 M KCl solution for a period to create an outer medium with high IS for effective accumulation of ejected 655-QDs.

TopVision Agarose was used to prepare 2.0 % agarose gels in 1x TAE buffer (pH 8.3 at 23.9°C). The agarose gel was formed into a pie shape with a thickness of 0.6 cm and a diameter of 1.0 cm. Then it was immersed into 3 M KCl solution in an Eppendorf Flex-tube for one hour as shown in Figure 5.1. When the agarose gel became fully immersed in the 3 M KCl solution instead of floating on the surface, the agarose gel was ready for use.

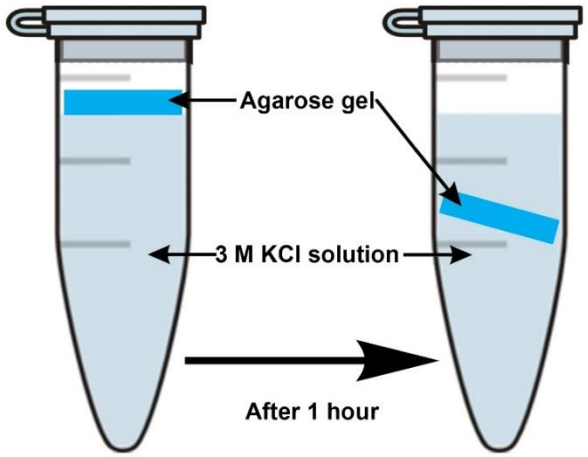

Figure 5.1 | Schematic illustration of creating agarose gels with high IS.

5.2.3 Microelectrophoresis of QDs

For both methods, fresh 655-QDs-17 suspensions (see section 2.3.5) were prepared and filled into micropipettes with tip ID estimated at 130 nm.

5.2.3.1 Long-term ejection method: measurement of the accumulation of ejected QDs on the counter electrode

The experiment apparatus of the *long-term ejection* method is shown in Figure 5.2, which was placed on a vibration-proof table in a dark environment to avoid photobleaching of 655-QDs. A glass capillary with a length of 80 mm and an ID of 1.0 mm was fully filled with 60 μL centrifuged 0.01 M KCl solution as the outer medium. As discussed in Chapter 2, 0.01 M KCl solution can provide the required electrolytic conductivity for Ag/AgCl electrodes and avoid rapid QDs aggregation at the same time. The micropipette filled with fresh 655-QDs-17 suspension was held by the pipette holder on the micromanipulator and inserted with the Ag/AgCl working electrode from the blunt end. The micropipette was slowly inserted into the outer medium via micromanipulator from one end of the capillary. Then the Ag/AgCl counter electrode was carefully inserted into the KCl solution from the other end without touching the tip of micropipette. The two Ag/AgCl electrodes were connected to the headstage of the intracellular bridge mode amplifier to form a complete electrical circuit.

Figure 5.2 | The experiment apparatus of the *long-term ejection* method (side view). The area **a** and **b** designated with red frames were observed under the fluorescence microscope after microelectrophoresis.

5.2.3.2 3M KCl accumulation method: measurement of the accumulation of ejected QDs under agarose gels

The experiment apparatus of the *3M KCl accumulation* method is shown in Figure 5.3, which was also placed on a vibration-proof table in a dark environment to avoid photobleaching of 655-QDs. The micropipette filled with 655-QDs-17 suspension was inserted with the Ag/AgCl working electrode from the blunt end and held by the pipette holder on the micromanipulator. The micropipette was confined in a glass capillary with relatively larger ID that was stuck on the glass slide to avoid the vibration of micropipette. The micropipette was slowly inserted into the agarose gel via micromanipulator from one side. Then the Ag/AgCl counter electrode was carefully placed into the surrounding 3 M KCl solution from the other side without touching the agarose gel. The coverslip was to prevent water evaporation. The two Ag/AgCl electrodes were connected to the headstage of the intracellular bridge mode amplifier to form a complete electrical circuit.

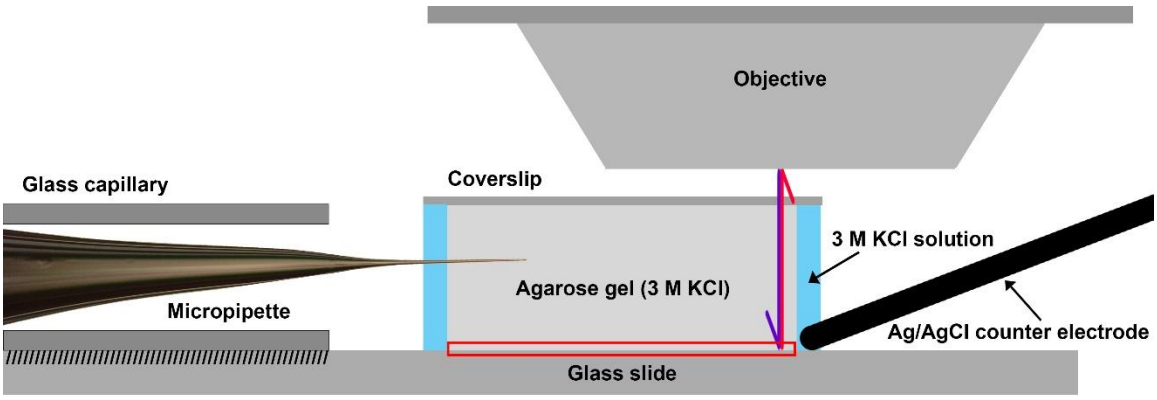

Figure 5.3 | The experiment apparatus of the *3M KCl accumulation* method (side view). The area of glass slide designated with red frame was observed under the fluorescence microscope after microelectrophoresis.

5.2.3.3 Fluorescence microscopy: measurement of the fluorescence signals of ejected QDs

In the *long-term ejection* method, after the microelectrophoresis, the Ag/AgCl counter electrode was carefully taken out. The area a and b of the counter electrode that are indicated with red frames in Figure 5.2 were observed under the fluorescence microscope (see details in section 4.2.4) to detect the fluorescence signals of ejected 655-QDs.

In the *3M KCl accumulation* method, after the microelectrophoresis, the micropipette, Ag/AgCl counter electrode and agarose gel were carefully removed. The area of glass slide that is designated with a red frame in Figure 5.3 was observed under the fluorescence microscope to detect the fluorescence signals of ejected 655-QDs.

5.3 Results and discussion

5.3.1 Aggregation of QDs in 3 M KCl solutions

To confirm that QDs can rapidly aggregate in solutions with high IS, the size distribution of 655-QDs that were suspended in 3 M KCl solution was measured by Zetasizer nano ZSP. The size distribution result of Sample "655-QDs_3M-KCl" is presented in Figure 5.4 and Table 5-1 with two peak sizes, the SD of three measurements, and the number percentage of each peak is listed.

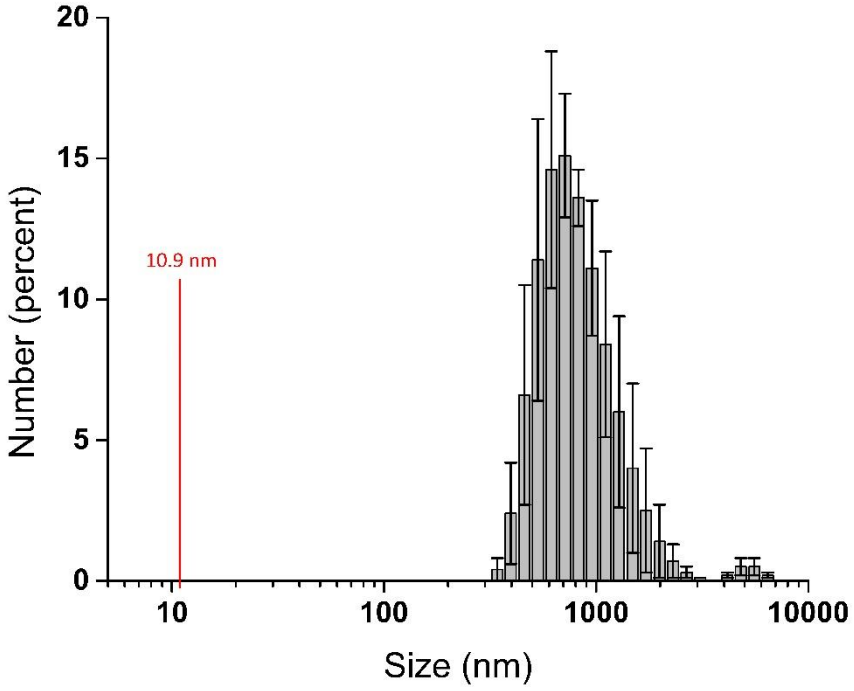

Figure 5.4 | The size distribution by number (percent) of Sample "655-QDs_3M-KCl". Error bars, ± 1 SD with *n*=3 each. The red line indicates the primary size of 655-QDs at 10.9 nm.

Table 5-1 | The size distribution result of Sample "655-QDs_3M-KCl". The sequence of the peaks is ascending with the peak size (± 1 SD with *n*=3 each).

Peak 1 Size ± SD (nm)	Peak 2 Size ± SD (nm)
1046 ± 211	5251 ± 138
Peak 1 Number ± SD (percent)	Peak 2 Number ± SD (percent)
98.5 ± 0.7	1.5 ± 0.7

As shown in Table 5-1, most of particles in Peak 1 are 1046 nm in diameter. Therefore, it is assumed that 655-QDs formed a large amount of aggregates due to the high IS of 3 M KCl solution. The large size of Peak 2 is assumed to be caused by the presence of air bubbles or dust. The hydrodynamic radii of most 655-QDs aggregates is 1046 nm, which is much larger than the primary size of

655-QDs (10.9 nm). Thus, it can be concluded that the high IS of 3 M KCl solution can completely shield the repulsive energy barrier between QDs and result in substantial QDs aggregation. This is useful for the accumulation of ejected 655-QDs in agarose gels that are immersed in 3 M KCl solutions. The ejected 655-QDs can rapidly aggregate and result in a high local concentration and fluorescence intensity of 655-QDs for fluorescence detection, which can validate the successful microelectrophoresis.

5.3.2 Microelectrophoresis of QDs

5.3.2.1 Long-term ejection method: detection of ejected QDs on the counter electrode

A successful microelectrophoresis requires no tip blockage during ejection. To examine whether 655-QDs aggregate in the tip and cause tip blockage, the resistance of micropipette was checked occasionally by applying a small known current (1 nA) across the micropipette. An irreversible increase of the resistance can indicate a blockage occurring at the tip, whereas an irreversible decrease of the resistance means that the tip of the micropipette is broken [3]. The resistance of the micropipette filled with 655-QDs-17 suspension was 122 MΩ consistently during microelectrophoresis for four hours. As a reference, another micropipette that was manufactured with the same program and filled with 0.01 M centrifuged KCl solution, had a resistance of consistently 125 MΩ under the same condition. The resistance of QDs-filled micropipette is comparable with that of the 0.01 M KCl-filled micropipette, which excludes the possibility of QDs aggregation. The slight difference between the two resistances is caused by the unavoidable change in the tip ID of micropipettes manufactured with the same program. Thus, it can be concluded that there was

no aggregation of 655-QDs occurring at the tip and the tip remained intact during microelectrophoresis. The amplifier generated a small negative current, -0.4 nA, and ejected 655-QDs for four hours.

The Ag/AgCl counter electrode was taken out after the microelectrophoresis and observed under the fluorescence microscope. As shown in Figure 5.5, two large areas and many small areas in the **a** part (as indicated in Figure 5.2) of the counter electrode show bright red fluorescence. Besides, the **b** part of the counter electrode that was not immersed in the 0.01 M KCl solution during microelectrophoresis shows no red fluorescence. Thus, it can be concluded that the bright red fluorescence in part **a** is from ejected 655-QDs, which clearly demonstrates the successful microelectrophoresis.

Based on the resistance change of micropipette and the fluorescence imaging results, the microelectrophoresis process in the *long-term ejection* method can be explained in detail as the following:

655-QDs that were ejected out of the micropipette continuously moved to and accumulated on the counter electrode under the applied electric field, resulting in high fluorescence intensity of 655-QDs for successful fluorescence detection. In addition, the ejecting current, -0.4 nA, is much less than the upper limit of intracellular microelectrophoresis (± 100 nA), which has the potential to preserve the intracellular electrical activities of target cells [3, 4].

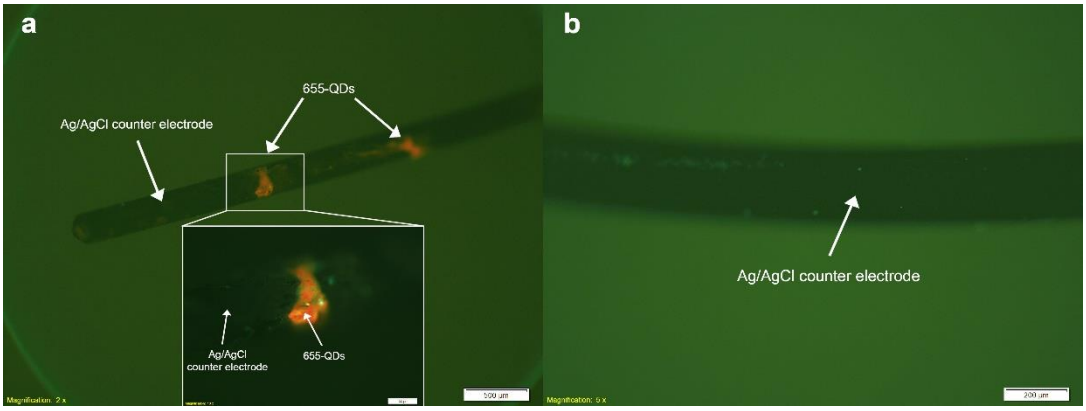

Figure 5.5 | Fluorescence image of the Ag/AgCl counter electrode after microelectrophoresis in the *Long-term injection* method (filter 2; exposure time: 121.1 ms). **a,** The area **a** of Ag/AgCl counter electrode. Scale bar, 500 μm. Inserted with the magnified red fluorescence region designated with the white frame. Scale bar, 100 μm. **b,** The area **b** of the Ag/AgCl counter electrode. Scale bar, 200 μm.

5.3.2.2 3 M KCl accumulation method: detection of ejected QDs under agarose gels

As described previously, the resistance of micropipette in the *3M KCl accumulation* method was checked occasionally by applying a small known current (1 nA) across the micropipette. The resistance of the micropipette filled with 655-QDs-17 suspension was 16 MΩ when the micropipette was placed in the surrounding 3 M KCl solution. Its resistance remained the same when it was slowly inserted into the agarose gel. However, the resistance increased to 40 MΩ after an -4.0 nA current was applied for 20minutes. The increase of resistance indicated that the tip was partly blocked. The blockage sign was reversible, and the resistance reduced to 23 MΩ after applying electrical clearing. During clearing, large amounts of positive or negative currents and buzz function with powerful high-frequency oscillations were used to clear the tip. Then a 1.5 nA current was applied for 5 minutes and the resistance reduced to 22 MΩ. After that, an -2.0 nA current was applied for 5 minutes, the tip was blocked again, and the resistance increased to 40 MΩ. The tip was cleared by

the same method and the resistance deduced to 17 MΩ. The blockage occurred again when the ejection current decreased to -0.5 nA, -0.1 nA and -0.06 nA respectively. The final resistance was 30 MΩ. The total ejection duration was 1 hour and 30 minutes.

As a reference, the resistance of another micropipette filled with 655-QDs-17 suspension was 20 MΩ when the tip of micropipette was immersed in the surrounding 3 M KCl solution and reduced to 19 MΩ after applying -4 nA current for 1 hour and 30 minutes. The resistance of another micropipette filled with 0.01 M centrifuged KCl solution was consistently 15 MΩ when the tip of micropipette was immersed in the surrounding 3 M KCl solution and slowly inserted into the agarose gel.

After the microelectrophoresis, the micropipette, Ag/AgCl counter electrode and agarose gel were carefully removed. The area of glass slide that is designated with a red frame in Figure 5.3 was observed under the fluorescence microscope to detect the fluorescence signals of ejected 655-QDs. As shown in Figure 5.6a, bright red fluorescence was observed around the KCl crystals under 330-385 nm excitation range. Because the emission peak wavelength of semiconductive QDs should remain the same under different excitation ranges [5], another excitation range, 400-440 nm, was used to excite the area to confirm the red fluorescence was emitted from 655-QDs. As shown in Figure 5.6b, bright red fluorescence was still observed at the same spot. Therefore, it is convincing that 655-QDs were successfully ejected via microelectrophoresis.

Using two different excitation ranges, it can also be concluded that the violet and green objects near ejected 655-QDs on the glass slide are specks of dust, as they only reflect light in the excitation bands rather than having featured

emission wavelength. They could have dropped from the air during the longtime microelectrophoresis.

Based on the resistance change of micropipette and the fluorescence imaging results, the microelectrophoresis process in the *3M KCl accumulation* method can be explained in detail as follows:

The 3 M KCl buffer within the agarose gel facilitated the rapid flocculation of ejected QDs. The large QDs aggregates partially blocked the tip and tended to move through the agarose gel to the Ag/AgCl counter electrode that was placed against the glass slide. They accumulated around the KCl crystals on the glass slide due to the gradual evaporation of water, resulting in a high local concentration and fluorescence intensity for successful fluorescence detection.

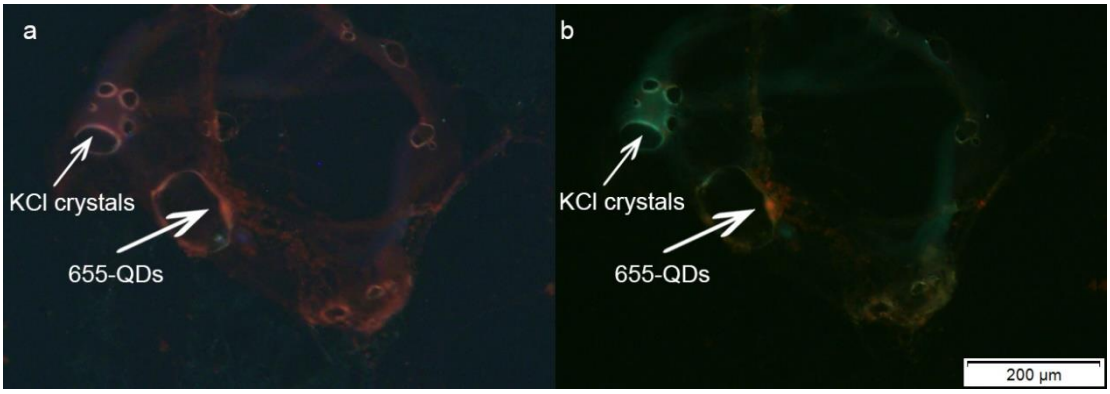

Figure 5.6 | Fluorescence image of ejected QDs near KCl crystals on the glass slide after microelectrophoresis in the *3M KCl accumulation* method. Scale bar, 200 µm. **a,** Filter 1; exposure time: 959.4 ms. **b,** Filter 2; exposure time: 292.9 ms.

However, there are several remaining questions for these two methods that deserve further investigation:

1. In the *long-term ejection* method, ejected 655-QDs formed several pieces of agglomerations on the Ag/AgCl counter electrode rather than a coating that evenly covers the electrode as a substrate (Figure 5.5). It is assumed that 655-QDs were physically adsorbed onto the counter electrode via electrostatic interaction rather than electroplating. The adsorption mechanism between them should be investigated in future studies.

2. The purpose of the long ejection duration (four hours) in the *long-term ejection* method is to eject enough amount of 655-QDs and result in strong fluorescence of 655-QDs on the Ag/AgCl counter electrode for fluorescence imaging. However, for intracellular microelectrophoresis, the ejection duration should be as short as possible to avoid physical damage to target cells but at the same time be long enough to reach a high intracellular concentration of ejected QDs above the detection limit of fluorescence microscopy. The ejection duration should be tuned for different type of target cells in future studies.

5.4 Conclusions

The successful microelectrophoretic ejection of QDs was demonstrated by two methods. In the *long-term ejection* method, ejected QDs moved through the outer medium (0.01 M KCl solution) and accumulated on the Ag/AgCl counter electrode. In the *3M KCl accumulation* method, ejected QDs rapidly flocculated and formed large aggregates due to the high IS of the agarose gel buffer solution (3 M KCl). QDs aggregates moved through the agarose gel to the

Ag/AgCl counter electrode and accumulated near the KCl crystals on the glass slide due to water evaporation. In both methods, bright red fluorescence from ejected QDs was observed under the fluorescence microscope. In addition, the micropipettes used in both methods had tip ID estimated at 130 nm and the ejecting currents were much less than the upper limit of intracellular microelectrophoresis (± 100 nA), which could avoid physical damage to the cell membrane and preserve their intracellular electrical activities at the same time [3, 4].

For future studies, it is exciting to demonstrate the feasibility of applying microelectrophoresis technique for delivering QDs into live cells. Several parameters need to be further optimized for intracellular delivery. For example, the ejection duration and current magnitude should be tuned for different cell types to achieve high intracellular fluorescence intensity of QDs for successful fluorescence imaging but at the same time preserve their intracellular electrical activities. In addition, the tip ID of micropipettes should be adjusted based on different cell sizes to avoid physical damage to the cell membrane and cell distortion.

5.5 References

1. Zhang, W., *Nanoparticle aggregation: principles and modeling*, in *Nanomaterial*. 2014, Springer. p. 19-43.
2. Merkoçi, A., *Biosensing using nanomaterials*. 2009: John Wiley & Sons.
3. Purves, R., *Microelectrode methods for intracellular recording and ionophoresis*. 1981: Academic Press.
4. Mobbs, P., et al. *Techniques for dye injection and cell labelling*. in *Microelectrode techniques. The Plymouth workshop handbook. Cambridge, UK: The Company of Biologists Ltd*. 1994. Citeseer.
5. Smith, A.M. and S. Nie, *Semiconductor Nanocrystals: Structure, Properties, and Band Gap Engineering.* Accounts of Chemical Research, 2010. **43**(2): p. 190-200.

6 Conclusions

The motivation of this thesis was to provide a new method for the intracellular delivery of semiconductive QDs and various biocompatible nanoparticles via microelectrophoresis technique for biological sensing and labelling. There are two main difficulties with this technique. Firstly, QDs tend to aggregate due to their colloidal instability, which can cause blockages in the tip of micropipettes during ejection. Secondly, the micropipette tip sizes are required to be large enough to allow the ejection of QDs but as small as possible to avoid physical damage to target cells. Chapter 2 presents an efficient experimental protocol for preparing conductive and monodispersed QDs suspensions for filling micropipettes. Then, Chapter 3 describes the fabrication of micropipettes with suitable tip IDs for successful ejection of QDs. Finally, Chapter 4 and 5 demonstrate the successful microinjection and microelectrophoresis of QDs respectively.

The pioneering work and success of microelectrophoretic ejection of QDs described in this thesis build the foundation for further studies and application of microelectrophoresis technique for delivering biocompatible nanoparticles into target cells for various biological research. Microelectrophoresis has the potential to precisely deliver monodispersed nanoparticles into target cells with negligible cell membrane damage and cell distortion. In addition, it can record the intracellular electrical activities of target cells at the same time. Thus, it has the potential to overcome some of the limitations of current techniques, such as the endosomal degradation of QDs in passive and facilitated deliveries, high cell mortality and aggregation of QDs in electroporation, and the cell locating difficulty of microinjection technique. However, it should be also noted that microelectrophoresis has its inherent limitation of low throughput

as it can only manipulate one cell at a time and can be only applied to deliver charged nanoparticles.

Future work should focus on the intracellular microelectrophoretic delivery of nanoparticles and investigate their subsequent intracellular distribution and possible endocytosis or aggregation. In the meantime, a better method for preparing nanoparticles suspensions or a better design of nanoparticles surface functionalization should be further investigated to achieve better stability and mobility of nanoparticles for microelectrophoresis. Furthermore, the shelf life of prepared nanoparticles suspensions should be investigated, i.e., the zeta potential and size distribution of nanoparticles should remain the same for a long period. In practical use, it is unrealistic and time-consuming for researchers to prepare fresh nanoparticles suspensions every time before the microelectrophoresis. Thus, it is much easier to have stock suspensions with good stability that are ready for use, which requires less operation before each experiment. Finally, the quantification of the minute number of ejected nanoparticles that varies with current magnitude and ejection duration should be investigated, which is critical to the precise intracellular delivery. The brief idea is to calibrate the number of ejected nanoparticles per cell on the basis of the fluorescence intensity emitted.

Appendix

Materials and Instruments

All materials and instruments that were mentioned in this thesis are summarized in Table A-1 with their catalogue numbers, manufacturers and linked chapters listed. They are categorized into two main schemes, i.e., preparation-related and characterization-related items, and further divided into several subcategories according to their application.

Table A-1 | All materials and instruments that were mentioned in this thesis. They are sorted by initials in each subcategory.

Preparation-related Items		
Chemical reagents		
Item	**Catalogue number; Manufacturer**	**Linked chapter(s)**
10 x TAE buffer	T8280; Sigma-Aldrich Pty Ltd, NSW, AU	4, 5
Ethanol, Undenatured 100%, Analytical Reagent (AR)	EA043; Chem-supply, SA, AU	2, 4
Gum rosin	60895; Sigma-Aldrich Pty Ltd, NSW, AU	2
Hydrochloride acid, 32%, AR	HA020; Chem-supply, SA, AU	2
pH buffer tablet (4.00 ± 0.02 at 20.0 °C)	331542Q; VWR, Radnor, Pennsylvania, US	2
pH buffer tablet (7.00 ± 0.02 at 20.0 °C)	331552S; VWR, Radnor, Pennsylvania, US	2
pH buffer tablet (9.22 ± 0.02 at 20.0 °C)	331562U; VWR, Radnor, Pennsylvania, US	2
Potassium chloride, AR	PA054; Chem-supply, SA, AU	2, 5
Qdot® 655 ITK™ Amino (PEG)	Q21521MP; Thermo Fisher Scientific, Waltham, MA, USA	2, 4, 5

Rhodamine b	R6626; Sigma-Aldrich Pty Ltd, NSW, AU	4
Sodium chloride, AR	27788.297; VWR, Radnor, Pennsylvania, US	1
Sodium hydroxide pellet, AR	SA178; Chem-supply, SA, AU	2
TopVision Agarose	R0491; Thermo Fisher, Massachusetts, US	4, 5
Ultrapure water	Milli-Q® Advantage A10 Water Purification System; Merck Millipore, Massachusetts, US	2, 4, 5
General laboratory components		
1 mL Tuberculin syringe	SS-01T; Terumo Medical Corporation, Somerset, NJ	2, 4, 5
100 mL erlenmeyer flask	028.01.103; Isolab, Wertheim, Germany	4
34 Gauge MicroFil™ flexible plastic syringe needle	Warner Instruments, Hamden, CT	4
Ag wire	782500; A-M Systems; Sequim, WA, US	1
Eppendorf Flex-Tubes, 1.5 mL, colourless	022364111; Eppendorf, Hamburg, Germany	2, 4, 5
Fume cupboard	2012; Conditionaire International Pty Limited, NSW, AU	2
Glass slide	1000000; Paul Marienfeld GmbH & Co.KG, Germany	4, 5
Microfuge 16 Centrifuge	A46473; Beckman Coulter, California, US	2, 4
pH meter	827 pH lab; Metrohm, Herisau, Switzerland	2
Platinum electrode	298093-425MG; Sigma-Aldrich Pty Ltd, NSW, AU	1
PYREX ® 1000 Low Form Griffin Beaker 10 mL	COR-1000-10; Corning Incorporated, New York, US	2
PYREX ® 1000 Low Form Griffin Beaker 20 mL	COR-1000-20; Corning Incorporated, New York, US	2
Agitation		
Ultrasonicator	Soniclean 80TD; Soniclean, Thebarton, AU	2, 4, 5
Vortex mixer	VM1; Ratek Instruments Pty Ltd, Victoria, AU	2, 4, 5

Mechanical components		
Intracellular bridge mode amplifier	BA-03X; npi electronic GmbH Company, Tamm, Germany	2, 5
Micromanipulator	MM-33; ALA Scientific Instruments, NY, US	2, 4, 5
Pico-litre injector	PLI-10; Warner Instruments, Hamden, CT	4
Pipette holder	PPH-1P-BNC; ALA Scientific Instruments, NY, US	4, 5
Micropipette fabrication		
Aluminosilicate glass capillary	30-0108; Harvard Apparatus, Massachusetts, US	3
Box filament	FB255B; Sutter Instrument, Novato, CA, USA	3
Micropipette puller	Model P-97 Flaming/Brown; Sutter Instrument, Novato, CA, USA	1, 2, 3
Characterization-related Items		
Electron microscopy		
FEI Quanta 450 FEG Environmental SEM	FEI Corporate, Hillsboro, US	2, 3
FEI Tecnai G2 Spirit TEM	FEI Corporate, Hillsboro, US	1, 2
Philips CM 200 TEM	FEI Corporate, Hillsboro, US	2
Optical and fluorescence microscopy		
405 nm laser	iBeam smart-S; TOPTICA Photonics, Munich, Germany	4
iHR320 imaging spectrometer	Horiba, Japan	4
Mercury Burner	USH-1030L; Olympus Corporation, Tokyo, Japan	4
Optical microscope	BX51; Olympus Corporation, Tokyo, Japan	4, 5
UV-visible transparent optical fibre	Ocean Optics, Florida, USA	4
Zetasizer and accessories		
Folded capillary cell	DTS1070; Malvern Instrument, Worcestershire, UK	1, 2, 5

Zetasizer	Nano ZSP; Malvern Instruments, Worcestershire, UK	1, 2, 5

Zetasizer parameter setting

In Zetasizer nano ZSP, Henry's function $f(K_a)$ was set as 1.50. The dispersant was set as water (Temperature 25.0 °C; Viscosity 0.8872 cP; Refractive Index: 1.330; Dielectric constant: 78.5) and its viscosity was used as the viscosity of the sample. The material properties, refractive index and absorption of 655-QDs, were entered as 2.550 and 0.010 in Zetasizer [1]. The temperature equilibrium time was set as 120 seconds at 25.0 °C. The real-time temperature value was recorded when pH reading was carried out since the measurement temperature in Zetasizer nano ZSP can cause fluctuations of actual pH values during measurement. But, the change of pH value of each sample is the same for the same temperature and has no influence on data interpretation.

The quality of zeta potential data

The quality of zeta potential data can be assessed by examining several parameters [2]. As described in Chapter 1, in Zetasizer nano ZSP, the incident laser beam illuminates the particles and the scattered light at a certain angle is collected by the detector. Count rate (in kcps) is the number of photons per second reaching the detector, which is an indication of the detection capability of the instrument [3]. Phase plot displays the difference between the phase of the light scattered by the particles and the phase of the reference beam [3]. A good phase plot should show well defined, alternating slopes of the phase difference with time that result from the rapid reversal of the applied field [3], followed by either a smooth positive or negative peak that results from the

slow field reversal [2]. The frequency plot displays the difference between the reference beam and the scattered beam due to the movement of particles, which is proportional to particle velocities [2]. A good frequency plot should have smooth baselines and the calculated zeta potential distribution should have no change with measurement duration or different applied voltages.

As 655-QDs particles have the most stable state around pH 9.81, Sample 8 is used to assess the quality of data. The count rate of three measurements of Sample 8 is 162.9, 207.5, 194.8 kcps respectively, which is acceptable based on the instrument manufacturer's specifications (a minimum count rate of 10 kcps). The phase plots, frequency plots and zeta potential distributions of three measurements of Sample 8 are presented in Figure A.1. The phase plots have alternating slopes with time followed by a smooth negative peak. The frequency plots have smooth baselines and the zeta potentials have no change with measurement duration or different applied voltages. Thus, the zeta potential data of Sample 8 has a good quality.

Appendix

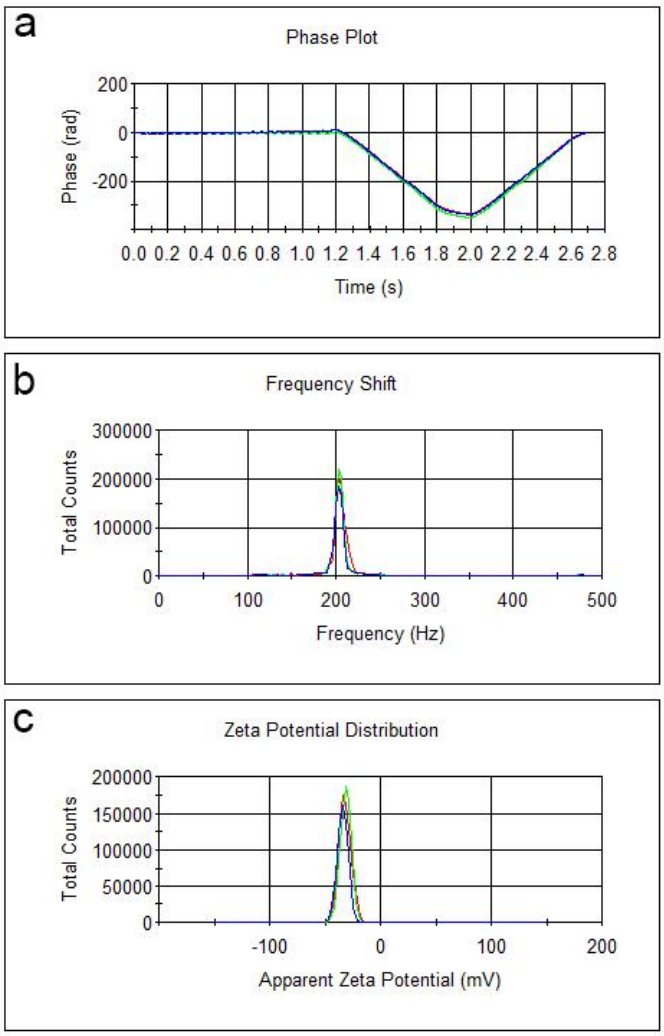

Figure A.1 | The phase plots, frequency plots and zeta potential distributions of three measurements of Sample 8 (pH 9.81 at 22.8°C). Rad=Radian.

References

1. Hondow, N., et al., *Quantitative characterization of nanoparticle agglomeration within biological media.* Journal of Nanoparticle Research, 2012. **14**(7): p. 977.
2. Clogston, J.D. and A.K. Patri, *Zeta Potential Measurement*, in *Characterization of Nanoparticles Intended for Drug Delivery*, S.E. McNeil, Editor. 2011, Humana Press: Totowa, NJ. p. 63-70.
3. Tantra, R., P. Schulze, and P. Quincey, *Effect of nanoparticle concentration on zeta-potential measurement results and reproducibility.* Particuology, 2010. **8**(3): p. 279-285.